Order Number 8914770

Transport and optical properties of n-CdSe

Levy, Miguel, Ph.D.

City University of New York, 1988

U·M·I
300 N. Zeeb Rd.
Ann Arbor, MI 48106

TRANSPORT AND OPTICAL PROPERTIES OF n-CdSe

by

Miguel Levy

A dissertation submitted to the Graduate Faculty in Physics in partial fulfillment of the requirements for the degree of Doctor of Philosophy, The City University of New York.

1988

This manuscript has been read and accepted for the Graduate Faculty in Physics in satisfaction of the dissertation requirement for the degree of Doctor of Philosophy.

9/27/1988
Date

Myriam P. Sarachik
Chair of Examining Committee

9/28/88
Date

Executive Officer

Professor Myriam P. Sarachik

Dr. Stanley Geschwind

Professor Joseph Birman

Professor Frederick W. Smith

Professor Frederick J. Cadieu

Supervisory Committee

The City University of New York

Abstract

TRANSPORT AND OPTICAL PROPERTIES OF n-CdSe

by

Miguel Levy

Adviser: Professor Myriam Sarachik

Transport measurements were performed on n-type CdSe near the metal-insulator transition above and below 4.2 K. The determination of compensation on the basis of transport data above 50 K is discussed. Use is made of some recent treatments of electron screening.

The resistivity of three insulating samples with carrier concentrations between 0.73 and 0.80 of the critical concentration follow a temperature dependence consistent with Mott variable range hopping in the temperature range between 1.25 K and 4.2 K. The Hall coefficient is also consistent with $R_H \sim \exp [T_{oH}/T]^{1/4}$ in that range. We compare our results with available theory and with those of other workers and point out some discrepancies.

Luminescence and Excitation spectra of metallic n-type CdSe were also obtained. We compare our results with available theory and find some discrepancies, which leads us to introduce some

modifications into the theory. In particular, we consider the effect of compensation on band gap renormalization. We also look for and find evidence of acceptor states in the luminescence spectra.

ACKNOWLEDGEMENTS

I thank my mentor, Myriam Sarachik, for her support, encouragement and competent advice. Her assistance was invaluable in enabling me to get back into physics after a seven year hiatus. Her constant concern and readiness to discuss physics at the spur of the moment are greatly appreciated. I also thank very specially Dr. Stanley Geschwind of AT&T Bell Laboratories, who played a central role in the development of this thesis. Dr. Geschwind initially suggested the study of CdSe, provided a large part of the samples, and suggested the study of the luminescence and excitation spectra in CdSe. I have learned a great deal from Stan's incisive criticisms and intellectual honesty and forthrightness. I thank Professors Joseph Birman, Fred Smith and Fred Cadieu for serving in my commitee.

My deep gratitude also goes to the following people. Professor Mel Lax, for many illuminating discussions and for pointing out to me the new treatments of electron screening and their incorporation in the formulation of electron mobility for degenerate semiconductors, included in this thesis. Gill Danan of AT&T Bell Laboratories and Wing-Kee Lee of City College, who were of great assistance in the luminescence experiments reported here. The transport experiments on CdSe below 4.2 K were done in collaboration with Apurba Roy, with whom I had many useful and illuminating discussions during our four years together at City College. Mark Turner, for many useful discussions and for being a

veritable encyclopedia and constant source of information, from geology to astronomy, and Les Isaacs for his help and for providing the Heli-Tran cold finger for the transport experiments above 4.2 K.

My very special thanks to George Devlin, a magnificent scientist, for his constant help, advice and suggestions during my stay at Bell Laboratories. The technical assistance of Jose Valladares is also very much appreciated. I also thank Drs. Aron Pinczuk and Herman Cummins for allowing me to use their equipment for the luminescence and excitation spectra experiments, and Vinay Ambegaokar, my mentor at Cornell University, for his many years of guidance and support.

TABLE OF CONTENTS

LIST OF TABLES

LIST OF ILLUSTRATIONS

INTRODUCTION

This thesis is divided into three main chapters, dealing with different experiments and analysis performed on heavily doped CdSe samples spanning the metal-insulator transition. Chapter I concerns transport measurements carried out at temperatures above 4.2 K. It contains a detailed analysis of the effect of various types of scattering mechanisms on the value of the electron mobility, and presents an attempt to extract the value of compensation for samples on the metallic side of the transition. As far as we know this is the first time that some recent treatments of screening presented below have been used to attempt to extract the value of compensation for the case of degenerate samples.

Chapter II concerns transport measurements carried out at temperatures below 4.2 K for insulating CdSe samples near the metal-insulator transition. The resistivity of these samples follows a temperature dependence consistent with Mott variable range hopping. We have been able to measure the Hall coefficient of these samples and find that it obeys $R_H \sim \exp [T_{oH}/T]^{1/4}$. This is significant given the paucity of data on the Hall coefficient in the variable range hopping regime. We compare our results with available theory and with those of other workers and point out some discrepancies.

Chapter III concerns luminescence and excitation spectra studies carried out on metallic n-CdSe samples. We compare our

results with available theory and find some discrepancies, which lead us to introduce some modifications into the theory. In particular, we consider the effect of compensation on band gap renormalization. We also look for and find evidence of acceptor states in the luminescence spectra. To our knowledge, this is the first observation of electron recombination into acceptor states for heavily doped n-type semiconductors on the metallic side of the metal-insulator transition.

Appendices are attached which contain discussions of some experimental and theoretical aspects of this work; in particular, Appendix III presents a correction to the van der Pauw formula for the determination of the Hall coefficient.

CHAPTER I
TRANSPORT MEASUREMENTS OF n-DOPED CdSe ON BOTH SIDES OF THE METAL-INSULATOR TRANSITION ABOVE 4.2 K.

INTRODUCTION

The transition from insulating to metallic behavior which occurs in semiconductors as the dopant concentration is increased has been the subject of numerous studies in recent years. Attention has focused largely on doped silicon and germanium, which have the important advantage that the dopant levels can be well controlled and the concentration of unwanted impurities can be kept very small. These materials have indirect fundamental band gaps, however, a fact which may introduce complications in the interpretation of results and which also makes some interesting measurements, such as Faraday rotation, very difficult to perform and analyze. On the other hand, direct band gap semiconductors such as CdS and CdSe are much more difficult to prepare cleanly and controllably. In addition to having non-negligible concentrations of unintended impurities, some degree of self-compensation is unavoidable. In order to shed further light on the metal-insulator transition, useful studies of these materials require full and careful characterization using a variety of different experimental probes. The aim is to obtain information regarding impurity content, the energy level diagram

including impurity levels, impurity bands and, if possible, the degree of compensation.

In this chapter, a careful analysis of Hall coefficient and resistivity data obtained for n-CdSe with indium dopant concentrations spanning the metal-insulator transition is used to estimate the degree of compensation and thus both the number of donors and acceptors. Although this has been done for semiconductors on the insulating side of the M-I transition, albeit not always with great care, we show that the application of recent theory yields similar information regarding the compensation for metallic samples. In particular, we make use of recent treatments of screening to improve upon estimates of the compensation based on measurements of the mobility. It should be pointed, however, that multi-ion screening, an effect not taken into account in the calculations presented below, may have a non-negligible effect on the value of the electron mobility and thus introduce an error in our determination of compensation for metallic samples. There have been some attempts to introduce the effect on multi-ion screening in theoretical treatments for the case of uncompensated samples on the metallic side of the metal-insulator transition, as discussed in this chapter, but no treatment exists as yet for the case of compensated material.

In the following, we describe our experimental methods, and based on theory and on preliminary data taken down to 1.2 K, we make an estimate of the critical concentration n_c. We discuss the overall features of the Hall coefficient and resistivity data; we attribute the experimentally observed transport at high

temperatures to carriers activated into the conduction band, and we argue that the behavior at intermediate temperature is very likely associated with impurity band conduction. Using the temperature dependent mobility and Hall coefficient measurements, we then show in detail using available recent theory for the insulating, intermediate and metallic cases, how to extract the compensation for samples on the metallic as well as the insulating side of the transition.

APPARATUS

Transport data above 4.2K was taken in an Air Products and Chemicals LT-3-110 Liquid Transfer Heli-tran System. This system provides refrigeration by a controlled transfer of liquid helium. The helium flows at a constant rate through a high efficiency transfer line to the sample holder interface. A micrometer needle valve permits precise control of the flow rate.

Temperature Control

Figure (I-1) shows a schematic view of the LT-3-110 Heli-tran end. A 44 Ω control heater wire is wound close to the sample holder attachment. Temperature sensing is effected by a Chromel-Gold with 0.07 atomic % iron thermocouple mounted on the Heli-tran cold tip.

A model 3700 Air Products temperature controller was used to control temperature between 5 K and 100 K. Alternatively, I also used a Lake Shore Cryotronics Model DRC-82C temperature

controller with a Carbon-Glass sensor mounted in the sample holder, shown in the next section.

Temperature stability was typically better than 20 mK in the temperature range between 5 K and 20 K. Temperature stability at higher temperatures was better than 0.1 K.

Sample Holder

A schematic view of the sample holder is shown in Fig. (I-2). It was machined of a single copper piece, and held the sample plus two resistor thermometers as shown. Sample lead electrical connections were made to four of six available binding posts connected to external measuring circuits.

The sample holder was screwed onto the bottom end of the Heli-tran cold tip. Conductive grease ensured good thermal contact between the sample holder and the Heli-tran tip.

A calibrated Lake Shore Carbon Glass CGR-1-1000 thermometer mounted as shown was used for temperature control when we operated with the Lake Shore controller. Temperature measurements were done with a calibrated Lake Shore GR-200A germanium thermometer. Samples were thermally anchored to the holder using Apiezon N grease. Electrical insulation was provided by cigarette paper, glued to the holder with GE7031 varnish.

The sample holder was encased in two radiation shields made out of aluminum, the colder of which was in thermal contact with the Heli-tran cryo tip. This system was encased in a vacuum shroud and evacuated by a diffusion pump. A schematic picture of the

radiation shields and vacuum shroud arrangement is shown in Fig. (I-3).

Magnetic Fields

The sample holder together with its vacuum shroud were designed to fit between the poles of an external magnet. Measurements were done up to 8 kilogauss, and the field intensity was determined by a Rawson-Lush Type 829M52 rotating coil gaussmeter.

All measurements were done with the magnetic field parallel to the c-axis of the CdSe samples.

Electronics

The Hall coefficient and resistivity were measured using the van der Pauw method[1]. This method requires measuring voltage and current across the sample in different configurations. Figure (I-4) shows the circuit we built for the purpose of facilitating these measurements.

Both voltage and current were measured with a Hewlett-Packard 3478A multimeter. Current was generated by a Hewlett-Packard 6181C DC current source.

Fig. (I-1) Schematic view of LT-3-110 Heli-tran end. *

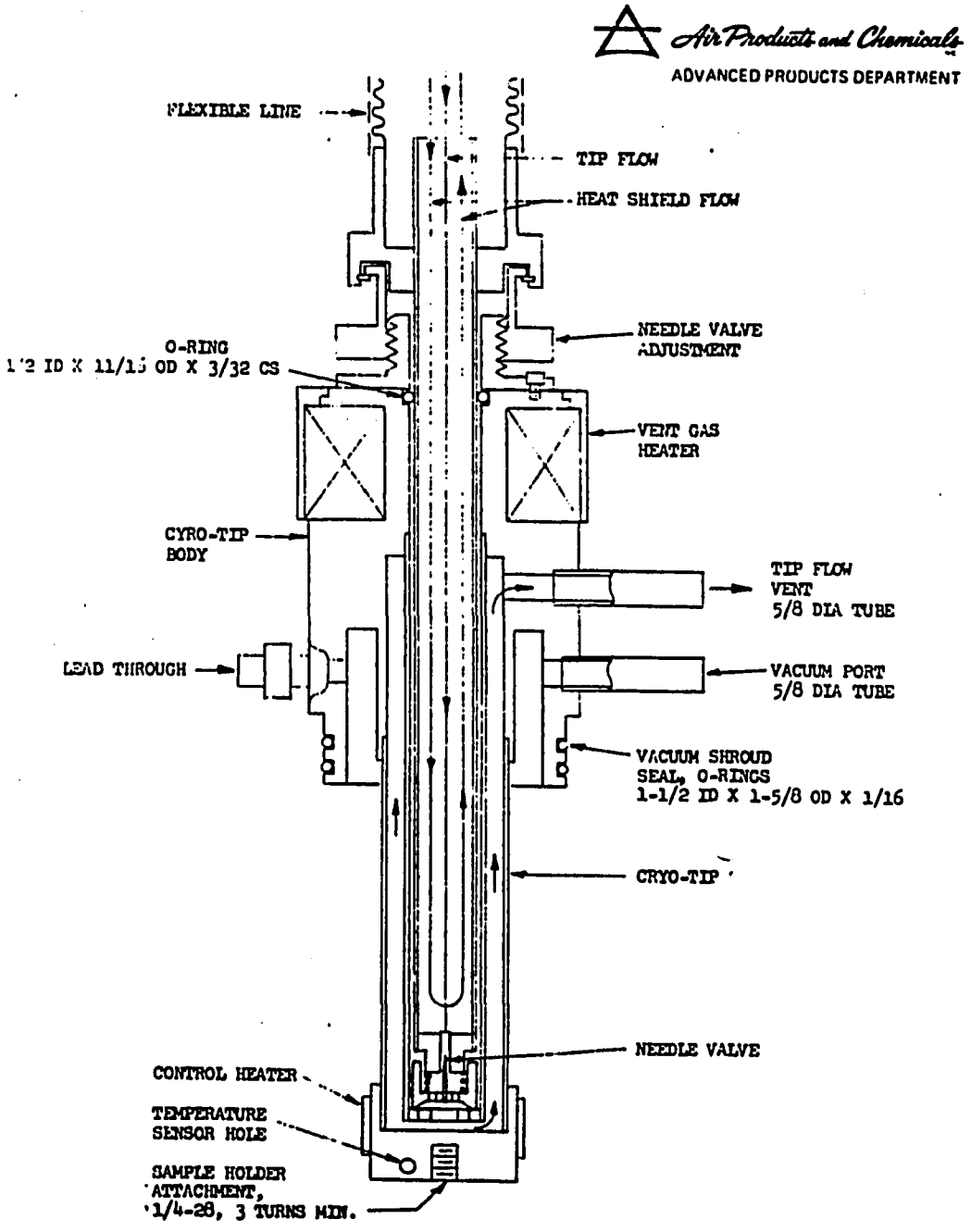

* Reprinted by permission of APD Cryogenics, Inc., Allentown, Pennsylvania.

Fig. (I-2) Schematic view of the sample holder.
Fig. (I-3) Radiation shields and vacuum shroud arrangement.

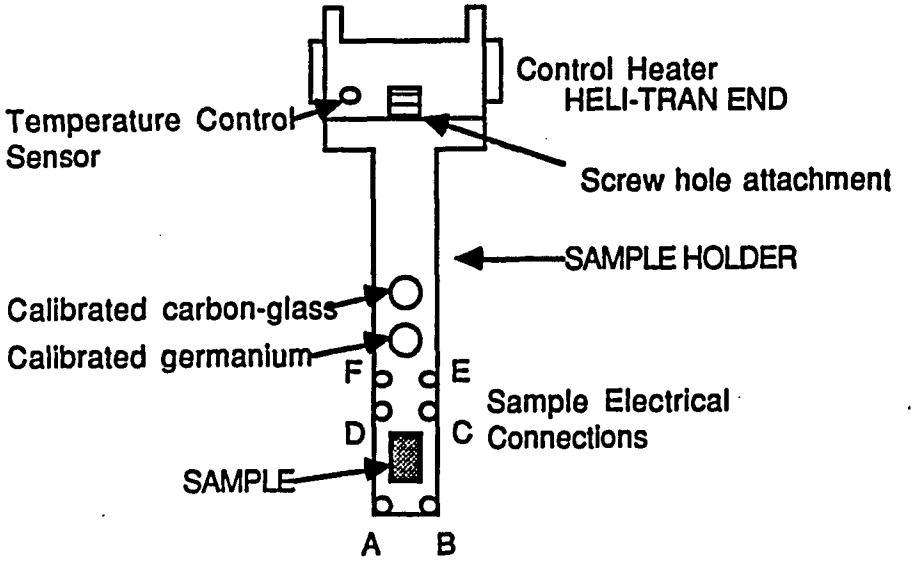

Fig. (I-2)

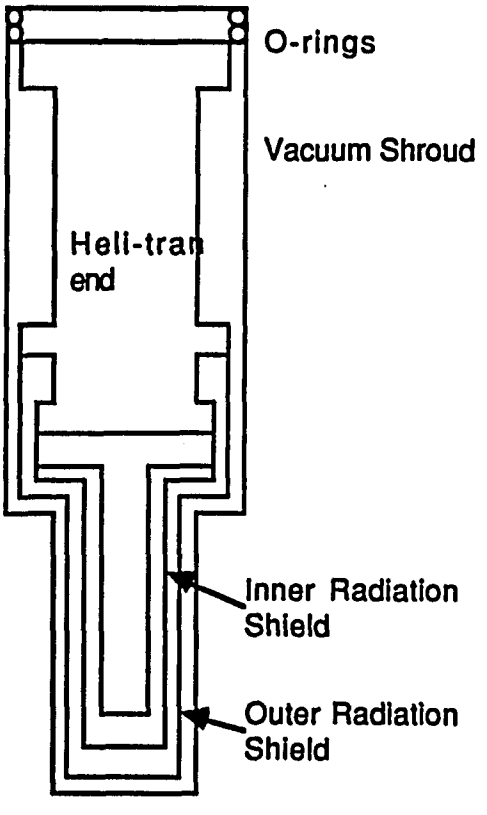

Fig.(I-3)

SAMPLES

Samples of n-CdSe doped with indium were obtained from two different sources, as specified in Appendix I. Six of the samples, of which four are on the insulating side of the transition, were purchased from Cleveland Crystals; the remaining samples were provided by the Institute of Physics, Polish Academy of Sciences in Warsaw. For ease of identification the prefixes I and M denote insulating and metallic, respectively.

Transport measurements above 8 K were carried out for samples I1 to I3, I6, M1 to M3, and M6. Transport measurements below 4.2 K were carried out for samples I4 to I6 and are the subject of Chapter II of this thesis.

Room temperature carrier concentrations and resistivities, as well as the Fermi temperatures of all these samples, calculated on the basis of the free-electron model, are listed in Appendix I.

Experimental Procedure

The samples were cut with their faces perpendicular to the c-axis to a size of approximately 3mm X 4mm X 0.8mm. Using the van der Pauw method, the resistivity and the Hall coefficient were determined both at room temperature, and in the Heli-tran cryostat between 8 K and 100 K.

In addition, data were obtained up to 200 K for sample M2, with a carrier concentration of 5×10^{17} cm^{-3}, and down to 1.25 K for sample I6, with a room temperature carrier concentration of 2.4×10^{17} cm^{-3}. These low temperature data were obtained in a different cryostat, and will be discussed in detail in Chapter II of

this thesis. Hall coefficients were obtained in magnetic fields up to 8 kilogauss. Within a given run, the resistivity and the Hall coefficient were determined to 0.5% and 3%, respectively; for both measurements, the reproducibility from run to run was 3 to 4%.

In measuring resistivity and Hall coefficient care was exercised to reverse current direction in order to eliminate thermal voltages. In order to extract the Hall coefficient we took measurements in opposite magnetic field directions. This enabled us to eliminate magnetoresistive effects in the measured voltages, as explained in detail in Appendix III.

Distortions due to ohmic heating of the sample were eliminated by making sure our currents were low enough that the voltage response was ohmic. Current versus voltage readings were taken at various temperatures for this purpose. Typical currents of 500 μA to 1 mA were used. Low temperature measurements, however, required currents as low as 20 to 50 μA in the case of our most resistive samples.

Fig. (I-4) Circuit for van der Pauw measurements of resistivity and Hall coefficient.

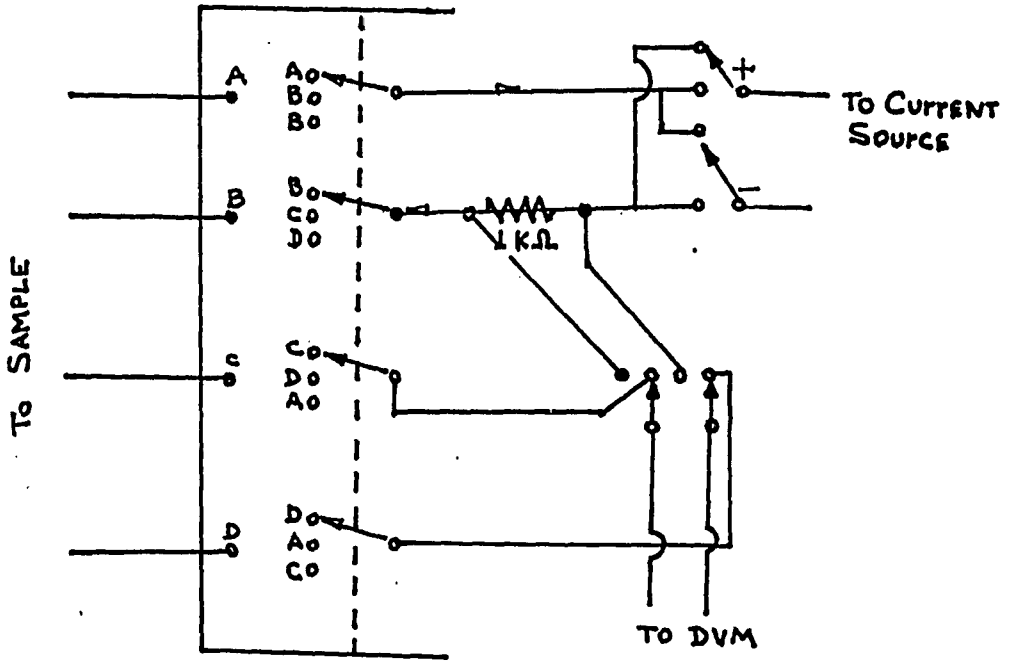

Carrier Concentration and Hall Factor

Carrier concentration n, and Hall coefficient R_H, are related by the expression, $n = r_H/eR_H$, where r_H is the Hall factor, defined as follows: $r_H = \mu_H/\mu_D$. μ_H and μ_D are the Hall and drift mobilities, respectively.

In determining the carrier concentration from room temperature measurements of the Hall coefficient, it is customary to set the Hall factor equal to 1, except in cases such as for silicon, where careful studies using methods other than transport, such as neutron activation,[2] have enabled an independent determination of the carrier concentration as a function of resistivity or Hall coefficient.

Nevertheless, it should be noted that for non-degenerate systems, the Hall factor can differ from unity by more than just a few percent. The studies of Mousty et.al.[2] show that near the metal-insulator transition r_H is as high as 1.3 for the case of silicon.

The Hall factor is given by $\langle\tau^2\rangle/\langle\tau\rangle^2$, where τ is the electron scattering time. Classical analysis indicates that for electron scattering by phonons, $r_H = 1.18$, and for ionized impurity scattering, $r_H = 1.96$, for the case of a Boltzmann distribution.[3] Thus the Hall factor is temperature and also compensation dependent, as the latter can affect the relative importance of one type of scattering over another.

In the study of the compensation of our insulating samples, we briefly consider the effect that changes in the Hall factor would have on our derived results.

I should emphasize, however, that our real interest lies in determining the compensation of samples on the metallic side of the transition. The reason is that compensation seems critically to affect band gap renormalization, which is an important element in our analysis of the luminescence spectra in metallic CdSe. For the case of degenerate materials, i.e. for most of our metallic samples, $\langle\tau^2\rangle/\langle\tau\rangle^2$ is exactly equal to one. In Appendix I we list the calculated Fermi temperatures for our different samples. We see that for most metallic samples this temperature is well above 100 K, making them degenerate at the temperatures where we extract compensations from the experimental values of the mobilities.

RESULTS AND DISCUSSION

A. Critical Concentration

Use of the Mott criterion,[4]

$$n_C^{1/3}\, a_H = 0.26 \pm 0.05, \qquad (1)$$

where a_H is the effective Bohr radius of the impurity center, yields a critical concentration $n_C = (3.1 \pm 1.4) \times 10^{17}$ cm^{-3} for uncompensated CdSe. Hirsch and Holcomb[5] studied the effect of compensation on the critical carrier concentration n_C in Si:P,B. Their results agree qualitatively with previous studies in compensated Ge, and show an increase of n_C with compensation $K = N_A/N_D$, where N_A is the density of acceptor impurities, and N_D the density of donor impurities. They find that the Ge data can be fit roughly by the form $n_C = n_C(K=0) / (1-K)$, whereas their Si data approximately follows the form $n_C = n_C(K=0) / (1- K)^{1/2}$. For typical values of the compensation in our

samples, either of these two forms would give corrections which are well within the error bars of our estimate for $n_c(K=0)$ for CdSe obtained from the Mott criterion.

Data on an extensive series of samples near the metal-insulator transition, presented in chapter II of this thesis, shows behavior consistent with Mott variable range hopping at low temperatures, for concentrations up to 2.4 X 10^{17} cm^{-3}. This suggests that (compensated) n-CdSe is probably insulating up to at least this concentration. On the other hand, zero temperature extrapolations of the conductivity for sample I6 (n_o = 2.4 X 10^{17} cm^{-3}), based on data down to 1.2 K do not tend to zero in the limit of zero temperature. This in itself does not mean that the sample is metallic, but that a more definitive determination of whether it is really insulating requires going down to lower temperatures. On the other hand, sample M1 with 3.7 X 10^{17} cm^{-3} exhibits metallic characteristics. We can, therefore, very tentatively place the critical concentration at (3.0 ± 0.6) X 10^{17} cm^{-3} on the basis of the data we have available at the moment.

B. Resistivity

B1.Insulating Samples

Figure (I-5) shows a semilogarithmic plot of resistivity versus inverse temperature for various CdSe samples on both sides of the metal-insulator transition. From this figure it is apparent that there are two distinct temperature ranges in which transport is characterized by different activation energies. The slopes of the straight lines observed at low values of 1/T (high temperatures)

yield the parameter ε_1, listed for samples I1 and I2 in Table I-1, which we associate with activation to the conduction band because they occur in the high temperature range of our data.

Conventional analysis of the conductivity of insulating doped semiconductors relies on the well-known expression:[6]

$$\sigma = \sigma_1 \exp(-\varepsilon_1/kT) + \sigma_2 \exp(-\varepsilon_2/kT) + \sigma_3 \exp(-\varepsilon_3/kT) . \qquad (2)$$

The first term refers to activation of electrons to the conduction band, the second describes activation to the mobility edge in an impurity D^- band of double occupancy states and the last term, which becomes dominant at low temperatures in compensated materials refers to Miller-Abrahams (fixed-range) hopping. The prefactor σ_2 of the second term is the Mott minimum metallic conductivity

$$\sigma_{min} = 0.026\, e^2 / \hbar d_c, \qquad (3)$$

where d_c is the average separation between impurities at the critical concentration n_c.

Fig. (I-5) Resistivity as a function of inverse temperature of n-type CdSe spanning the metal-insulator transition. The prefixes I and M denote insulating and metallic samples, respectively.

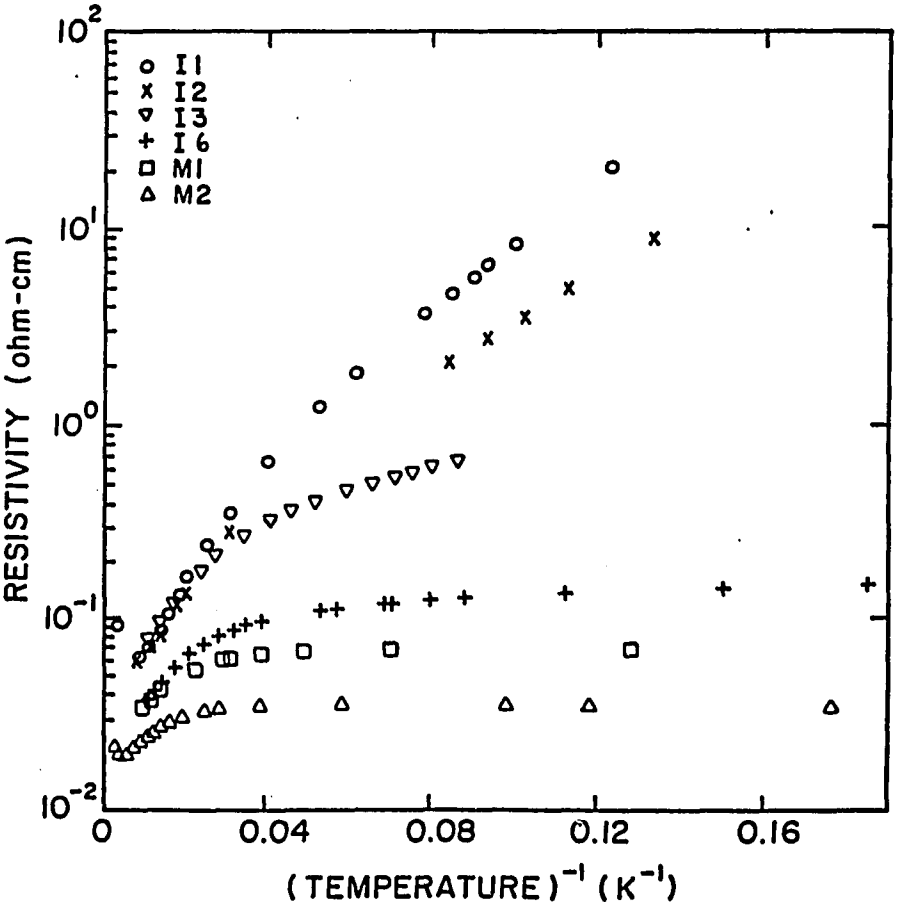

Fits of Eq. (2) to the straight line behavior at high values of 1/T (lower temperatures) give for samples I1 and I2 the prefactors σ_2 and activation energies ε_2 listed in Table I-1.

TABLE I-1. For samples I1 and I2, the parameters listed are ε_1, ε_1^H, ε_2, ε_2^H, and σ_2. Here ε_1, ε_2, and σ_2 are determined by fitting the measured conductivity to $\sigma = \sigma_1 \exp(-\varepsilon_1/k_BT) + \sigma_2 \exp(-\varepsilon_2/k_BT)$. The values ε_1^H and ε_2^H are obtained from the measured Hall coefficient. Energies are determined within 0.2 meV.

Sample	ε_1(meV)	ε_1^H(meV)	ε_2(meV)	ε_2^H(meV)	$\sigma_2(\Omega\text{-m})^{-1}$
I1	8.7	5.4	2.7	2.2	290 ± 10
I2	6.2	4.3	2.3	1.3	380 ± 10

We suggest that the results of this fit are consistent with an identification of the transport in this temperature range with activation to double occupancy states above the mobility edge in an impurity band. This is based on the fact that the experimentally determined prefactor σ_2 of Eq. (2) agrees fairly well with theoretical predictions for the value of Mott's minimum metallic conductivity in CdSe, and that compensation levels are low enough, as we shall show later, that a D^- band still exists which can support doubly occupied electron states. At the critical concentration for CdSe the average distance d_C between impurity centers, Eq. (3) yields a Mott minimum metallic conductivity σ_{min} of about 690 $(\Omega\text{-m})^{-1}$ for uncompensated material. This number must be corrected for the presence of compensation, which reduces the inter-impurity

separation d_C and shifts the critical concentration n_C upwards.[4,7] An estimate of such a correction for typical compensations in our samples yields an approximate value of about 800 $(\Omega\text{-m})^{-1}$. For compensated samples, however, Fritzsche[4] has argued that a correct calculation of the statistics of correlated electrons yields a Fermi energy which is a decreasing function of temperature, with the consequence that the apparent (measured) prefactor can be substantially reduced for sufficiently large compensation. At K = 0.5, for example, this effect reduces σ_{min} by a factor of two, assuming a symmetric distribution for the density of states, and possibly even further when E_F lies in an exponentially decreasing tail of an asymmetric density of states g(E). This means that our theoretical estimate of σ_2 for $K \approx 30\%$ could be reduced from 800 $(\Omega\text{-m})^{-1}$ to perhaps 500 to 600 $(\Omega\text{-m})^{-1}$ which is quite comparable to our measured value of 300 to 400 $(\Omega\text{-m})^{-1}$. In contrast, available data on n-Ge for a wide range of compensations and concentrations yield much smaller values of σ_3/σ_{min} ranging between 10^{-2} and 10^{-3} for hopping processes.[4,5,8]

B2. Metallic Samples

The resistivity of the four remaining samples, which we have classified as metallic, is essentially independent of temperature except for the samples M1 and M2 shown in Fig. (I-5), which are closest to the transition. We note that in addition to giving information regarding the number of available carriers, the resistivity also reflects changes in their mobility. We suggest that the decrease in the resistivity observed for samples M1 and M2 as

the temperature increases above about 50 K reflects predominantly an increase in the mobility associated with reduced scattering from ionized impurities. Further, the qualitative features of the high temperature resistivity of the two samples straddling the transition, namely the insulating I6 sample and the metallic M1 sample, are very similar, and reflect the fact that at temperatures above approximately 50 K, electron transport for both takes place mainly in the conduction band.

C. Hall Coefficient

Turning now to the Hall coefficients of the four insulating samples shown in Fig. (I-6), one notes that they exhibit different activation energies in the same two distinct ranges of temperature as the resistivity. These ranges are separated by a small maximum or inflection point in the Hall coefficient which signals a change from one dominant transport process to another. Except in the vicinity of these crossover regions (or at very low temperatures), the Hall coefficient simply reflects the number of carriers, and not their mobility.[9]

The activation energies ε^{H}_{1} and ε^{H}_{2} deduced from the Hall measurements for insulating samples I1 and I2 are listed in Table I-1. One should note that ε^{H}_{1} is generally smaller than the ε_1 deduced from the resistivity, since the latter reflects changes in mobility with temperature as well as changes in carrier number. The metallic samples, of which we have plotted only M1, exhibit no structure at all, indicating that the number of carriers is constant within the range of temperature and the accuracy of our measurements.

An interesting feature of our data for the insulating samples is that the Hall coefficient and the resistivity exhibit apparently different activation energies in the "ε_2" range, namely, where the dominant mechanism is activation from the Fermi energy located in a D^0 impurity band of single occupancy states to a mobility edge in the D^- band of double occupancy states. Similar results have been observed in other materials. In particular, the activation energy deduced for sample I2 from the Hall coefficient is about half as large as that deduced from the resistivity data. The same factor of approximately 2 was found by Fritzsche[7,10] in his classic work on uncompensated (or low compensation) Ge:Ga over a reasonably extended range of dopant concentrations near the metal-insulator transition.

D. Magnetoresistance

The magnetoresistance at 4.2 K of two insulating CdSe samples I1 and I6, are plotted as a function of magnetic field up to 90 kG in Fig. (I-7). The resistivity decreases for fields up to 50 kG and then increases at higher magnetic fields. Similar results were obtained for n-CdSe by Jaroszynski and Dietl,[11] who ascribed the negative magnetoresistance at low fields to the delocalization associated with dephasing of backscattered waves, and the positive magnetoresistance to the shrinking of the donor wavefunctions and consequent shift in n_c at high magnetic fields.

Fig. (I-6) Hall coefficient as a function of the inverse temperature for n-type CdSe samples I1 to I3, I6 and M1.

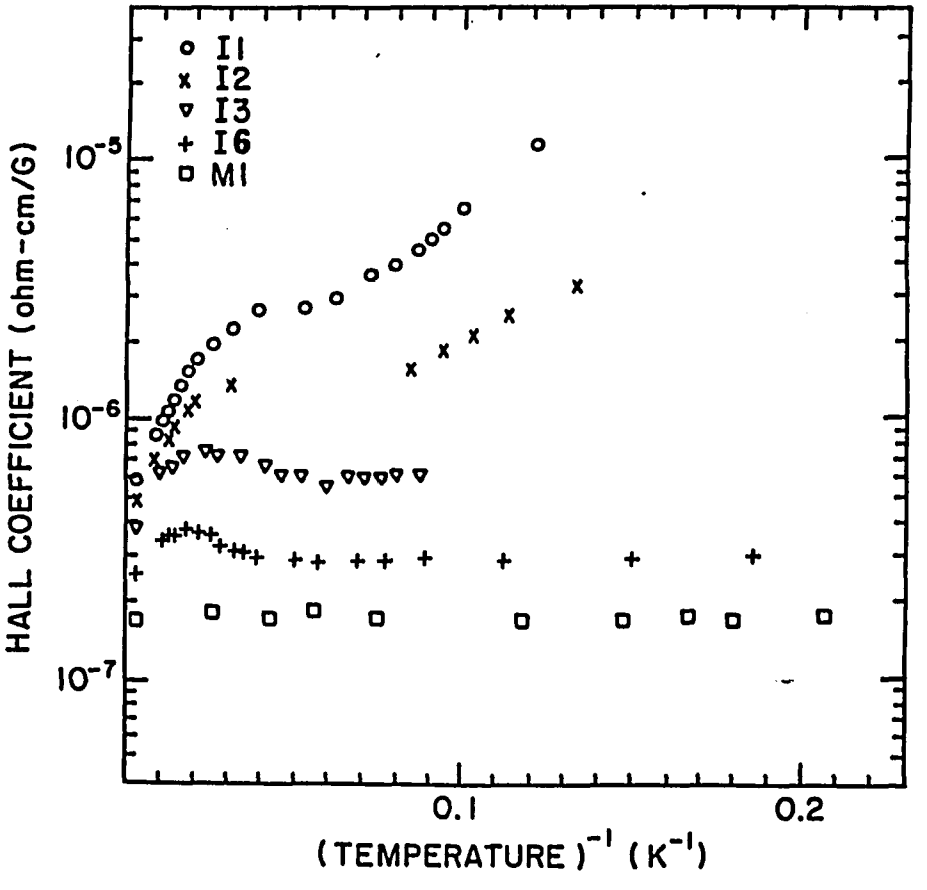

Fig. (I-7) The magnetoresistance at 4.2 K as a function of the magnetic field for two insulating n-type CdSe samples.

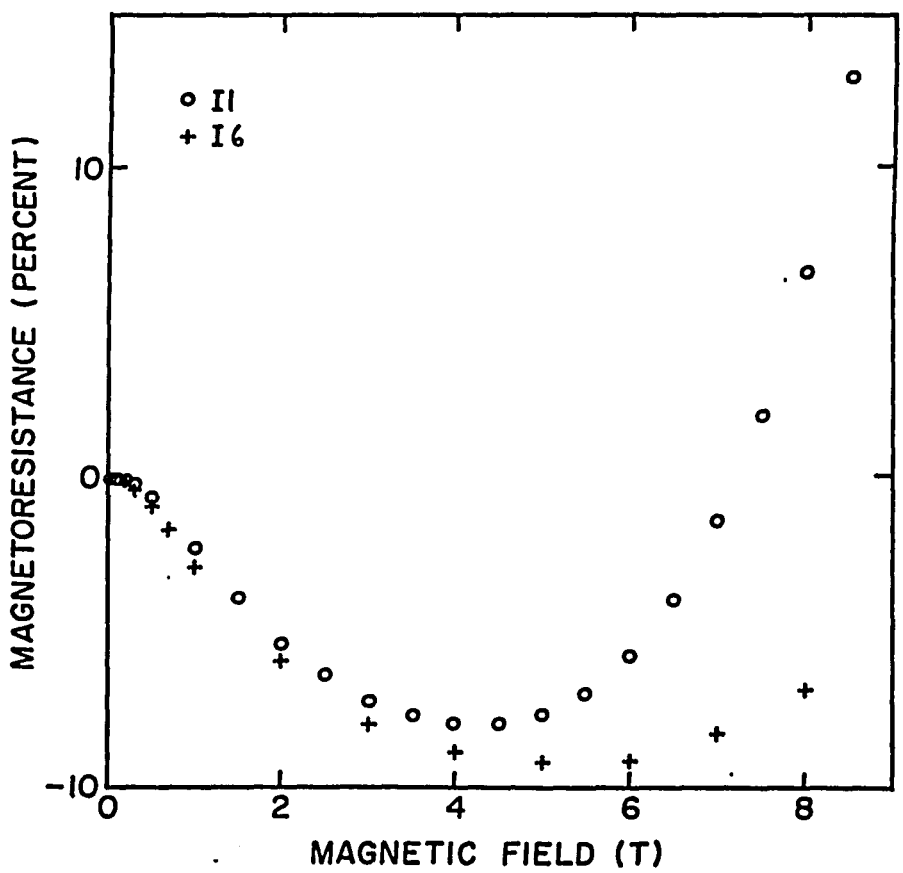

E. Mobility and Compensation

In this section we determine the compensation for samples on both sides of the metal-insulator transition from the value of the Hall mobility in the conduction band. The various scattering mechanisms which determine the mobility will be discussed.

E1. Insulating Samples

Fig. (I-8) shows a plot of the Hall mobility, calculated from the relation $\mu_H = R_H/\rho$, as a function of temperature for samples I1, I2, I6 and M1. For all samples, the mobility increases with increasing temperature between 15 K and 90 K.

We have argued that both the Hall coefficient and the resistivity data indicate that at temperatures above about 50 K, transport occurs mainly in the conduction band for insulating samples I1 to I6. As the temperature is lowered below 50 K, impurity band conduction begins to play an increasingly significant role.

SCATTERING MECHANISMS

In the temperature range between 50 K and 100 K, ionized impurity scattering constitutes the dominant scattering mechanism determining the mobility of conduction electrons, although neutral impurity scattering also plays an important role. Piezoelectric scattering gives a small, but non-negligible contribution, which we take into account in determining compensation.[12,13] Both polar-optical[13] and acoustic phonon[14] scattering are completely negligible below 80 K, although the first of these is comparable to piezoelectric scattering near 100 K.

Fig. (I-8) Mobility versus temperature for three insulating (I1, I2, and I6) samples and one metallic n-type CdSe sample.

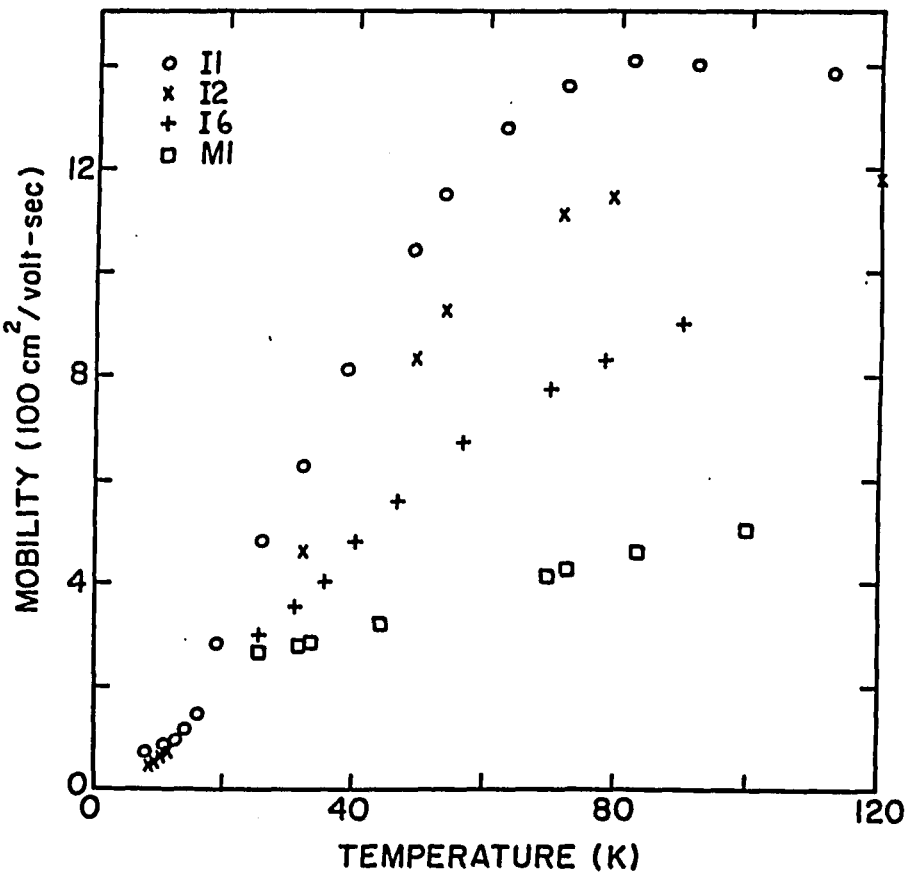

In Fig. (I-9) we plot the polar-optical scattering mobility μ_{po} for CdSe as a function of temperature, as determined by Burmeister and Stevenson.[13] We also plot the piezoelectric scattering mobility μ_{pz}.[12] These latter mobilities and also the acoustic-phonon scattering mobility μ_{ap} are decreasing functions of temperature. The acoustic-phonon scattering mobility is equal 29,000 cm^2/Vs at room temperature, and increases fairly rapidly as T goes down.

The mobility due to ionized impurity scattering, μ_I, is extracted from the Hall mobility, μ_H, by using the relation[15]

$$(1/\mu_I) = (1/\mu_H) - (1/\mu_N) - (1/\mu_{pz}) \tag{4}$$

Where μ_N is the mobility due to neutral impurity scattering and μ_{pz} is the piezoelectric scattering mobility for CdSe. The mobility μ_N due to neutral impurity scattering is determined from Erginsoy's[16] formula:

$$\mu_N = \frac{e^3 m^*}{20\hbar^3 \varepsilon N_N} . \tag{5}$$

Here N_N is the density of neutral impurities, m^* is the conduction band mass[17] in CdSe, and ε is the dielectric constant.

The piezoelectric scattering mobility is given by Hudson,[12]

$$\mu_{pz} = \frac{16(2\pi)^{1/2}}{3} \frac{h^2}{e m^{*3/2} (k_B T)^{1/2}} \left[\sum_{modes} \left[\frac{\langle K^2 \rangle_{av}}{\varepsilon} \right] \right]^{-1} , \tag{6}$$

Fig. (I-9) Theoretical predictions for the polar-optical phonon and piezoelectric scattering mobilities for CdSe. The first is due to Burmeister and Stevenson. The latter is based on the calculation of A. R. Hutson.

Fig.(I-9a) polar-optical scattering mobility

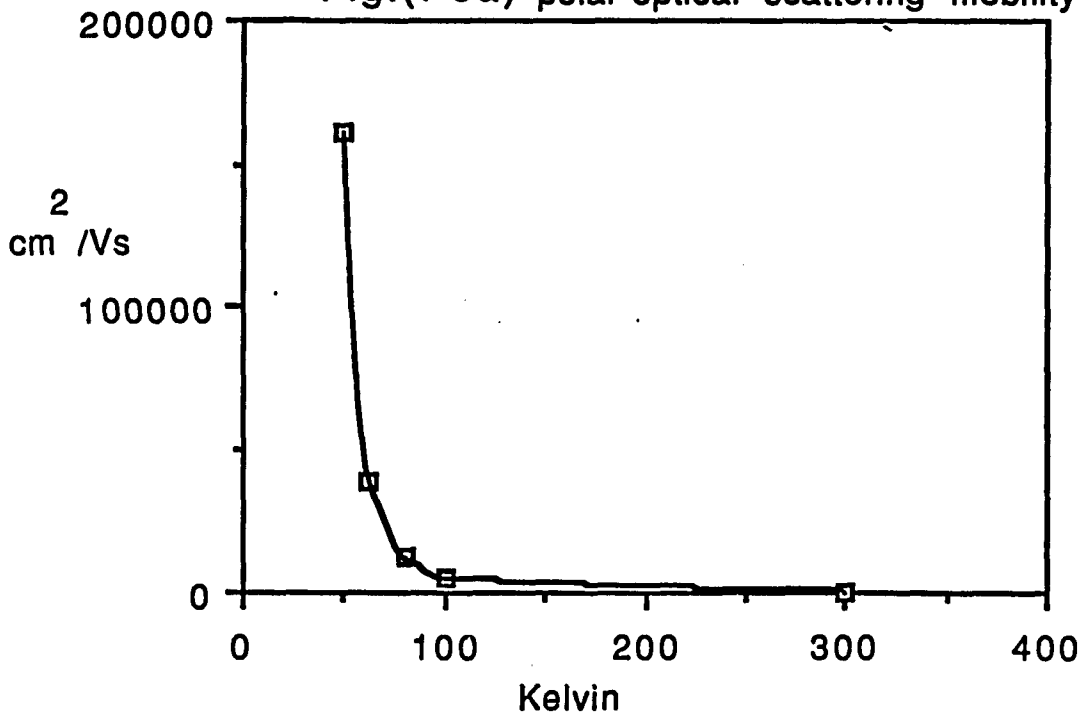

Fig.(I-9b) piezoelectric scattering mobility

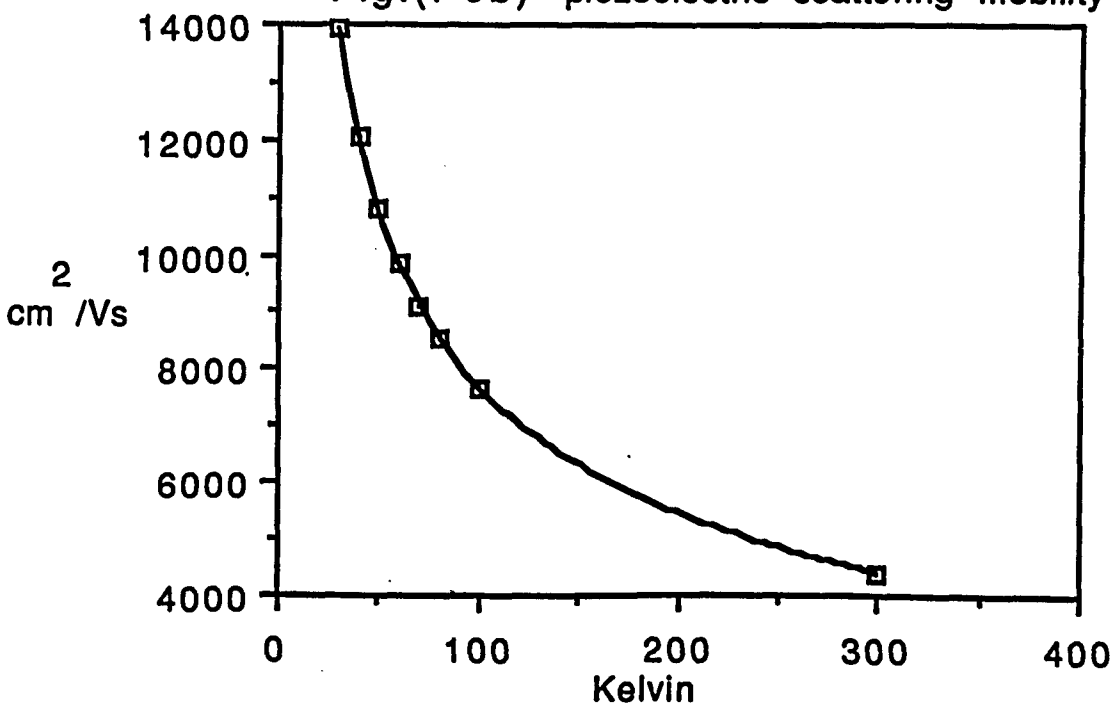

where k_B is Boltzmann's constant, e is the electronic charge, and K is an electromechanical coupling constant. The summation refers to longitudinal and shear modes, and the averaging procedure is described in reference 12.

The assumption in Eq. (4) that the scattering processes which determine the mobility are independent of each other is not strictly valid. Corrections to this formula would give a higher value for μ_I and, consequently, a lower value for the compensation.[18,19] We take the effect of electron-electron scattering into account in our determination of the compensation only for the metallic samples, where it plays a more significant role.

BROOKS-HERRING FORMULA

The compensation for the insulating samples I1 and I2 is obtained from the value of the mobility due to ionized impurity scattering by using the Brooks-Herring formula, suitably modified to take into account correlations between ionized scattering centers:[20]

$$\mu_I = \frac{2^{7/2}\varepsilon^2(k_B T)^{3/2}}{\pi^{3/2} m^{*1/2} e^3 N_I f(x)}, \tag{7}$$

where

$$f(x) = \left[\ln(1+x) - \frac{x}{1+x}\right]$$

and

$$x = \frac{6m^*\varepsilon(k_B T)^2}{\hbar^2 \pi n_s e^2}$$

Here ε is the dielectric constant, m^* is the effective conduction band mass, N_I is the number of impurity scattering centers ($N_I = n + 2N_A$), n is the number of charge carriers at temperature T, n_s is given by

$$n_s = n + (n + N_A)\left[1 - \frac{n + N_A}{N_D}\right] \tag{8}$$

and N_A and N_D are the number of acceptor and donor impurities, respectively. We have verified that we can indeed use the above formula, which is valid only for the non-degenerate limit, by comparing with results obtained from the expression of Mansfield[21] for the case of arbitrary degeneracy.

A fit of our data for samples I1 and I2 to Eq. (7) allows us to obtain an estimate of the number of ionized impurity centers, $N_I = n + 2N_A$, from which we extract the number of acceptors N_A. The donor density can then be determined from the room temperature Hall coefficient which gives the exhaustion-range electron density $n_0 = N_D - N_A$. This analysis yields estimates[22] for the compensation $K = N_A/N_D$ of 0.2 to 0.25 for sample I1, and of about 0.35 for sample I2, assuming a Hall factor of r_H=1. If we make the assumption that the Hall factor at the temperatures in question is close to the classical value of r_H = 1.96 for ionized impurity scattering, however, these values are shifted upwards quite strongly. In the case of sample I1, for example, K is shifted to a value close to 0.5.

Fig. (I-10) Brooks-Herring predictions for the compensation of n-type CdSe sample I1 as a function of temperature. Figure (I-10a) shows the results of the original Brooks-Herring formulation. Figure (I-10b) shows the results of the modified version (Eq. (7)) which takes into account correlations between impurity scattering centers.

Fig. (I-10a) Sample I1 Compensation
No correlations between scatterers

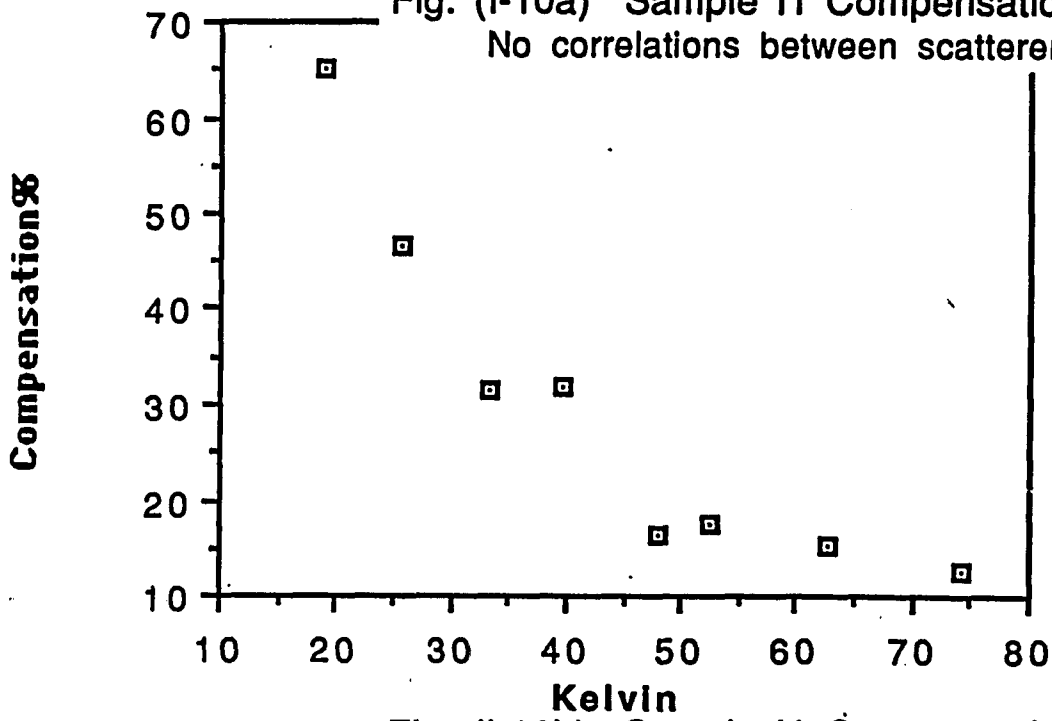

Fig. (I-10b) Sample I1 Compensation
Correlations between scatterers accounted for

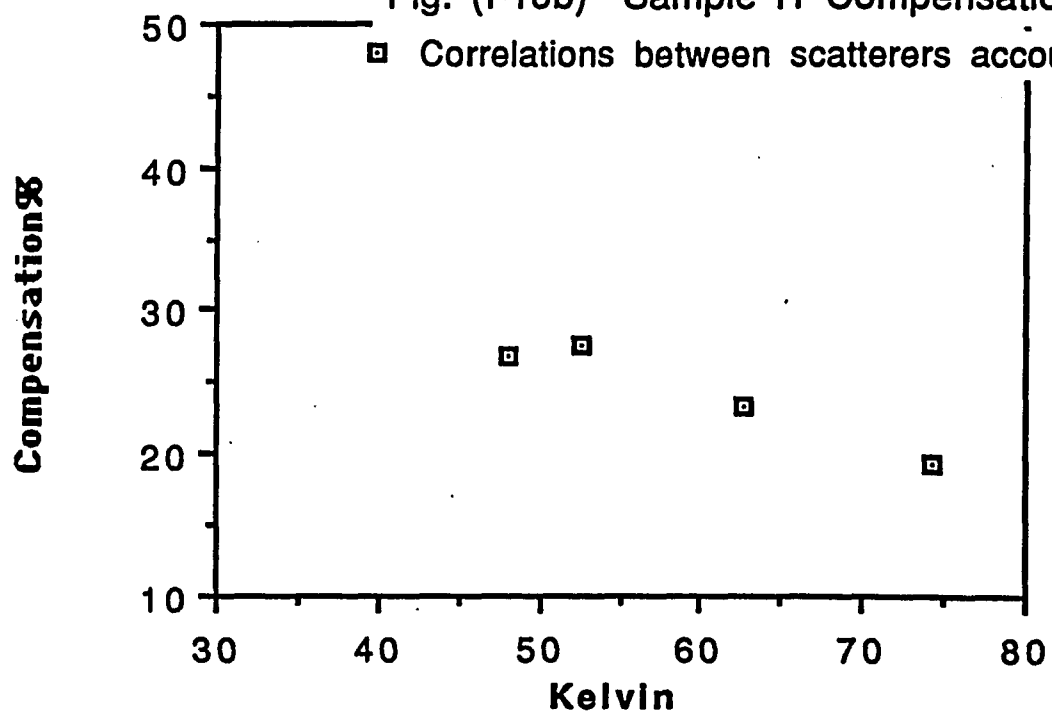

RANGE OF APPLICABILITY OF THE BROOKS-HERRING FORMULA

L. M. Falicov and M. Cuevas[20] have pointed out that the Brooks-Herring formula (Eq. (7)) is valid only if the electric potential resulting from the ionized impurities is small compared with the thermal energy k_BT. One would therefore expect the applicability of the formula to break down at sufficiently low temperatures. In Fig. (I-10) we have plotted the Brooks-Herring predictions for the compensation as a function of temperature for sample I1, for the case of the original Brooks-Herring formulation (a), and for the modified version (Eq. (7)) which takes into account correlations between impurity scattering centers (b). We note that both tend to a constant value as the temperature increases above 50 K. We take this constant value to be the true compensation. We have separately verified that in the range from about 45 K to 80 K the ionized impurity scattering mobility as extracted above is indeed consistent with a $T^{3/2}$ temperature dependence, as should be the case for the Brooks-Herring formula.

Comparisons with the predictions of the Brooks-Herring formula, and also of the modified theory of Falicov and Cuevas[18] for low temperatures[23,24] with our experimental results for μ_I below 60 K indicate that as we lower the temperature the contribution of ionized impurity scattering to the mobility drops faster than predicted by the theoretical expressions. We believe that this is probably due to the increasing importance of impurity band conduction. Below 15 K, where transport takes place mostly in the D- impurity band, the value of the mobility begins to saturate, as shown in Fig. (I-8), whereas the expression of Falicov and Cuevas

predicts that μ_I goes to zero as T -> 0. Use of the Brooks-Herring formula at too low a temperature can, therefore, lead to erroneous determinations of the compensation ratio K.

E2. Metallic Samples

The compensation for metallic samples M3 and M6 is determined from the mobility in much the same way as in the case of I1 and I2. However, we neglect neutral impurity scattering. This is justified to some extent by the fact that the Hall coefficient shows no freeze out of charge carriers.

The expression for μ_I is given in the degenerate limit by:

$$\mu_I = \frac{3h^3\varepsilon^2 n_0}{16\pi^2 e^3 N_I m^{*2} f(x)}, \qquad (9)$$

where all terms are defined above, but where x is now equal to $h^2\varepsilon(3n_0)^{1/3}/[2e^2m^*(8\pi)^{1/3}]$, and where we have lifted the condition that $n=N_I$ of reference 21.

Comparison with the results given by the full expression for arbitrary degeneracy confirms that these samples are indeed in the degenerate limit.

Equation (9) is obtained by treating the electronic screening of the ionized impurities in the Thomas-Fermi approximation, and assuming no electron-electron scattering, nor any correlations between the impurity centers.

Various treatments of electron screening which improve upon the above result are discussed by Lax and Narayanamurti.[25] All these schemes include the effects of electron exchange and

correlations, but not of correlations between ionized impurity centers. These calculations are:

(1) The Green's function technique of Toigo and Woodruff[26] with a Hartree-Fock type of decoupling of the expression for the dielectric response function[27]

$$1 - [1/\varepsilon(\mathbf{k},\omega)] = [4\pi e^2/k^2] \ll\rho_{\mathbf{k}}(t);\rho_{\mathbf{k}}^{+}(0)\gg^{ret}_{E=\omega},$$

where the symbol $\ll\ldots\gg^{ret}_{E=\omega}$ stands for the Fourier transform with respect to time of the retarded Green's function,

$$G_r = i\theta(t)\langle[\rho_{\mathbf{k}}(t),\rho_{\mathbf{k}}^{+}(0)]\rangle,$$
$$\rho_{\bar{k}}(t) = \sum_{\bar{q},\sigma} a^{+}_{\bar{q},\sigma}(t)a_{\bar{k}+\bar{q},\sigma}(t),$$

with a^{+} and a Fermi creation and annihilation operators in the Heisenberg representation.

The Green's function G_r satisfies an equation of motion which couples it to higher order Green's functions in the usual fashion of many-body theory. The decoupling mentioned above refers to a simplifying assumption about the higher order Green's functions, whereby these are expressed in terms of lower order Green's functions in order to make the problem tractable.

(2) The Wigner distribution function method of Brosens, Lemmens, and DeVreese[28,29,30] with a dynamic Hartree-Fock decoupling leading to a frequency dependent local field correction $G(q,\omega)$.

(3) An equation of motion technique of Singwi and co-workers[31,32,33] with a decoupling based on a density-dependent

equilibrium pair-correlation function combined with a self-consistent calculation of the pair-correlation function g(r) and $G(q) = G(q,\omega=0)$.

(4) A perturbation (in the electron-electron coupling) analysis of exchange and correlation corrections by Holas, Aravind, and Singwi[34] which leads to a dynamical "local field" $G(q,\omega)$ that can be compared with Geldart and Taylor[35] and with Brosens, DeVreese, and Lemmens.[29]

The corrections introduced by all these treatments can be subsumed in the f-function of the above expression for μ_I (Eq. (9)), so that the new expression for the ionized impurity scattering mobility becomes

$$\mu_I = \frac{3h^3\varepsilon^2 n_0}{32\pi^2 e^3 N_I m^{*2} f_{-1}(x)}, \qquad (10)$$

where $f_{-1}(x)$ is a function different from the previous f(x), and depends on the particular treatment of screening. For clarity, plots taken from reference 25 for $f_{-1}(x)$ are here reproduced in Fig. (I-11).

Table I-2 shows the values of the compensation for samples M3 and M6. We see that in all cases K is reduced from a Thomas-Fermi value of about 0.45 for both samples, to a value of 0.33 and 0.20, depending on the particular treatment. The calculation of Brosens *et al.* can give markedly different results from Toigo-Woodruff and Vashishta-Singwi, especially for small x.[36]

A reduction in the value predicted for the compensation is what one would expect as a result of the inclusion of electron

exchange and correlation effects. Coulomb repulsion and the Pauli exclusion principle will tend to keep the electrons further apart than in the absence of these effects, thus reducing the effectiveness of the screening of the impurity charges. This translates into a smaller value for the density of impurity scattering centers as derived from the theoretical expression for the mobility, since not as many scatterers are needed now to limit the electron mobility to a given experimental value. The result is a smaller value for the compensation prediction.

TABLE I-2. Values of the compensation K for samples M3 and M6 deduced from different treatments of the electron screening, as discussed in detail in the text.

Sample	Thomas-Fermi	Vashishta-Singwi	Toigo-Woodruff	Brosens *et al.*
M3	0.45	0.32	0.29	0.22
M6	0.45	0.32	0.30	0.24

Fig. (I-11) Plot of function f_{-1} from Ref. 25. Labels indicate the particular screening treatment employed in the calculation.

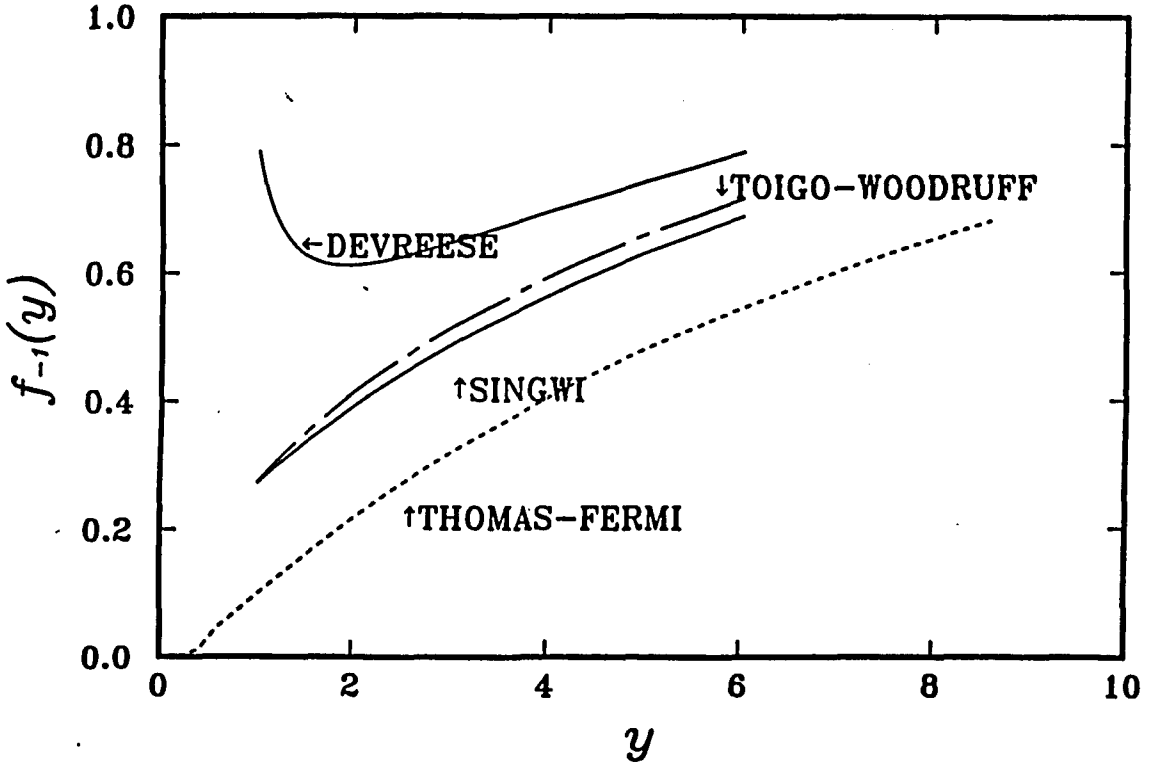

E3. Discussion of Uncertainties

Various authors have discussed the uncertainties[18,20,21,37] involved in theoretical formulations for the ionized scattering mobility in the non-degenerate case. Based on these works, we estimate the uncertainty in the compensation for insulating samples I1, and I2 to be very approximately 20 to 30%.

Uncertainties in theoretical determinations of μ_I in the degenerate case have not been heretofore discussed in detail. There are four main sources of possible error:

1) Errors incurred in extracting from the total measured mobility the mobility due only to ionized impurities; the largest contribution which we have neglected is due to piezoelectric scattering, which we estimate to be at most 5% of the total at the temperatures in question.

2) Use of the Born approximation to calculate the scattering rate, where the criteria for its validity are only marginally satisfied on the metallic side. According L. Schiff's *Quantum Mechanics* [38] the Born approximation is only applicable when the following two criteria are satisfied,

$$ka >> 1, \text{ and}$$

$$(2\pi e^2/hve) \ln ka << 1,$$

where k is the wave vector of the scattering electron, a is the scattering potential screening length, which is given by Mansfield[21] as

$$a = (\varepsilon h/4\pi e)[m^*(3n_0/\pi)]^{-1/2},$$

v is the velocity of the electron, ε is the dielectric constant in CdSe, h is Planck's constant, n_0 is the electron density and m^* is the

conduction band mass. Although the criteria for the validity of the Born approximation are not met very well, as shown in the table below, the departure from these criteria is not too severe.

Sample	$(2\pi e^2/hv\epsilon)$ ln ka	ka
M3	0.86	3.13
M6	0.81	3.30

Using as a guide estimates of uncertainties obtained in detailed studies of the non-degenerate case,[37] we suggest that this could lead to errors on the order of 10, or at most 15, percent.

3) Different treatments of the electronic screening of the impurity charges, which yield values of compensation which differ by as much as 30% for samples M3 and M6. Our overall estimate of the uncertainty in the compensation values due to the three preceeding sources is therefore very roughly 50%. It should be noted, however, that unlike the experimental error which is random and on the order of 5%, the uncertainty associated with the theoretical treatment is systematic in all instances. Thus, relative values of the compensation have been determined more reliably than their absolute values.

4) Neglecting the effect of multi-ion screening by the electron gas. This effect is discussed in detail by Meyer and Bartoli[39] for the case of uncompensated degenerate semiconductors. The treatment of Meyer and Bartoli is based on the realization that electrons are never able to screen a given ion in a multi-ion system as well as they can screen the same ion in a single-ion system. The

correctness of this claim is discussed by the authors. The basic idea is that any given electron charge is now shared by several impurity centers.

As in the case of electron correlation and exchange effects, the inclusion of multi-ion screening effects into the theory results in a reduction in the theoretically predicted effectiveness in the screening of the impurity scatterers. This results in smaller theoretical values for the ionized impurity scattering mobility and the compensation.

Meyer and Bartoli carry out phase-shift calculations for the electron mobility in uncompensated silicon and germanium including the effects of multi-ion screening and obtain often substantial corrections (as much as factor of 4) to the predictions of single-ion treatments. Their predictions appear to agree better with experiment.

Although it is hard to estimate at this point the error introduced by neglecting multi-ion screening in degenerate compensated semiconductors, it seems fairly safe to assume that this omission leads to a significant overestimation of the magnitude of the compensation. Our determinations of the compensation from transport data should therefore be taken more as an indication of the relative compensations of the samples than a measure of their actual compensations.

F. Comparison with Other Data for CdSe

Measurements of the resistivity and of the Hall coefficient as well as the magnetoresistance have been obtained by Finlayson et

al.[14] for Cr-doped CdSe with electron concentrations comparable to ours. We note that the features of their Hall coefficient data differ from ours for carrier concentrations comparable to samples I1 and I2 of the present studies. Whereas in our data the ε_1 and ε_2 regions are separated by an inflection point and there is a non-negligible slope in the ε_2 region, their data exhibit a clear maximum separating both regions and fairly flat behavior in the range of impurity band conduction. Finlayson et al.[14] claim that their Hall coefficient data at these temperatures can be ascribed to conduction above the mobility edge in a single occupancy impurity band. The claim that only a single occupancy lower D^o band exists is based on their conclusion that D^- levels are virtually non-existent due to the very heavy compensation of their samples, which they estimate, using the Brooks-Herring formula, at about 80%. We note, however, that we have applied this formula to their published values of the mobility at temperatures of 40 K and 50 K, for their sample with $n_o = 1.2 \times 10^{17}$ cm^{-3}, and we deduce compensations of 50% or less, which is considerably lower than the values they claim,[40] and which would imply that one may not be able to rule out the presence of a D^- band. Even if we assume a Hall factor r_H of 2, which is the value of r_H in the classical treatment of ionized impurity scattering,[3] we deduce a compensation no higher than 65%. This suggests to us that the observed differences in the Hall coefficient are more likely to originate with the different nature of the impurities ("magnetic" Cr compared to In) and/or the rather high densities of Cr added to the samples during the growth of their crystals, rather than the absence of a D^- band. Nevertheless we cannot rule out the latter possibility.

Summary and Conclusions

We have presented experimental data for the resistivity and Hall coefficient between about 8 and 80 K, and the magnetoresistance to 9 T, of a series of CdSe samples with donor concentrations spanning the metal-insulator transition. The general features of the data, and measurements on selected samples to lower temperature (1.2 K) yield a critical carrier concentration for (compensated) CdSe of (3.0 ± 0.6) X 10^{17} cm^{-3}, an energy ε_1 which we associate with carriers activated into the conduction band and an energy ε_2 which, we argue, is attributable to impurity band conduction at intermediate temperatures.

Using the Brooks-Herring formula for insulating material, and an appropriate expression for the ionized impurity scattering mobility in metallic samples, we have used the measured Hall mobility to estimate the (relative) level of compensation of our In doped CdSe material for metallic as well as insulating material. To our knowledge, this is the first application of recent theory to attempt to estimate compensation for metallic samples using transport data.

REFERENCES

[1] L. J. van der Pauw, Philips. Res. Repts. **13**, 1 (1958).

[2] F.Mousty, P.Ostoja, and L.Passari, J. Appl. Phys. **45**, 4576 (1974).

[3] V.I.Fistul', *Heavily Doped Semiconductors* (Plenum, New York, 1969).

[4] H. Fritzsche, Phil. Mag. B **42**, 835 (1980).

[5] M. J. Hirsch and D. F. Holcomb, in *Disordered Semiconductors,* edited by M. A. Kastner, G. A. Thomas and S. R. Ovshinsky (Plenum Press, New York, 1987) 45; Proceedings of the Eighteenth International Conference of the Physics of Semiconductors, Stockholm, August 11-15, 1986.

[6] N. F. Mott and E. A. Davis, in *Electronic Processes in Non-Crystalline Materials,* 2nd Edition (Clarendon Press, Oxford, 1979) 239.

[7] H. Fritzsche, Phys. Rev. **99**, 406 (1955).

[8] E. A. Davis and W. D. Compton, Phys. Rev. A **140**, 2183 (1965).

[9] This is not strictly correct if the Hall factor changes in going from, say, transport dominated by phonon scattering to transport dominated by ionized impurity scattering, in which case the Hall coefficient would also reflect these changes.

[10] H. Fritzsche, J. Phys. Chem. Solids **6**, 69 (1958).

[11] J. Jaroszynski and T. Dietl, Acta Physica Polonica, A **69**, 1017 (1986).

[12] A. R. Hutson, J. Appl. Phys. **32**, 2287 (1961).

[13] R. A. Burmeister and D. A. Stevenson, Phys. Status Solidi **24**, 683 (1967).

[14] D. M. Finlayson, J. Irvine and L. S. Peterkin, Phil. Mag. B **39**, 253 (1979).

[15] This is valid only under the assumption that the drift and Hall mobilities are equal. If the Hall factor is not equal to 1, one should properly use the drift mobility instead. Below we examine some implications of this for sample I1.

[16] C. Erginsoy, Phys. Rev. **79**, 1013 (1950).

[17] The value of the conduction band mass in CdSe is 0.13 m_e, where m_e is the free electron mass.

[18] M. Cuevas, Phys. Rev. 164, 1021 (1967).

[19] V. A. Johnson and K. Lark-Horovitz, Phys. Rev. 82, 977 (1951).

[20] L. Falicov and M. Cuevas, Phys. Rev.164, 1025 (1967).

[21] R. Mansfield, Proc. Roy. Soc. London B 69, 76 (1956). Mansfield's general expression for the conductivity is

$$\sigma_I = 32\varepsilon^2 m^*(k_BT)^3 f_2(\eta^*)/[N_I e^2 h^3 f(x)],$$

with

$$x = \langle\eta\rangle\,(k_BT)^{1/2}\varepsilon h/[e^2(2m^*)^{1/2} f'_{1/2}(\eta^*)],$$

where all parameters are as defined in the text. Here

$$f_k(\eta^*) = \int_0^\infty \frac{x^k dx}{\exp(x-\eta^*)+1}$$ (Fermi-Dirac functions)

with

$$f_k' = d\,f_k(\eta)/d\eta\ .$$

η^* is the reduced chemical potential $\eta^* = \mu/k_BT$, and $\langle\eta\rangle$ satisfies

$$(\langle\eta\rangle - 3)\exp(\langle\eta\rangle - \eta^*) = \langle\eta\rangle + 3.$$

It should be noted that Mansfield's expression does not take into account correlations between ionized scattering centers.

[22] Values for n_s and N_I (and thus, for $K=N_A/N_D$) were obtained from Eqs. (7) and (8) by starting with $n_s = n$ and itiratively adjusting N_I and n_s to be self-consistent.

[23] The results obtained from the Falicov and Cuevas expression (Eq. 2.17 of ref. 16) for m_I can only be considered as very approximate in our case since our samples do not meet their criterion that the density of ionized majority impurities approaches the same value as N_A. Nevertheless, we find that the compensation predicted by their formula is very close to the values given by the Brooks-Herring formula.

[24] Falicov and Cuevas (ref. 20) point out that the Brooks-Herring formula does not apply at very low temperatures for compensated materials because of the approximations introduced in the derivation of this formula.

[25] M. Lax and V. Narayanamurti, Phys. Rev. B 24, 4692 (1981).

[26] F. Toigo and T.O. Woodruff, Phys. Rev. B 2, 3958 (1970); 4, 371, 4312 (1971).

[27] D. N. Zubarev, Usp. Fiz. Nauk 71, 71 (1960) [Soviet Phys. Usp. 3, 320 (1960)].

[28] F. Brosens, L.F. Lemmens, and J. T. DeVreese, Phys. Status Solidi 74, 45 (1976).

[29] F. Brosens, J. T. DeVreese, and L. F. Lemmens, Phys. Rev. B **21**, 1363 (1980).

[30] J. T. Devreese, F. Brosens, and L. F. Lemmens, Phys. Rev. B **21**, 1349 (1980).

[31] K. S. Singwi, M. P. Tosi, R. H. Land, and A. Sjolander, Phys. Rev. **176**, 589 (1968).

[32] K. S. Singwi, A. Sjolander, M. P. Tosi, and R. H. Land, Phys. Rev. B **1**, 1044 (1970).

[33] P. Vashishta and K. S. Singwi, Phys. Rev. B **6**, 875 (1972).

[34] A. Holas, P. K. Aravind, and K.S. Singwi, Phys. Rev. B **20**, 4912 (1979).

[35] D. J. W. Geldart and R. Taylor, Can. J. Phys. **48**, 155 (1970).

[36] Our calculation assumes that both donor and acceptor scattering centers are singly ionized. Since they have twice the charge, double acceptors, such as Cd vacancies (or double donors) affect the scattering rate for conduction electrons differently, and would necessitate a modified treatment of the calculation of the number of acceptors (or donors) and thus of the compensation.

[37] J. R. Meyer and F. J. Bartoli, Phys. Rev. B **24**, 2089 (1981).

[38] Leonard I. Schiff, *Quantum Mechanics*, Third Edition, McGraw-Hill Book Company, 326.

[39] J. R. Meyer and F. J. Bartoli, Phys. Rev. B **36**, 5989 (1987).

[40] As pointed out earlier, use of the Brooks-Herring formula at too low temperatures can lead to erroneous determinations of the compensation ratio K.

CHAPTER II

TRANSPORT MEASUREMENTS OF n-DOPED CdSe BELOW 4.2 K.

INTRODUCTION

In this chapter we report on measurements of the resistivity and Hall coefficient in n-doped insulating CdSe near the metal-insulator transition, in the range from 1.2 K to 4.2 K. The resistivity in this range exhibits a temperature dependence consistent with Mott variable range hopping. More interesting, however, is the fact that we are able to detect a measurable Hall coefficient which also exhibits a temperature dependence of the form $R_H \sim \exp [T_{oH}/T]^{1/4}$, where T_{oH} is a constant which depends on magnetic field but not on temperature.

Variable range hopping occurs via quantum-mechanical phonon assisted hopping between localized sites and not via extented state conduction. Since the charge carriers cannot be assigned a classical velocity during hops from site to site, it is not immediately obvious that there should be a Hall effect in the temperature range where hopping transport is dominant. Theoretical work on the subject has shown that a non-vanishing Hall coefficient is nevertheless possible as a result of quantum interference.[1,2]

Before the work of Holstein[1] in 1961, theoretical treatments of the Hall effect in the hopping regime considered quantum mechanical transitions which involved only the initial site and the destination site for the localized electron and did not provide a mechanism for the presence of a Hall effect. By considering hopping paths between two sites which include multi-hop processes,

Holstein showed that the jump rate can depend on magnetic field. This field dependence comes about as a result of the interference between direct and indirect paths and is the source of a non-zero Hall voltage.

In line with a suggestion made by Friedman and Pollak[3], subsequent work by Gruenewald *et al.*[4] and Nemeth and Muhlschlegel[5] has predicted a temperature dependence for the Hall coefficient of the form $R_H \sim \exp[T_{oH}/T]^{1/4}$, in the variable range hopping regime. Up until very recently,[6,7] however, measurements of the Hall coefficient at low temperatures for heavily-doped semiconductors on the insulating side of the transition have either not been able to detect any Hall voltage or have only exhibited a temperature dependence consistent with conduction due to electrons activated above the impurity band mobility edge.[8,9,10,11,12]

Amitay and Pollak[8] and R. Klein[9] carried out ac Hall effect measurements in p-type germanium and n-type silicon, with room temperature charge carrier concentrations two orders of magnitude below the critical concentration for the metal-insulator transition. The purpose of such low carrier concentrations was to eliminate as much as possible the contribution to the Hall conductivity coming from activated carriers. Low temperature measurements failed to detect a Hall effect due to hopping conduction in the impurity band, setting an experimental upper bound for the hopping Hall conductivity a factor of six below the value predicted by Holstein's theory.

More recently, D. W. Koon and T. G. Castner,[6] claimed to have found evidence for a variable range hopping form of the Hall

coefficient temperature dependence in arsenic-doped silicon samples, with carrier concentrations in the range between 0.9 and 0.98 of the critical concentration. The measurements reported here, done at considerably lower fields than those used in ref. 6, are consistent with a $T^{-1/4}$ temperature dependence for the Hall coefficient in the variable range hopping regime, for samples with carrier concentrations close to the metal-insulator transition. The results differ in detail, however, from those of Koon and Castner, as discussed below. The proximity to the critical concentration means that there is quite significant wavefunction overlap between charge carriers. This would imply a much higher jump rate between localized sites according to Holstein's formulation for the Hall effect, since his expression for the tranfer integral depends on wavefunction overlap, which is a strong function of concentration. Correlation effects will possibly play a significant role in this case, requiring perhaps important modifications in Holstein's original formulation.

APPARATUS

Transport data below 4.2 K were taken in a cryostat designed by Dr. Apurba Roy and built at the CCNY Science machine shop. A schematic of the cryostat is shown below.

The sample chamber is under vacuum. Refrigeration is provided through thermal contact with a He4 pot; the He4 liquid in this pot can be pumped down to approximately 1.2 K.

The sample holder is a two stage holder made of annealed copper and screwed on to a copper extension connected to the He4

pot. Apiezon N grease was used to ensure good thermal contact to the pot. The sample was heat sunk with Apiezon N grease to one of the holder stages using a layer of cigarette paper glued to the copper with GE 7031 varnish. A calibrated carbon-glass thermometer was mounted in a hole drilled into one of the sample holder stages and heat sunk by a) applying Apiezon N grease to the body of the thermometer, and b) heat sinking the thermometer leads to the copper sample holder body over a length of 4 inches using cigarette paper and GE 7031 varnish. All temperature measurements were taken at zero magnetic field.

Temperature control was done with a Lakeshore pressure regulator. This allowed a temperature stability of about 2 mK. The magnetic field for Hall coefficient and magnetoresistance measurements was provided by a superconducting 9 tesla magnet.

Samples and Measurements

The samples used for transport measurements below 4.2 K are listed in Appendix I. They are labelled I4, I5 and I6 and their concentrations relative to the critical concentration n_c range from 0.73 to 0.80.

CdSe is self-compensating and is also very likely to contain various p-type as well as small amounts of other n-type impurities. Based on measurements of the temperature dependence of the Hall mobility above 7K, using the same set up described in Chapter I of

Fig. (II-1) Schematic of cryostat for transport measurements below 4.2 K

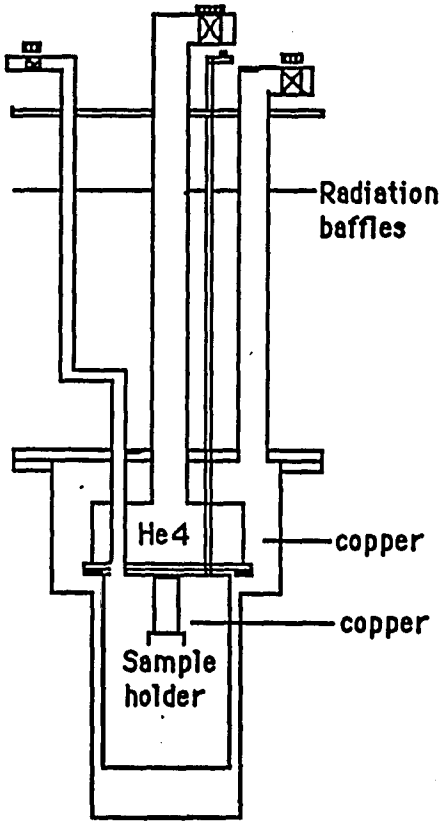

this thesis, and using rough theoretical estimates for the various scattering mechanisms as described in that chapter, we have estimated the compensation in these samples to be approximately 40 to 50%.

The resistivity and the Hall coefficient were measured using the van der Pauw[13] geometry and standard DC techniques. Data were obtained between 1.25 and 4.2 K in magnetic fields from 0.2 to 1T. In addition, the magneto-resistivities of samples I1 and I6 were measured to 8T.

Hall coefficient measurements were taken in opposite magnetic field directions, in order to eliminate magnetoresistive effects in the measured voltages, as explained in Appendix III. Currents were reversed in all measurements to eliminate thermal voltages. Heating effects were checked by studying the voltage versus current characteristics for all samples, at various temperatures. Currents were then limited to the linear portions of the I vs. V curves. Typical currents ranged from 100μA to 500μA.

Resistivity and Magnetoresistance

Except possibly for sample I6 which is closest to the transition, a good fit is obtained to the Mott variable range hopping form

$$\rho = \rho_o \exp (T_o/T)^{1/4} \qquad (1)$$

as demonstrated in Fig. (II-2a), where the logarithms of the resistivities of samples I4, I5 and I6 are plotted as a function of $T^{-1/4}$. Figures (II-2)(b) and (c) show that neither a T^{-1} plot, corresponding to activated conduction, nor a $T^{-1/2}$ plot, expected for a Coulomb gap associated with electron-electron correlations, offer as good a fit. It should be mentioned, however, that the measured resistivity of sample I6 which is closest to the metal insulator transition is consistent also with an exponent smaller than 1/4 (but greater than zero). The weaker temperature dependence may beassociated with some measure of delocalization in these samples in the range of temperature of these experiments.

The slopes of the curves of Fig. (II-2a) decrease as the metal-insulator transition is approached and represent the parameter T_o of Eq. (1) given by the expression

$$T_o = \beta/(k_B\, N\,(E_F)\, \xi^3) \qquad (2)$$

Here, ξ is the localization length, $N(E_F)$ is the density of (localized) states at the Fermi energy, k_B is Boltzmann's constant, and the constant β is approximately equal to 18. The parameters T_o deduced from our data are listed in Table II-1 for samples I4, I5 and I6. It should be noted that although earlier measurements of the resistivity of sample I6 to higher temperatures indicate that the variable range hopping behavior extends to even higher temperatures of about 10K, the low value of T_o deduced for this sample implies that some delocalization is expected in the range of temperature of these experiments, so that parameters deduced for

Fig. (II-2a) Semilogarithmic plot of the resistivities of samples I4, I5 and I6 versus $T^{-1/4}$, showing a good fit to the Mott variable range form given by Eq. (1). The resistivity is in Ω-cm.

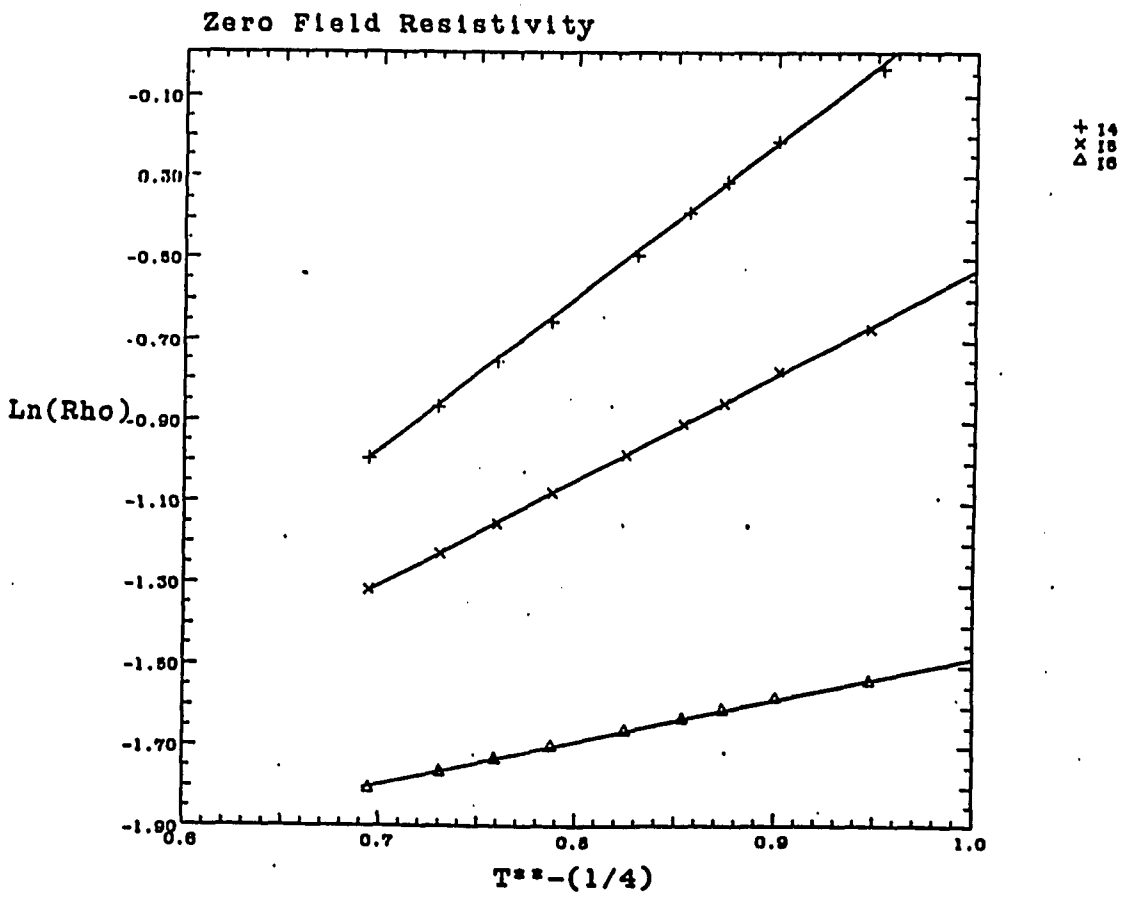

Fig. (II-2b) Semilogarithmic plot of the resistivity of sample I5 versus T^{-1}, showing that the activated conduction form does not provide a good fit to our data. The resistivity is in Ω-cm.

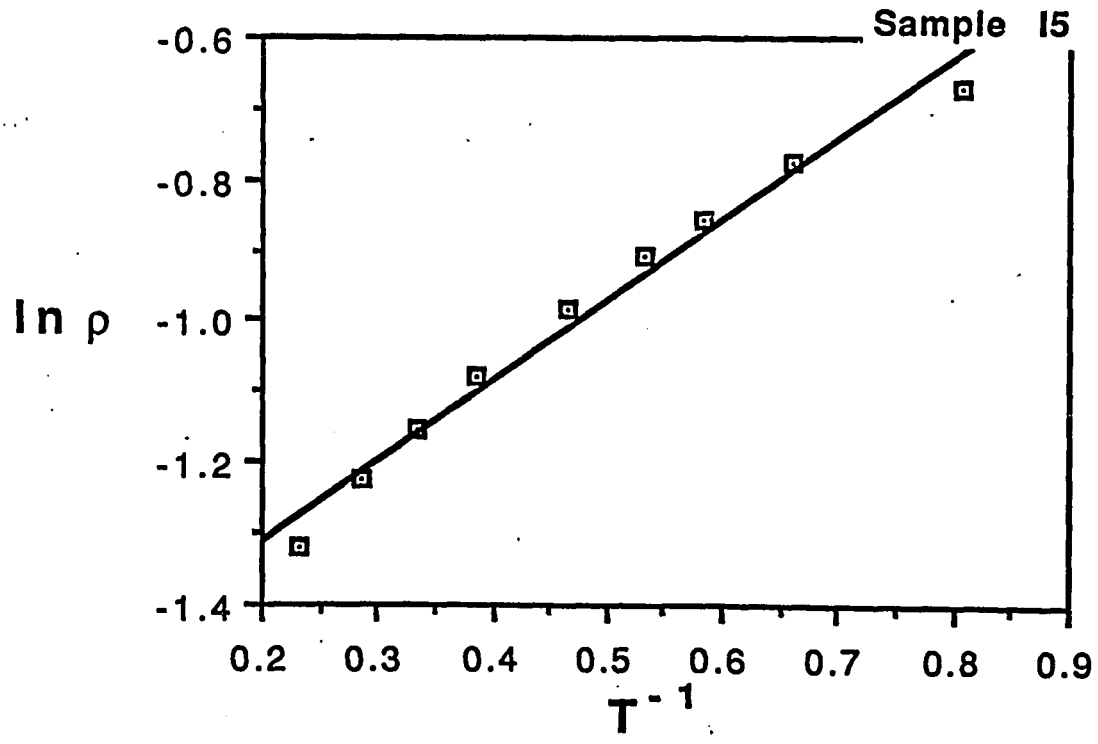

Fig. (II-2c) Semilogarithmic plot of the resistivity of sample I5 versus $T^{-1/2}$, showing that the form expected for the presence of a Coulomb gap associated with electron-electron correlations does not provide as good a fit as $T^{-1/4}$ to our data. The resistivity is in Ω-cm. $T^{-1/2}$ temperature dependence is not completely ruled out, however.

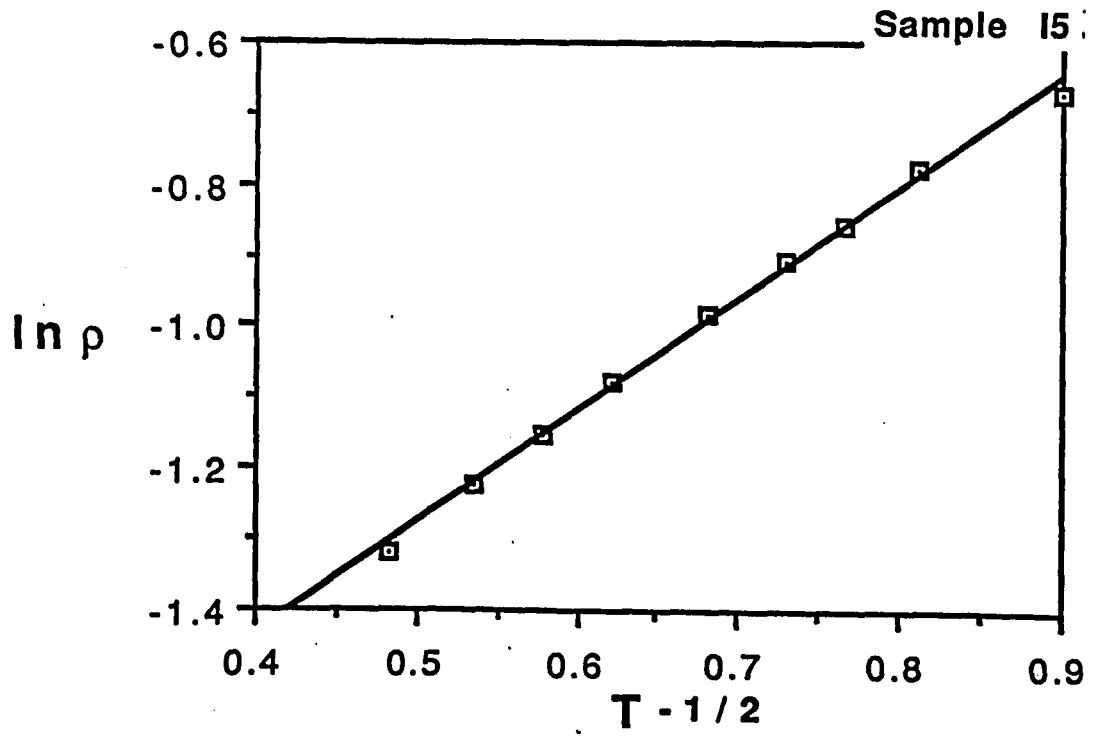

this sample in the analysis given below should be viewed with some caution.

TABLE II-1. Important parameters of samples I4, I5 and I6. ξ is the localization length, R is the hopping length at 4.2 K, d is the inter-donor separation. All lengths are in angstroms. T_o is in kelvin.

SAMPLE	T_o	R/ξ	ξ	R	d
I4	197.3	0.98	361	355	127
I5	44.5	0.68	593	402	127
I6	1.3	0.28	1912	539	123

Using Eq. (2) and the expression for the hopping length

$$R = [8\pi k_B T N(E_F)/(9\xi)]^{-1/4} \qquad (3)$$

to eliminate the density of states $N(E_F)$, we obtain the relation

$$\frac{R}{\xi} = \left[\frac{9}{8\pi\beta}\right]^{1/4}\left[\frac{T_o}{T}\right]^{-1/4} \qquad (4)$$

Values of R/ξ deduced from this expression at 4.2 K are listed in Table II-1. Also listed in Table II-1 are the hopping length R and the localization length ξ deduced from a very rough estimate for $N(E_F)$ of $2\times10^{19}(\text{ev-cm}^3)^{-1}$, and the average distance between donors, $d=N_D^{1/3}$, where N_D is the number of donors.

We note that the hopping length is larger than d, as should be the case for variable range hopping. Less reassuring, however, is

that in the range of these measurements the hopping length is comparable with the localization length for sample I4, and R/ξ becomes progressively smaller for I5 and I6. It should be noted, however, that the resistivity does nevertheless fit the variable range hopping form given by Eq. (1) measurably better than a number of other forms, including activated conduction, formulations which include electron correlations (this formulation may not be excluded, on the basis of our data) and the simple power law behavior expected for near-neighbor hopping diffusion within a localization length. Similar behavior consistent with Eq. (1) in a range of temperature where one can infer that R is appreciably smaller than ξ has been observed by Ovadyahu[14] for insulating, disordered, three-dimensional vanadium oxide films with carrier concentrations near the metal-insulator transition. One should, nevertheless, bear in mind that this experimentally observed temperature dependence could possibly derive from a process other than Mott variable range hopping, particularly for samples near the transition.

The logarithm of the resistivity of sample I5 at various fixed magnetic fields between 0.3 and 1T is shown in Fig. (II-3), again as a function of $T^{-1/4}$. The variable hopping form continues to describe the resistivity in magnetic fields up to 1T; if any deviations occur, they are quite small. As evidenced by the decreasing slope, the parameter T_o decreases with increasing magnetic field, an effect presumably associated with the delocalizing effect of the field and a consequent increase in the localization length ξ, as further discussed below.

Fig. (II-3) The logarithm of the resistivity of sample I5 at various fixed magnetic fields, as a function of $T^{-1/4}$. The slope decreases with magnetic field, an effect presumably associated with the delocalizing effect of the magnetic field. The resistivity is in Ω-cm.

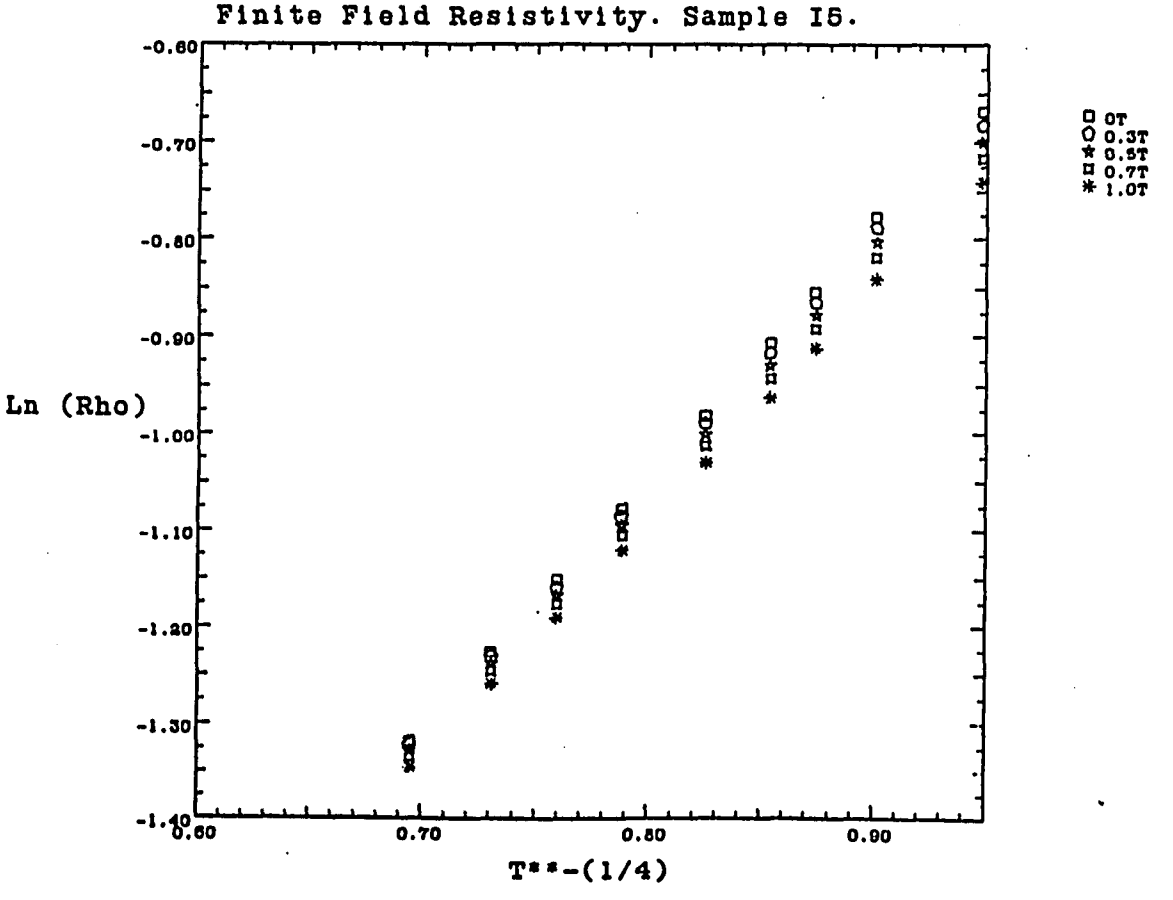

The effect of a magnetic field is clearly demonstrated in Fig. (II-4) where the magnetoresistance at 4.2 K is shown as a function of field to 8T for samples I1 and I6. As in most materials near the metal-insulator transition, the magnetoresistance is net negative at low fields; in both the weakly localized and the hopping regimes, this has been ascribed to field-induced changes of phase. The dominant effect at higher fields is to shrink the impurity wave functions, leading to an increase in the resistivity. It is clear from this figure, and Fig. (II-5) which shows the magnetoresistance of sample I5 at various temperatures in fields to 1T, that the mechanism which gives rise to negative magnetoresistance is dominant in this range of magnetic fields. It should be noted that the Hall coefficient data presented and discussed later were all taken in magnetic fields no higher than 1T.

Returning to Fig. (II-3), it is evident that the parameter T_o varies with magnetic field, becoming smaller as the field increases. Values of $T_o(H)$ deduced from least mean square fits to the data at different magnetic fields are listed in Table II-2. If we assume that the density of states $N(E_F)$ does not vary with field, and we assign the observed field dependence of T_o entirely to a change in the localization length ξ, then Eq. (2) gives the relation

$$[T_o(0)/T_o(H)]^{1/3} = [\xi(H)/\xi(0)], \qquad (5)$$

where $T_o(0)$, $\xi(0)$ and $T_o(H)$, $\xi(H)$ refer respectively to the values of the parameters at zero field and finite field H. A plot of this quantity is shown in Fig. (II-6) as a function of magnetic fields to

1T for samples I4 through I6. In all cases the localization length increases with magnetic field, and this increase becomes more pronounced as the critical concentration n_c is approached.

TABLE II-2. Values of the parameter $T_o(H)$ at different magnetic fields for sample I5. Notice the decrease in $T_o(H)$ with increasing magnetic field.

Magnetic Field (tesla)	$T_o(H)$ (kelvin)
0	44.5
0.3	42.0
0.5	39.3
0.7	36.8
1.0	33.7

Hall Coefficient and Mobility

The Hall Coefficient $R_H(H)$ was measured in several fields up to 1T at temperatures between 1.25 and 4.2 K. Care was taken to insure that the results were independent of measuring current, which was typically held below 10^{-3} amp. Data obtained at 1T for samples I4, I5 and I6 are shown in Fig. (II-7a). Data at lower fields are comparable, although somewhat noisier. All results are

Fig. (II-4) Magnetoresistance at 4.2 K as a function of magnetic field, for samples I1 and I6.

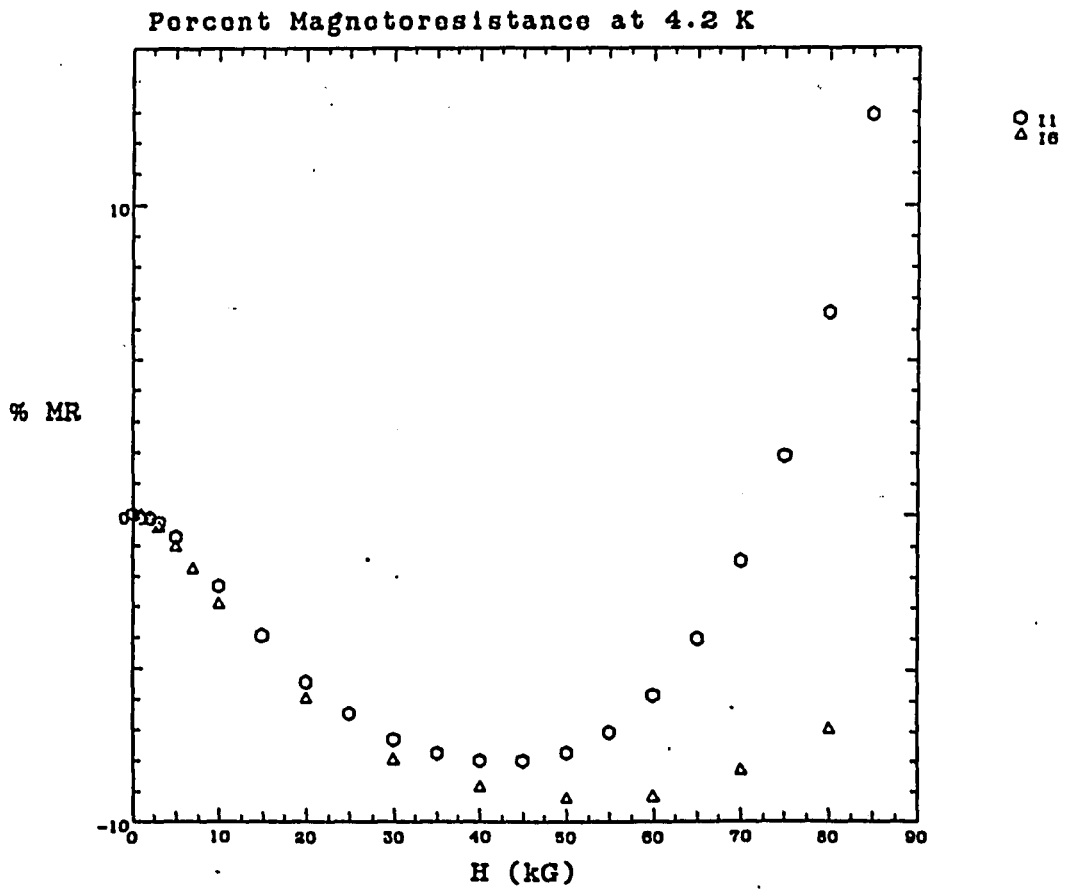

Fig. (II-5) Magnetoresistance of sample I5 at various temperatures in fields to 1T. Figures (II-4) and (II-5) show that the mechanism which gives rise to negative magnetoresistance is dominant in the range of magnetic fields used in the measurements discussed in this chapter.

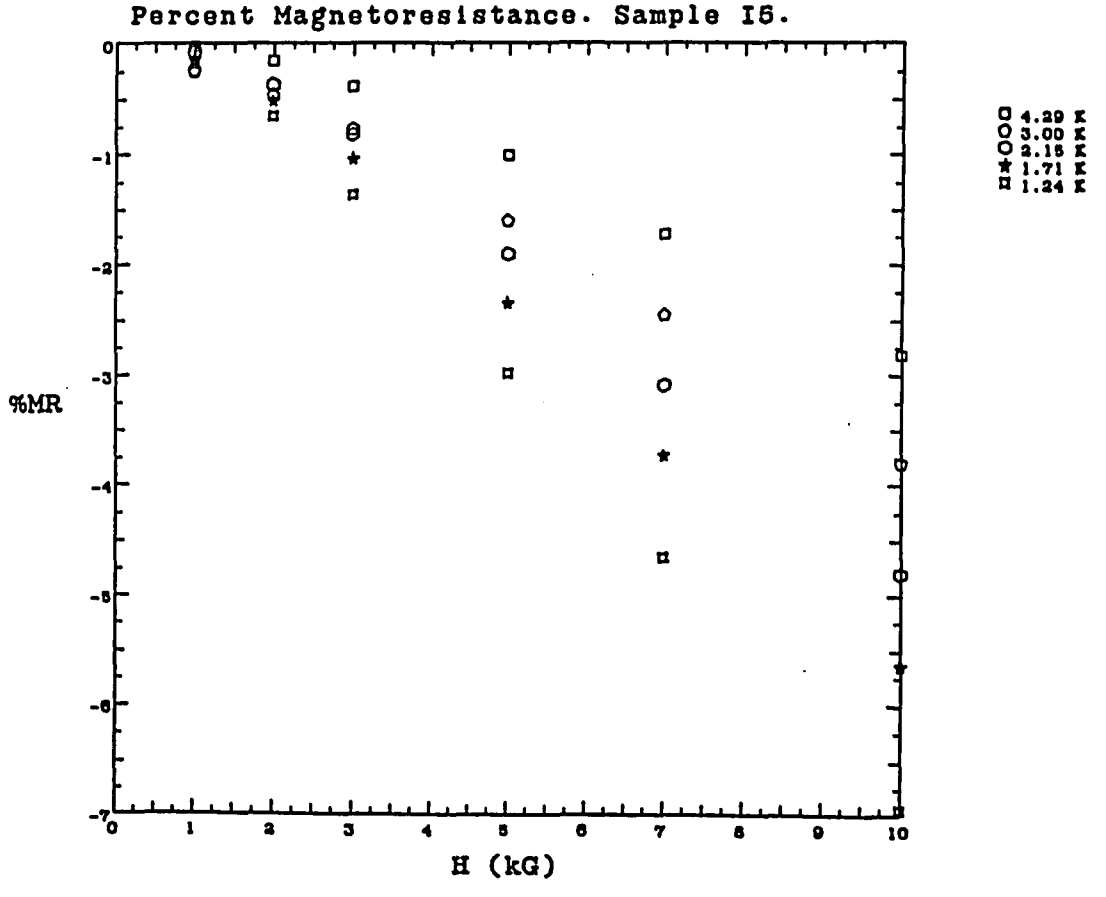

Fig. (II-6) Plot of $\xi(H)/\xi(0)$ as a function of magnetic field to 1T for samples I4 through I6. In all cases the localization-length increases with magnetic field, and this increase becomes more pronounced as the critical concentration n_c is approached.

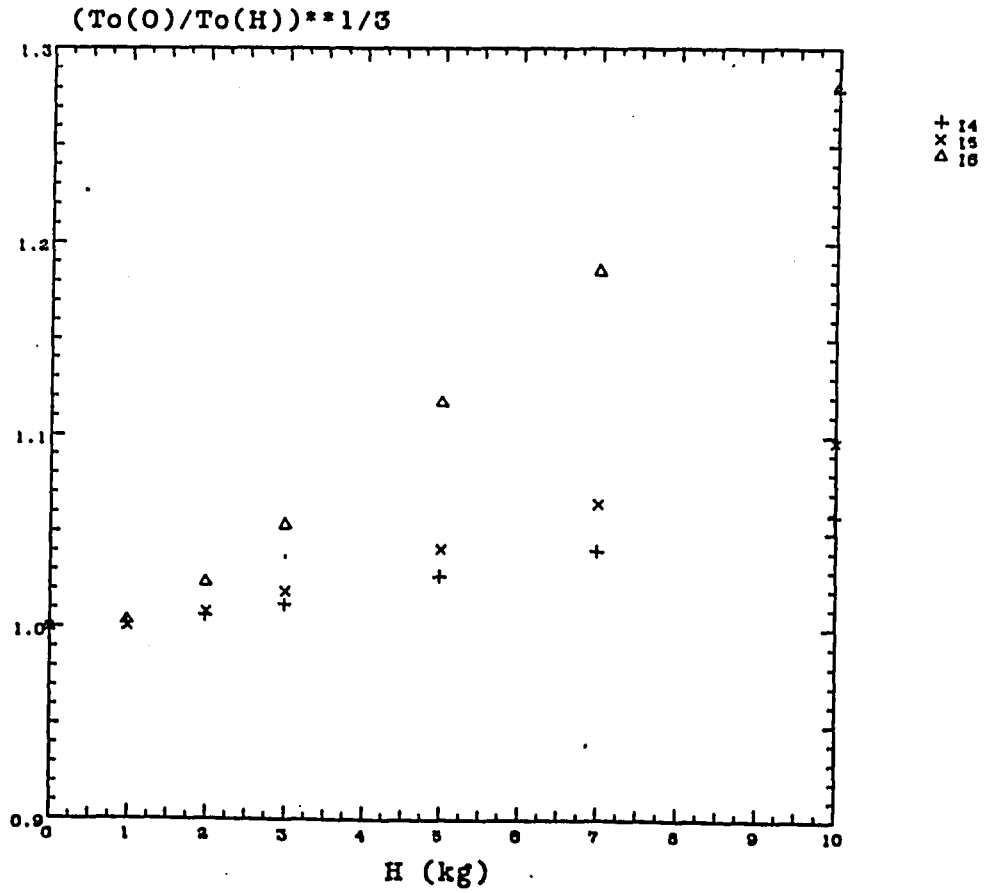

consistent with an expression similar to that which describes the variable range hopping resistivity, namely,

$$R_H(H, T) \propto \exp\left[K_{Hall}(H)\left[\frac{T_0(H)}{T}\right]^{-1/4}\right], \qquad (6)$$

where we have allowed for the possibility that $K_{Hall}(H)$ derived from the slope of the curves of Fig. (II-7a) varies with magnetic field. We also plot the logarithm of $R_H(H)$ versus T^{-1} to show that the Hall coefficient does not fit an activated form. Figure (II-7b) shows that we cannot eliminate a $T^{-1/2}$ dependence on the basis of our data; it should be noted, however, that there appears to be no theoretical basis for expecting such behavior. [3,4,5] A least mean square fit to Eq. (6) of data for all samples at various magnetic fields to 1T yields values for $K_{Hall}(H)$ listed in Table II-3.

TABLE II-3. Values of the parameter $K_{Hall}(H)$ at various magnetic fields for samples I4, I5, and I6.

SAMPLE	0.3 T	0.5 T	0.7 T	1.0 T
I4	0.30	0.34	0.37	0.40
I5	0.29	0.34	0.37	0.39
I6	0.37	0.45	0.46	0.48

Fig. (II-7a) Logarithm of the Hall coefficient at 1T for samples I4, I5, and I6 plotted as a function of $T^{-1/4}$.

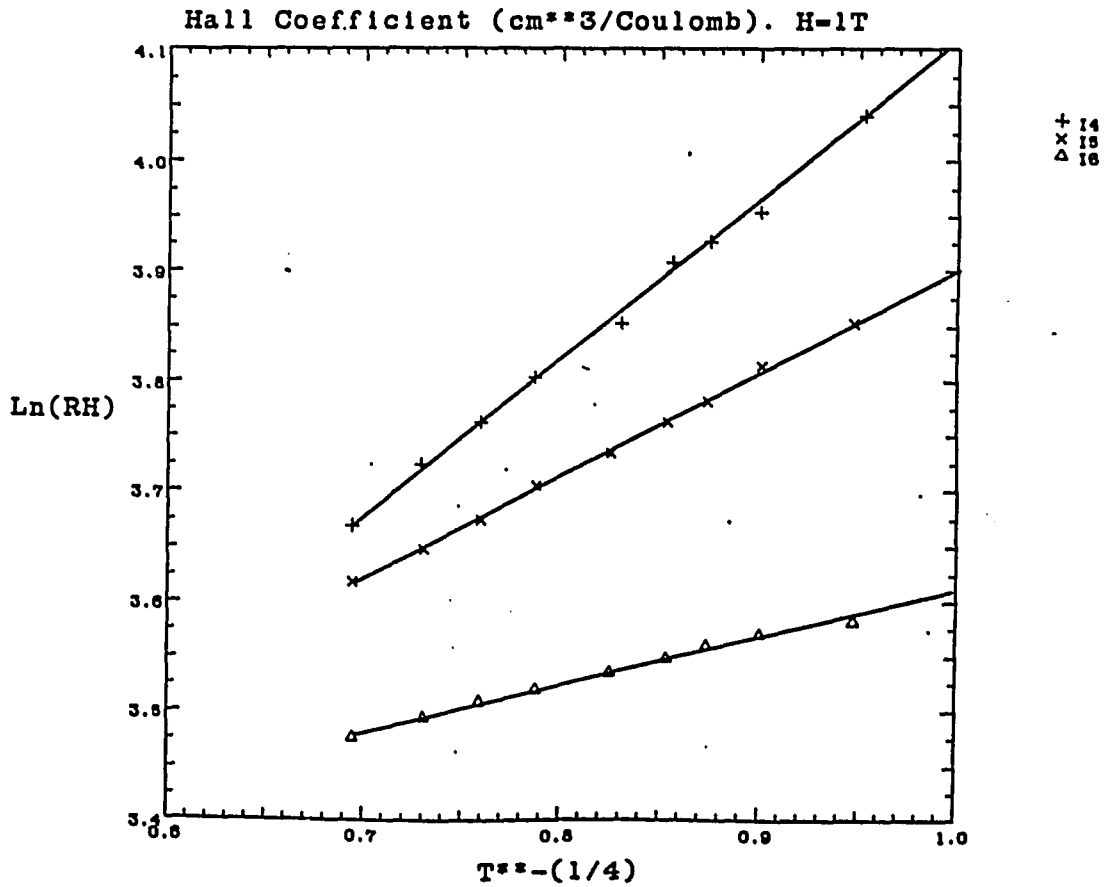

Fig. (II-7b). Logarithm of the Hall coefficient at 1T for sample I5, plotted as a function of T^{-1}. We also plot a straight line whose slope is obtained from a least mean squares fit to the data. The Hall coefficient is in cm^3/Coulomb.

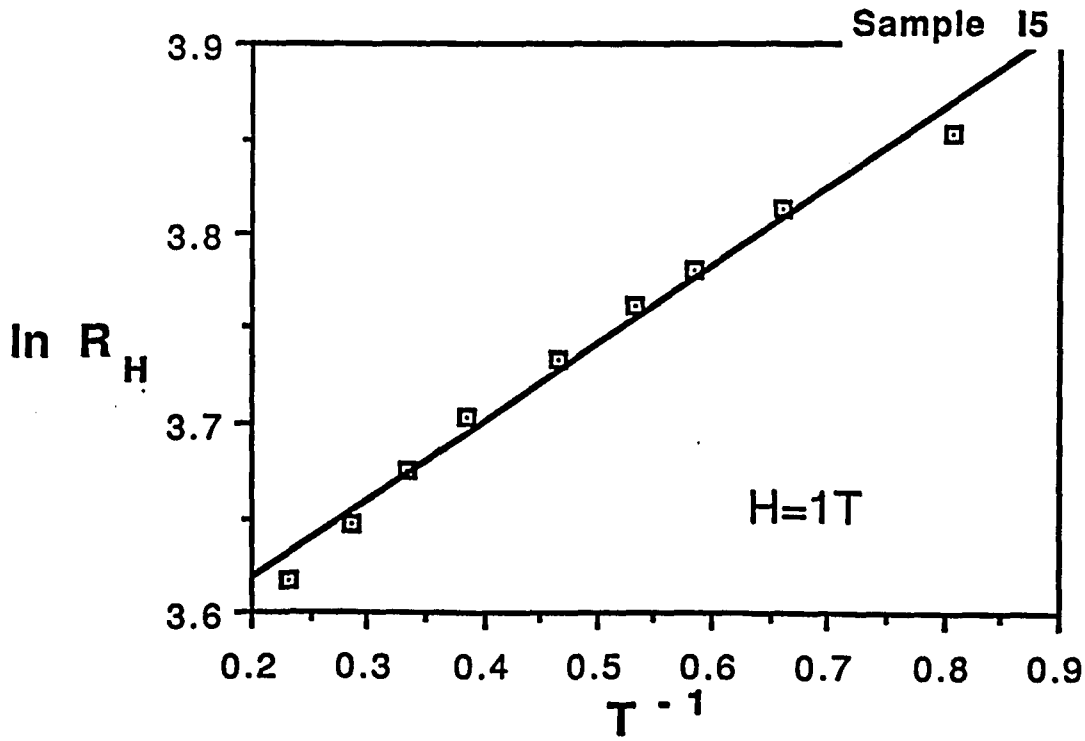

Fig. (II-7c) Logarithm of the Hall coefficient at 1T for sample I5, plotted as a function of $T^{-1/2}$. We also plot a straight line whose slope is obtained from a least mean squares fit to the data. The Hall coefficient is in cm^3/Coulomb.

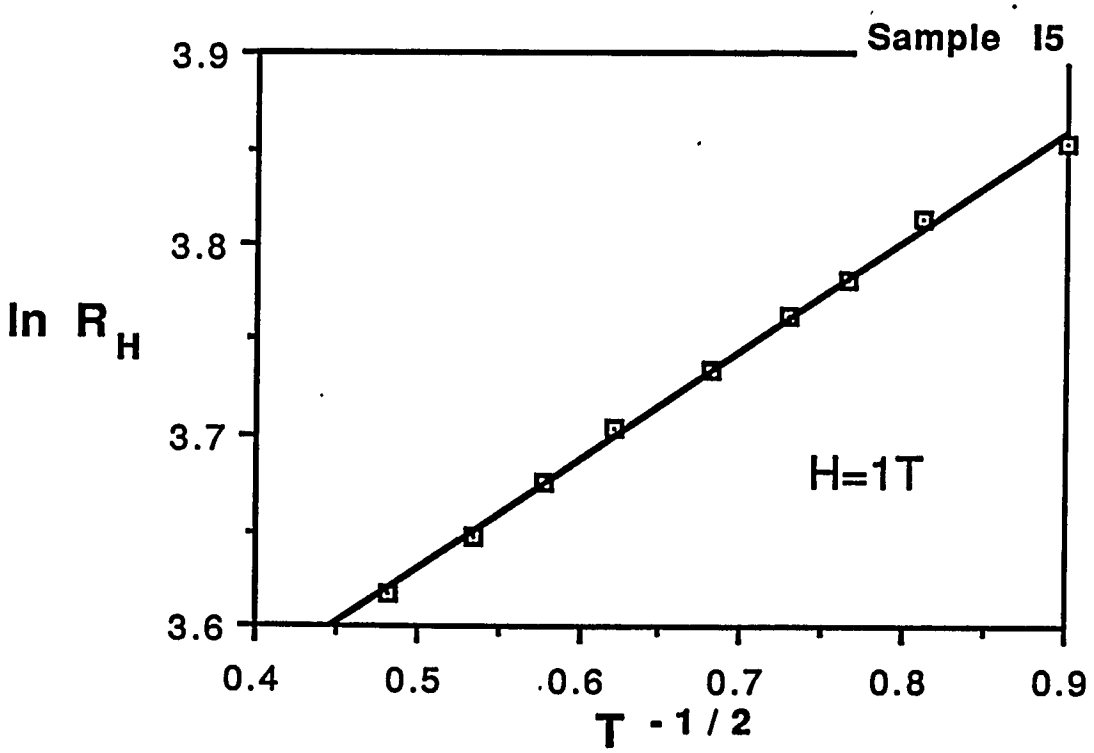

The logarithm of the Hall mobility, $\mu_H = R_H/\rho$, is plotted as a function of $T^{-1/4}$ for samples I4 through I6 at 1T in Fig. (II-8), and for sample I5 in various magnetic field in Fig. (II-9). Given that both R_H and ρ are consistent with the variable range hopping form, it follows that the Hall mobility which is their ratio, fits the same experimental form equally well. In particular, it is clear from Eqs. (2) and (6) that

$$\mu_H \propto \exp\left[-(1-K_{Hall})\left[\frac{T_0(H)}{T}\right]^{1/4}\right] \qquad (7)$$

As is true for the resistivity shown in Fig. (II-2a), the mobility exhibited in Fig. (II-8) continues to obey the same temperature dependence in finite field as it does at zero field.

The theory of the Hall effect for hopping conduction was initially developed by Holstein[1] and Friedman[2] who showed that a non-vanishing Hall effect was possible as a result of quantum interference. On the basis of these ideas, Gruenewald *et al.*[4] carried out a percolation path calculation for the conductivity and Hall mobility for the variable-range-hopping case, using three-site clusters. Their results reproduce Mott's expression for the conductivity, Eq. (1) above, and predict for the Hall mobility,

$$\ln \mu_H \sim -3/8\ (T_0/T)^{1/4} \qquad (8)$$

where T_0 is given by Eq. (2). This implies that a zero field $(1-K_{Hall}) = 3/8$ and the parameter K_{Hall} of Eq. (5) which characterizes the behavior of the Hall coefficient in the limit of zero field has the value 5/8.

The parameters K_{Hall} deduced from our data and listed in Table II-3 are plotted in Fig. (II-10) as a function of magnetic field for samples I4, I5 and I6. We find that K_{Hall} is a weak function of magnetic field (except possibly at the lowest field of 0.3T, where measurements involve the largest error), and extrapolations to zero field yield values which are approximately the same for all three samples within the accuracy of our measurements. The resulting values of K_{Hall} are considerably smaller than the 5/8 predicted by Gruenwald *et al.*

In a recent study of a series of insulating Si:As samples near the metal-insulator transition, Koon and Castner[6] have claimed that the Hall coefficient follows a variable range hopping form similar to the temperature dependence we report here for n-CdSe. Unlike our results in CdSe, however, they claim that K_{Hall} for their system extrapolates to the expected value of 5/8 at the critical concentration. Several factors may account for these differences. Our results were obtained for compensated CdSe while their data were for uncompensated Si:As. A more important difference may stem from the fact that the results on Si:As were obtained from extrapolations of data taken at considerably higher fields above 1T. The magnetoresistance is positive in this range of magnetic fields, and the physical processes giving rise to the Hall coefficient may be significantly different from what they are at lower fields.

Fig. (II-8) Logarithm of the Hall mobility plotted as a function of $T^{-1/4}$ at 1T for samples I4, I5, and I6.

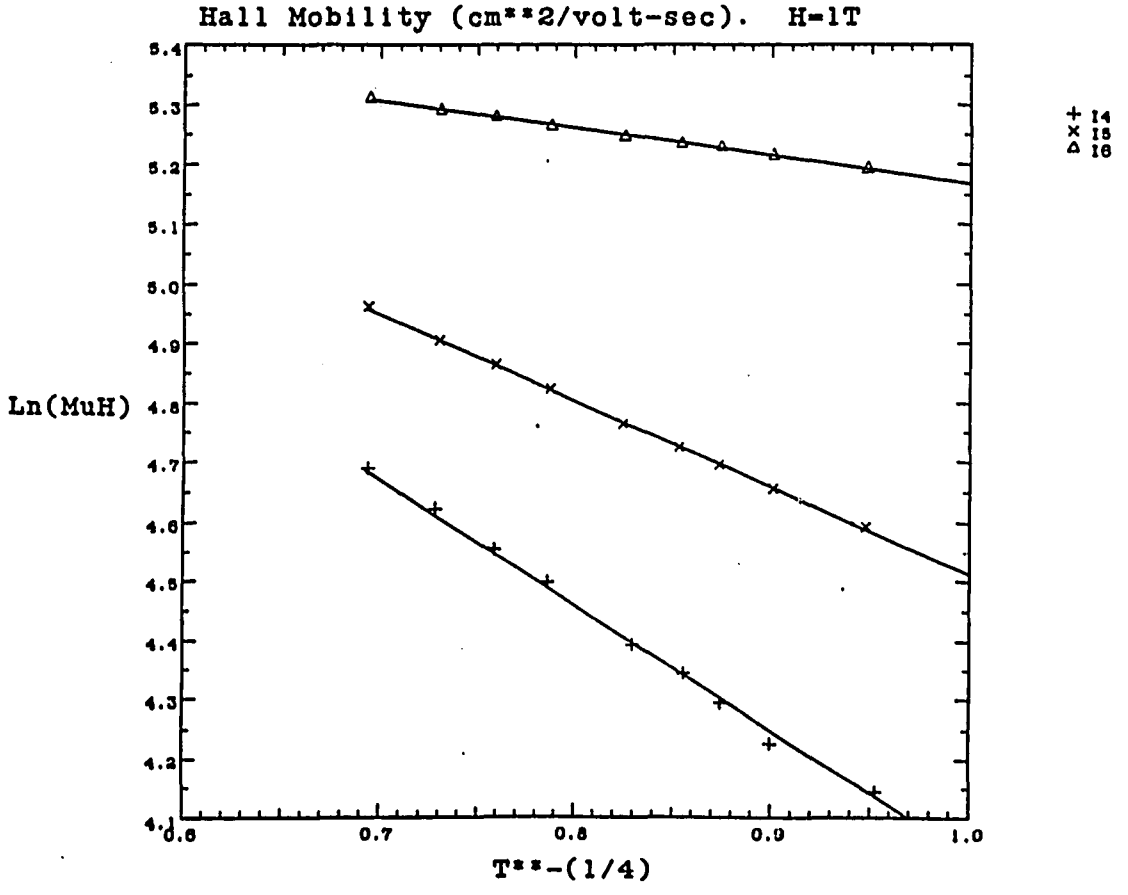

Fig. (II-9) Logarithm of the Hall mobility plotted as a function of $T^{-1/4}$ at various magnetic fields for sample I5. The Hall mobility is in $cm^2/V\text{-}s$.

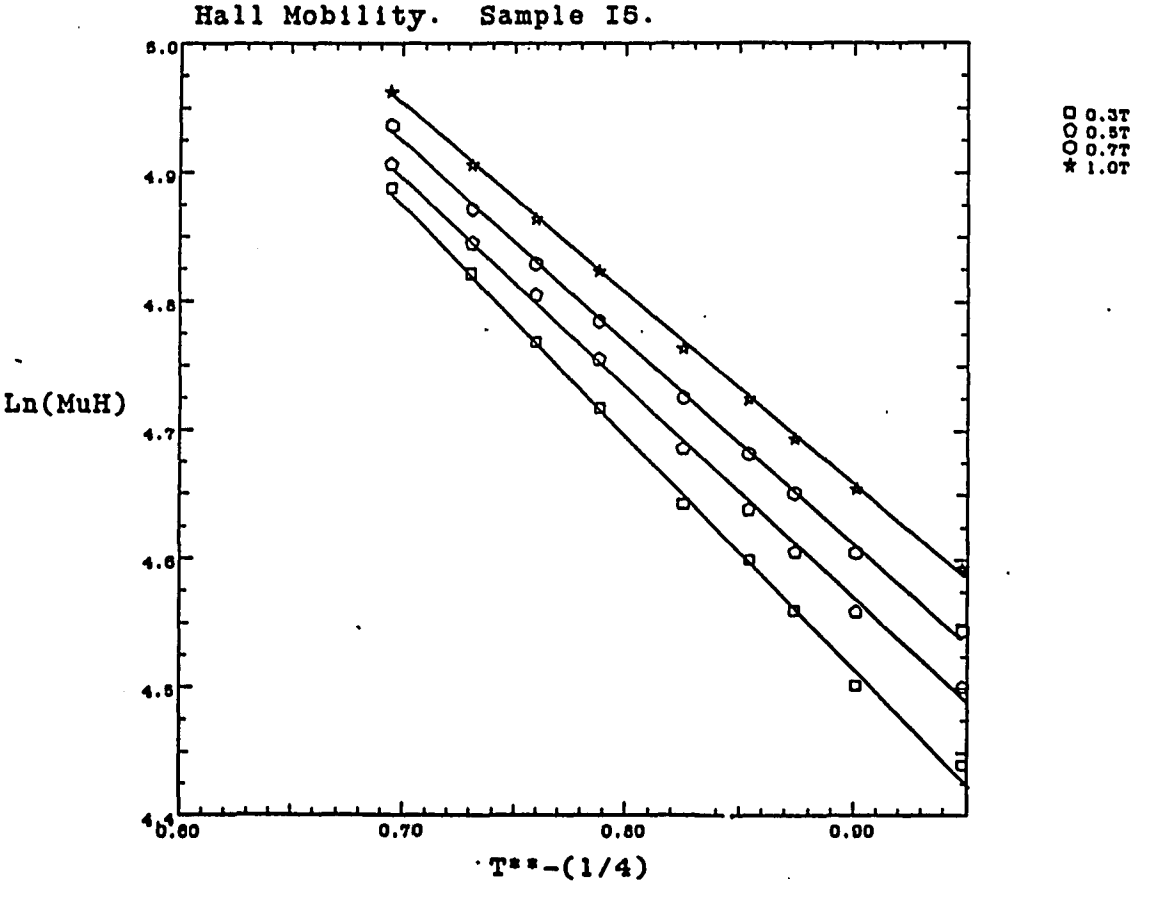

Fig. (II-10) Plot of the parameter K_{Hall} as a function of magnetic field for samples I4, I5, and I6. Zero field extrapolations yield values considerably smaller than the 5/8 predicted by Gruenewald *et al.*

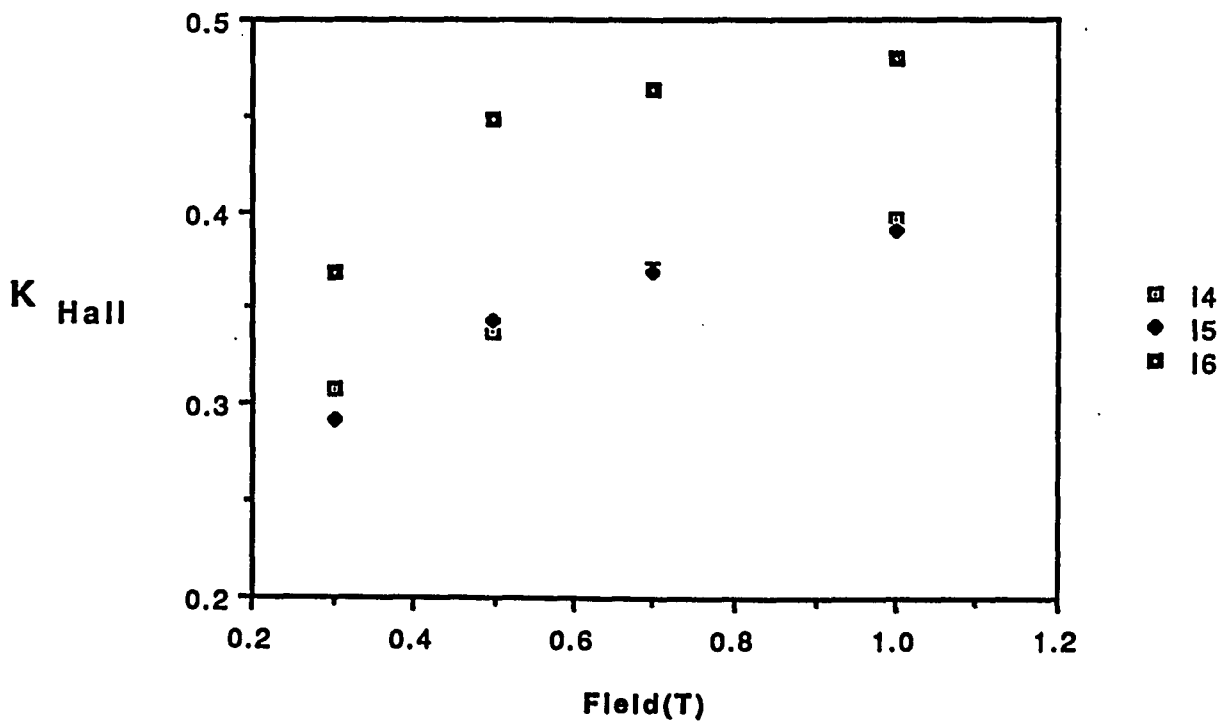

REFERENCES

[1] T. Holstein, Phys. Rev. **124**, 1329 (1961).

[2] L. Friedman and T. Holstein, Ann. Phys. **21**, 494 (1963).

[3] L. Friedman and M. Pollack, Phil. Mag. B38, 173 (1978).

[4] M. Gruenewald, H. Mueller, P. Thomas, D. Wuertz, Solid State Commun. **38**, 1011 (1981).

[5] R, Nemeth and B. Muhlschlegel, Solid State Commun. **66**, 999 (1988).

[6] D. W. Koon and T. G. Castner, Solid State Commun. **64**, 11 (1987).

[7] W. Sasaki, Phil. Mag. B52, 427 (1985).

[8] M. Amitay and M. Pollak, J. Phys. Soc. Jpn. Suppl. **21**, 549 (1966).

[9] Robert S. Klein, Phys. Rev. B **31**, 2014 (1985).

[10] M. J. F Le Hir, J. Phys. (Paris) **28**, 563 (1967).

[11] F. R. Allen and C. J. Adkins, Phil. Mag. **26**, 1027 (1972).

[12] D. M. Finlayson, J. Irvine and L. S. Peterkin, Phil. Mag. **39**, 253 (1979).

[13] L. J. van der Pauw, Philips Res. Repts. **13**, 1 (1958). See also Chapter I of this thesis.

[14] Tzvi Ovadyahu, preprint.

CHAPTER III

LUMINESCENCE AND EXCITATION SPECTRA OF HEAVILY DOPED n-TYPE CdSe ON THE METALLIC SIDE OF THE METAL-INSULATOR TRANSITION.

I. INTRODUCTION

In this chapter we discuss the results of a study of heavily doped n-type CdSe on the metallic side of the metal-insulator transition using luminescence and excitation spectra as probes. This is the first time that luminescence and excitation spectra have been obtained for n-type CdSe samples on the metallic side of the transition, although luminescence spectra for heavily doped n-type CdS on the metallic side of the transition had previously been obtained by S. Geschwind[1] and by Kukimoto *et al.*[2]

The luminescence spectra for metallic n-CdSe and n-CdS are very similar. They are both quite asymmetric and exhibit a high-energy threshold and a low energy tail. Figures (III-4) and (III-5) show plots of these spectra for CdSe. The CdS spectra were studied theoretically by S. M. Girvin[1] who proposed a model to explain the carrier concentration dependence of the energy at which these high-energy thresholds occur. This model successfully explains the monotonic progression of the thresholds with carrier concentration found experimentally for CdS, and is able to predict their location to within 10 meV, a quite remarkable achievement in light of the fact

that a simple Burstein shift[3] calculation of these thresholds is off by as much as 100 meV for some of the samples Girvin analysed.

Our experimental determination of the high-energy thresholds for CdSe exhibit an unexpected non-monotonic progression with carrier concentration. We have applied Girvin's model to the case of CdSe and compared these predictions with our experimental results. This is discussed in Sect. VII of this chapter. We find that although the predictions are still approximately within 10 meV of the experimentally determined thresholds, the model fails to explain the non-monotonic progression of the threshold locations with carrier concentration. A plot of this progression is shown in Fig. (III-6), and a plot of the predictions based on Girvin's model is shown in Fig. (III-12).

Section VIII of this chapter presents a modification proposed by us of the original Girvin model and based on work by L. Vina and M. Cardona.[4,5] This modification, which consists of a model to account for the effect of compensation on the size of the fundamental band gap, an effect not included in the original Girvin treatment, is able to explain the non-monotonic progression of the threshold energy with carrier concentration. Given the limited amount of data available to us, however, we are not able to definitely establish the correctness of the modified Girvin model which we propose, but we discuss some of the features which make it quite plausible.

The key role played by band gap renormalization due to compensating impurities in explaining our experimental results led us into a search for acceptor impurities in metallic n-type CdSe. In particular we wanted a more definitive proof of the presence of

acceptors than the indirect evidence already available to us from the transport studies of these samples. Section VI, on the long wavelength luminescence of n-type CdSe on the metallic side of the metal-insulator transition, presents what we believe are the first observations of luminescence due to electron recombination into acceptor states in metallic n-doped semiconductors.

II. SAMPLES

A list of the metallic samples investigated is presented in appendix I. We include their room temperature charge carrier concentration, Fermi wave vector and Fermi temperature.

III. EXPERIMENTAL PROCEDURES

A. Sample Preparation

Samples were treated to eliminate the surface oxide layer that forms when the crystals are exposed to air, and to minimize surface defects which could mask the true bulk luminescence of the crystals. Two different surface treatment methods were used for the experiments carried out at The City College of New York and at the AT&T Bell Laboratories, respectively. The luminescence experiments were repeated on the same samples at both facilities with identical results, thus confirming the correctness of the experimental data.

At AT&T Bell Laboratories the sample surfaces were polished with 3 micron grain aluminum oxide and subsequently polished with a slow edging solution of bromine methanol. They were then stored in a dessicator for less than 24 hours and transferred into the optical cryostat the day of the experiment. At The City College of New York the samples were cleaved along the crystal c-axis minutes before the experiment and immediately transferred into the cryostat. Once in the cryostat the samples were either kept in vacuum or in a Helium liquid or gas environment.

All sample crystals had also been oriented prior to the experiments, but it was found that the luminescence spectra were

independent of sample orientation or direction of polarization of the excitation radiation. At City College the samples were oriented by the Laue technique of x-ray diffraction. This allowed us to determine the direction of the crystal c-axis to within 5 degrees. At the Bell Laboratories samples were oriented using an x-ray orientation goniometer by finding the Bragg peak for reflection of the K_α line copper radiation off the 001 plane in the CdSe crystal. The crystal c-axis was determined to better than 20 minutes of arc by this method.

B. Apparatus and Technique

B1. Luminescence I

This work was carried out at The City College of New York, in the laboratories of Professor H. Cummins. I gratefully acknowledge the assistance of Dr. Wing-Kee Lee.

The experimental set up is shown in Fig. (III-1). Radiation of wavelength 5145 A or 4880 A from a Coherent Model 52 Argon Ion laser operating in single mode is focused by lens L1 (focal length of approximately 13 cm) onto the sample surface. The luminescence light is collected by the lens L2 (focal length of approximately 10 cm) and then focused at the entrance slit of a Spex 1401 double monochromator spectrometer with a resolution of about 4 cm^{-1} (approximately 0.5 meV). The signal, typically on the order of thousands of photons per second near the spectral peak, is then detected by a photomultiplier tube and the data stored in an IBM PC microcomputer.

The irradiated area on the sample is about 100 mm in diameter and the power at the surface is close to 0.13 mW. This means that the intensity at the sample surface is on the order of 1 W/cm^2, which is many orders of magnitude below the excitation energy densities needed to produce electron-hole plasmas or even high density exciton systems in insulating CdSe.[3] We can therefore safely neglect any effect of the laser light on the electron population density in the sample.

Freshly cleaved samples were put into a Janis Model 8DT optical cryostat. The samples were immersed in superfluid Helium, and the temperature, measured by a carbon-glass thermometer, was close to 2 K.

Fig. (III-1) Experimental set-up used at CCNY for luminescence experiment.

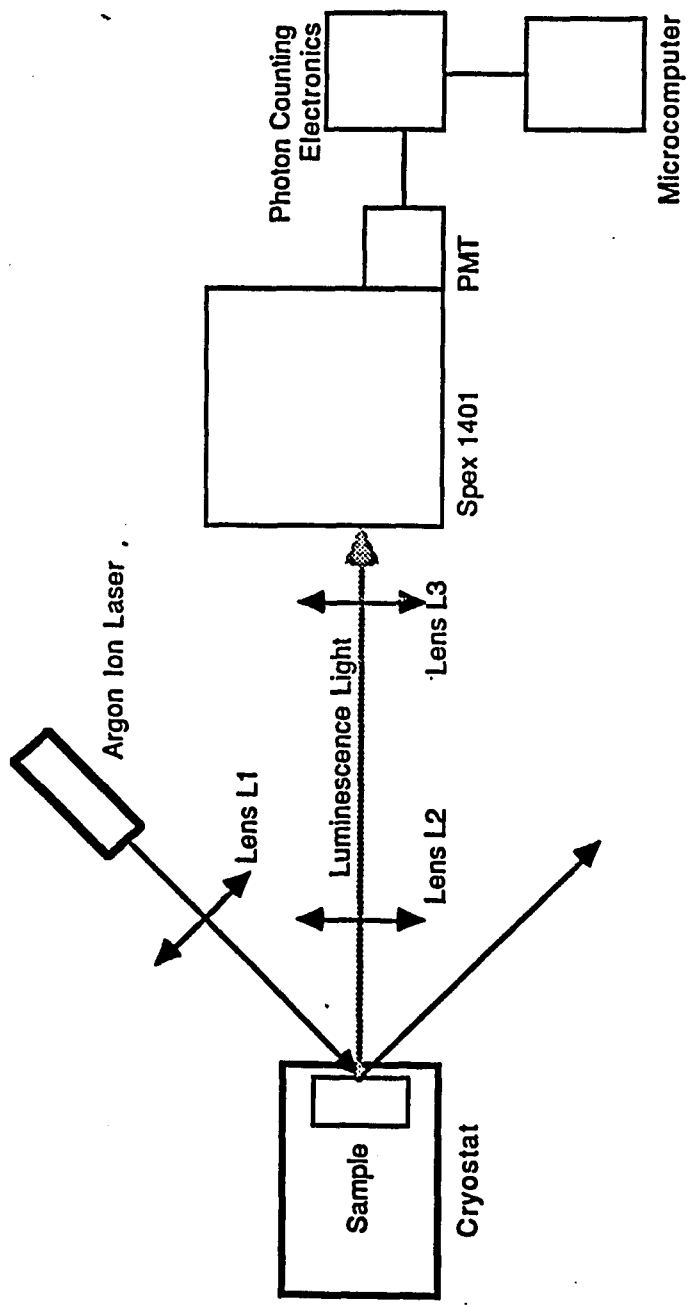

Fig. (III-2) Experimental set-up used at AT&T Bell Laboratories for obtaining excitation and luminescence spectra.

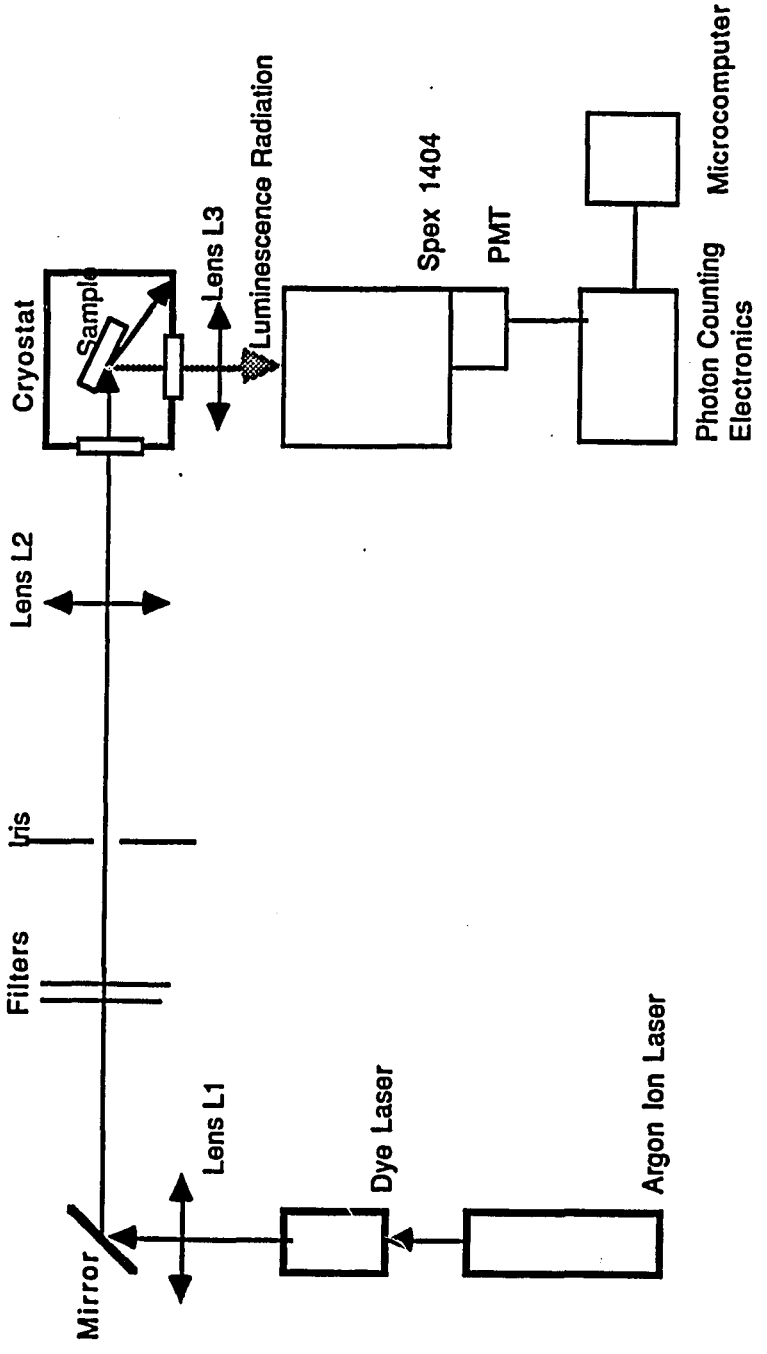

B2. Luminescence II and Excitation Spectra

This work was carried out at the AT&T Bell Laboratories in Murray Hill, New Jersey, in the laboratories of Dr. A. Pinczuk. I gratefully acknowledge the assistance of Dr. Gillard Danan.

The experimental set up is shown in Fig. (III-2). Monochromatic radiation of wavelength in the range from 6600 A to 7000 A from a Coherent Model CR- 599 dye laser is focused by a cylindrical lens (L2; focal length of approximately 50 mm) onto the sample surface. The fluorescence light is collected by lens L3 (focal length of approximately 300 mm) and then focused at the entrance slit of a Spex 1404 double monochromator spectrometer with a resolution of about 1 A (approximately 0.25 meV at these wavelengths). The signal is detected by a photomultiplier tube and the data stored in an AT&T microcomputer.

The samples are immersed in superfluid Helium, in a Janis Model 8DT optical cryostat. The operating temperature, measured by a carbon-glass thermometer, was 1.7 K in most instances. Some measurements were performed by cooling the samples with vapor from a pumped Helium bath. The temperature was then 3 K. No noticeable difference in the spectral linewidths was detected on account of this temperature difference.

The dye laser was supplied with DCM dye. This dye lases in the range from 6200 A to 7000 A. The birefringent filter in the laser then selects a single output wavelength, with a resolution of better than a fraction of an angstrom. The dye laser was pumped by 5145 A light from a Spectra Physics Model 171-01 Argon Ion laser.

The output intensity of the dye laser was about 150 mW. This radiation was then filtered down to nearly 10 μW, a quite adequate pumping intensity for the strongly luminescent CdSe crystals at these low temperatures. Typical luminescence signals were on the order of thousands of photon counts per second per wavelength, for a noise to signal ratio of better than 5 percent.

The irradiated area on the samples was close to 0.2 mm^2, making the intensity at the surface about 5 mW/cm^2. At these excitation energy densities the perturbing effect of the laser light on the conduction band electron population density in the CdSe crystals is completely negligible.[6]

Cryostat. Fig. (III-3) shows a schematic diagram of the 8DT Janis optical cryostat. Light enters the cryostat through one of the windows shown near the bottom of the cryostat. It then impinges on the sample and the luminescence radiation is collected by lens L3 after exiting through a window at right angles to the incident light path. The sample surface is so oriented that most of the exciting radiation is scattered away from the exit window. In the experiment at The City College of New York, the luminescence radiation exits through the same window as the incoming laser radiation, but the latter impinges on the sample surface at an angle so that most of the exciting light is scattered away from the spectrometer. This is shown in Fig. (III-1).

The temperature of the Helium bath in the sample chamber can be controlled to some extent by a needle valve near the top of the cryostat. The valve connects the sample tube with the Helium

reservoir. The temperature of the bath also depends on the vacuum pumping speed. The location of the sample space pumping port is shown in the diagram in Fig. (III-3).

For those measurements where the sample is cooled by Helium vapor, a Cryogenics Research Model TC-103 temperature controller was used to maintain a stable temperature of 3 K. This controller energized a heater wire placed above the sample holder.

Photon Counting. The luminescence light from the CdSe crystals is focused on the spectrometer, where it is diffracted twice by a double grating arrangement. A single frequency component of this light (within a wavelength resolution of one angstrom at the Bell Laboratories set up, or a wavenumber resolution of 4 cm^{-1} at City College) exits the spectrometer through an exit slit and is detected by a photomultiplier tube.

At the AT&T Bell Laboratories set up the signal from the photomultiplier is fed into an ORTEC 9315 photon counter and the corresponding count is stored in a computer. The photon counter is connected to the computer through an ORTEC 779 interface controller.

The photon counter also controls the dwell time for each wavelength, which was set to one second. The spectrometer is driven by a Compu-Drive Cd2A system.

For the experiment at City College the data was processed by an IBM data acquisition and control card and interfaced into an IBM PC microcomputer. Here the spectrometer was driven at a constant scanning speed of 0.625 cm^{-1}/sec, with a detection dwell time of one second.

Fig. (III-3) Janis 8DT Optical Cryostat.*

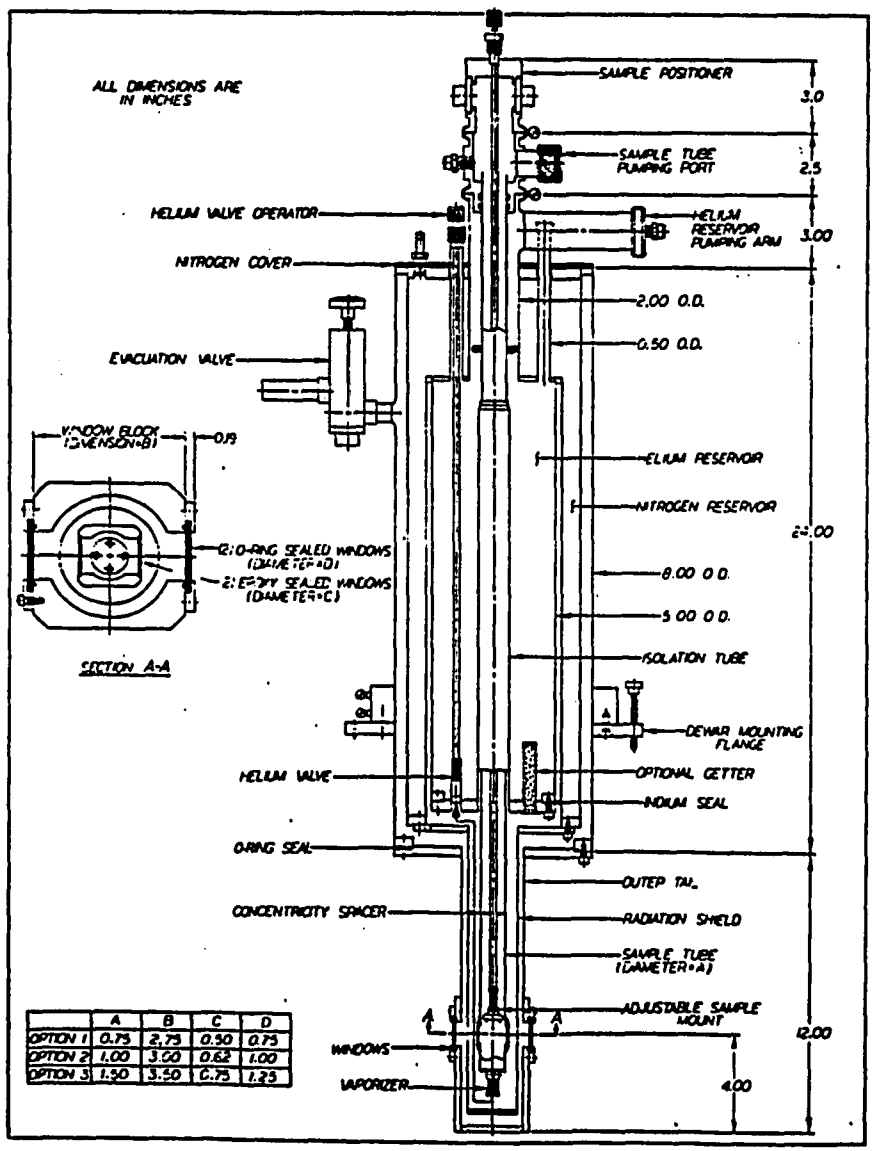

* Reprinted by permission of Janis Research Corporation, Wilmington, Massachusetts.

Excitation Spectra. Excitation spectra are obtained using the same experimental set up described above and shown in Fig. (III-2). An electrical motor rotates the birefringent filter in the dye laser, changing the wavelength of the emitted radiation at a constant rate. The speed of rotation of this filter is controlled by an Oriel Model 18009 dual controller.

Detection takes place at a fixed wavelength, chosen to lie far into the low energy tail of the luminescence spectra of the samples. Typical detection wavelengths ranged from 6870 A to 6900 A. The spectrometer is set to detect light only at this wavelength and excitation of the CdSe crystals takes place with radiation of shorter wavelengths up to the spectrometer setting.

The data was plotted directly on a chart recorder.

IV. RESULTS I

High-Energy Threshold in Metallic Samples: Luminescence

Luminescence spectra of metallic n-doped CdSe for several different doping densities are shown in Fig. (III-4). Figures (III-5)(a to d) show[7] the spectra plotted separately. As can be seen, each spectrum exhibits a threshold on its high-energy side. This threshold, whose position was taken as the energy corresponding to the midpoint of the steeply rising portion of the spectrum --the "threshold"--, occurs at different energies for different doping levels, and generally tends to increase in energy with increasing carrier concentration. Further, we notice that the spectra are quite asymmetric, with a long tail towards low energies.

Notice, however, that the high-energy threshold for sample M3 occurs at a higher energy than those for samples M4 and M5, which have higher carrier concentrations. This is also shown in Fig. (III-6), where we plot the position of the high-energy threshold versus carrier concentration. This feature of our spectra is somewhat unexpected. It was not observed in the luminescence spectra for metallic n-doped CdS taken by S. Geschwind[1], where it was strictly true that the threshold increased in energy with increasing charge carrier density for the samples studied.

These latter CdS spectra were analysed by S. M. Girvin[1], who calculated the position of the upper threshold assuming that it arose from the annihilation of a thermalized valence hole with a Fermi-surface electron. As we shall see below, Girvin's model predicts a monotonically increasing high-energy threshold for CdSe. Therefore, as it stands, Girvin's original formulation cannot account for the detailed features of our CdSe spectra. In this chapter we discuss a modification of this model which is able to explain the non-monotonicity of the upper threshold with carrier concentration, exhibited in our data.

It is possible that this threshold does not correspond, in some of the samples at least, to recombination with a valence hole but with a hole in an acceptor trap above the top of the valence band. This could explain the break in monotonicity in the high-energy threshold with increasing carrier concentration. However, our results for the excitation spectra and long-wavelength luminescence of the same n-doped CdSe samples indicate that the high-energy thresholds are not caused by recombination into impurity traps in

the band gap. These results are described below. We therefore also assume, as Girvin did, that the high-energy thresholds for all samples arise from the annihilation of a thermalized valence hole with a Fermi-surface electron.

With regards to the low energy tail, it is due to the decay of electrons below the Fermi level into the thermalized valence hole.

Fig. (III-4) Luminescence spectra obtained at CCNY. They are plotted as a function of energy.

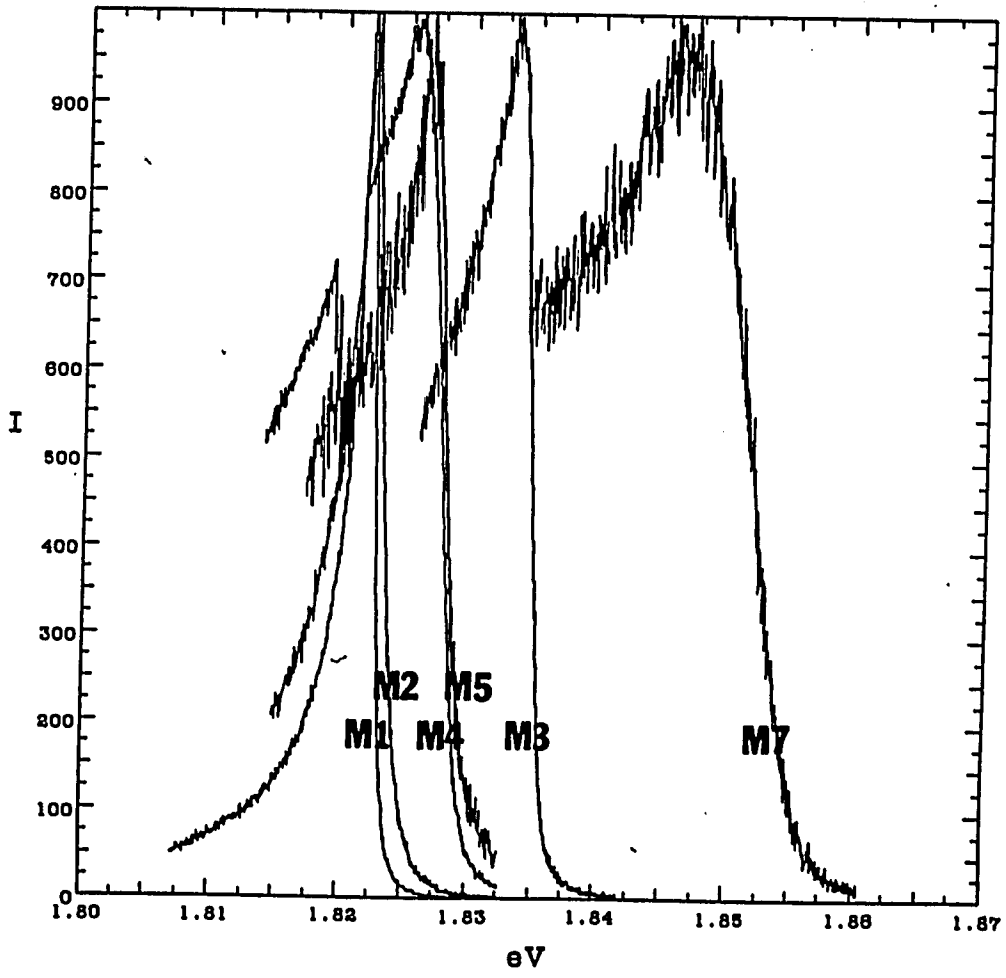

Fig. (III-5a) Luminescence spectrum of sample M1. All the spectra plotted in Figs. (III-5)(a to d) were obtained at AT&T Bell Laboratories. They are plotted as a function of wavelength. They give the same position for the spectra thresholds as the experiments carried out at CCNY.

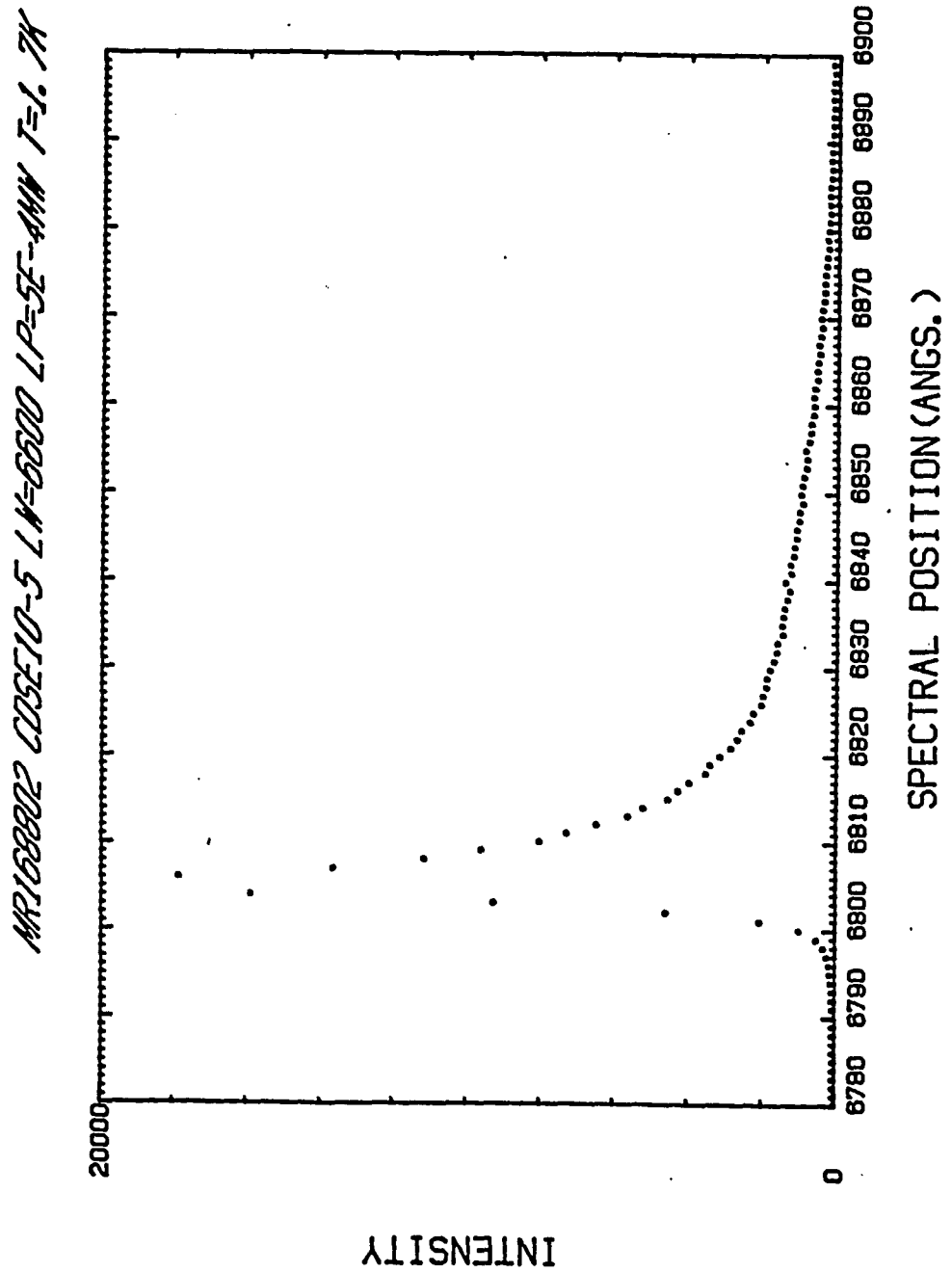

Fig. (III-5b) Luminescence spectrum for sample M3.

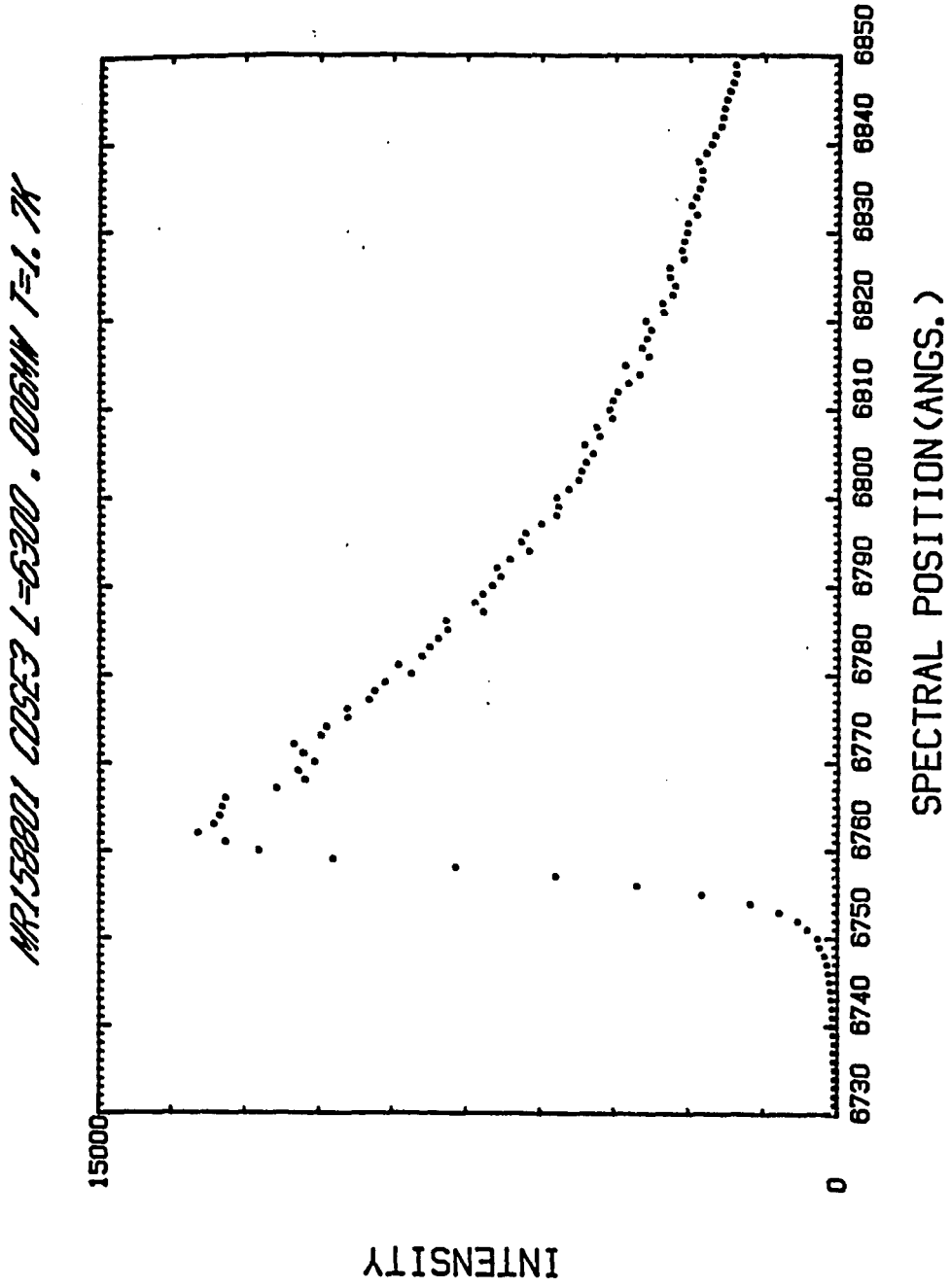

Fig. (III-5c) Luminescence spectrum for sample M4.

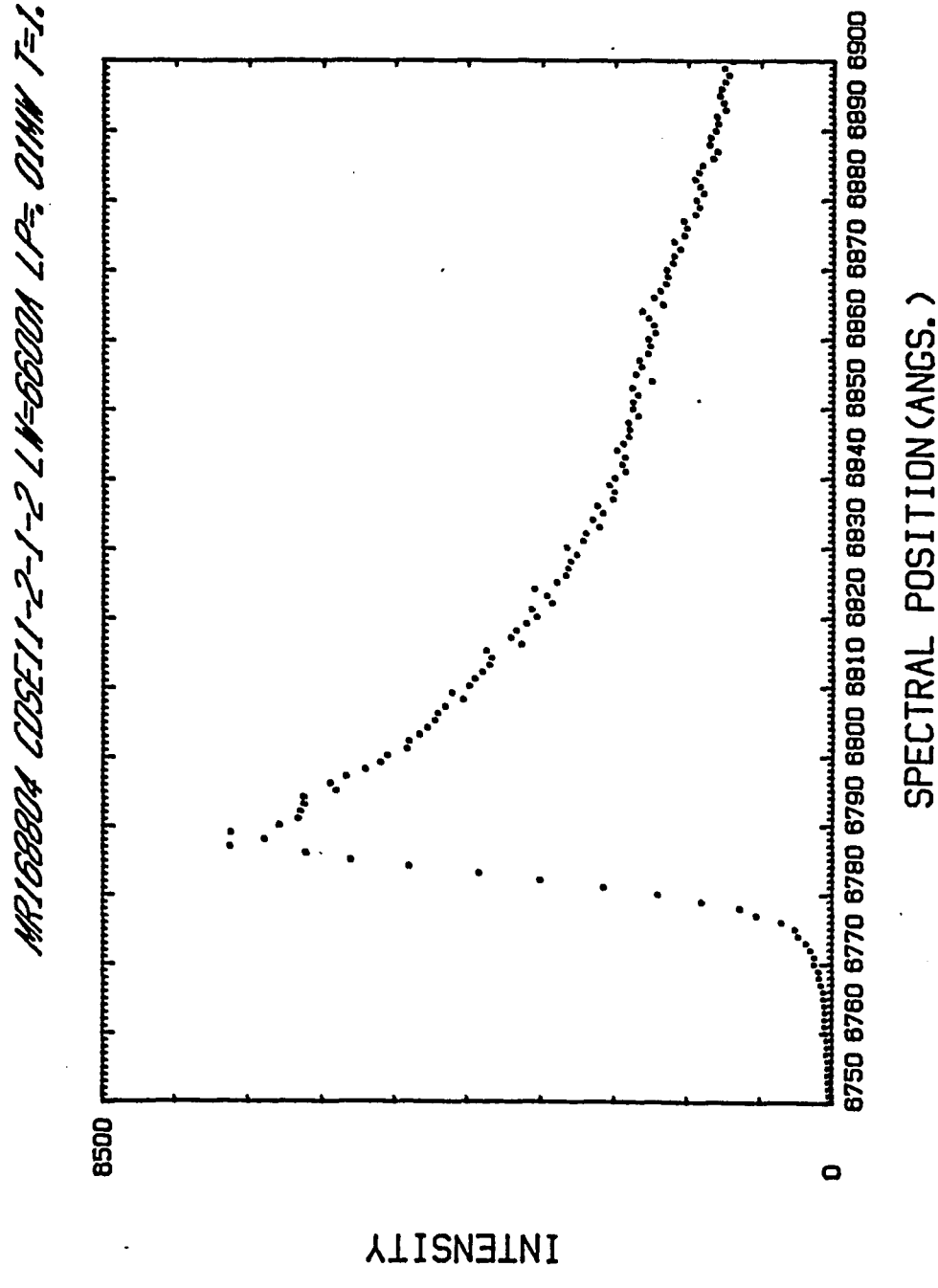

Fig. (III-5d) Luminescence spectrum for sample M5.

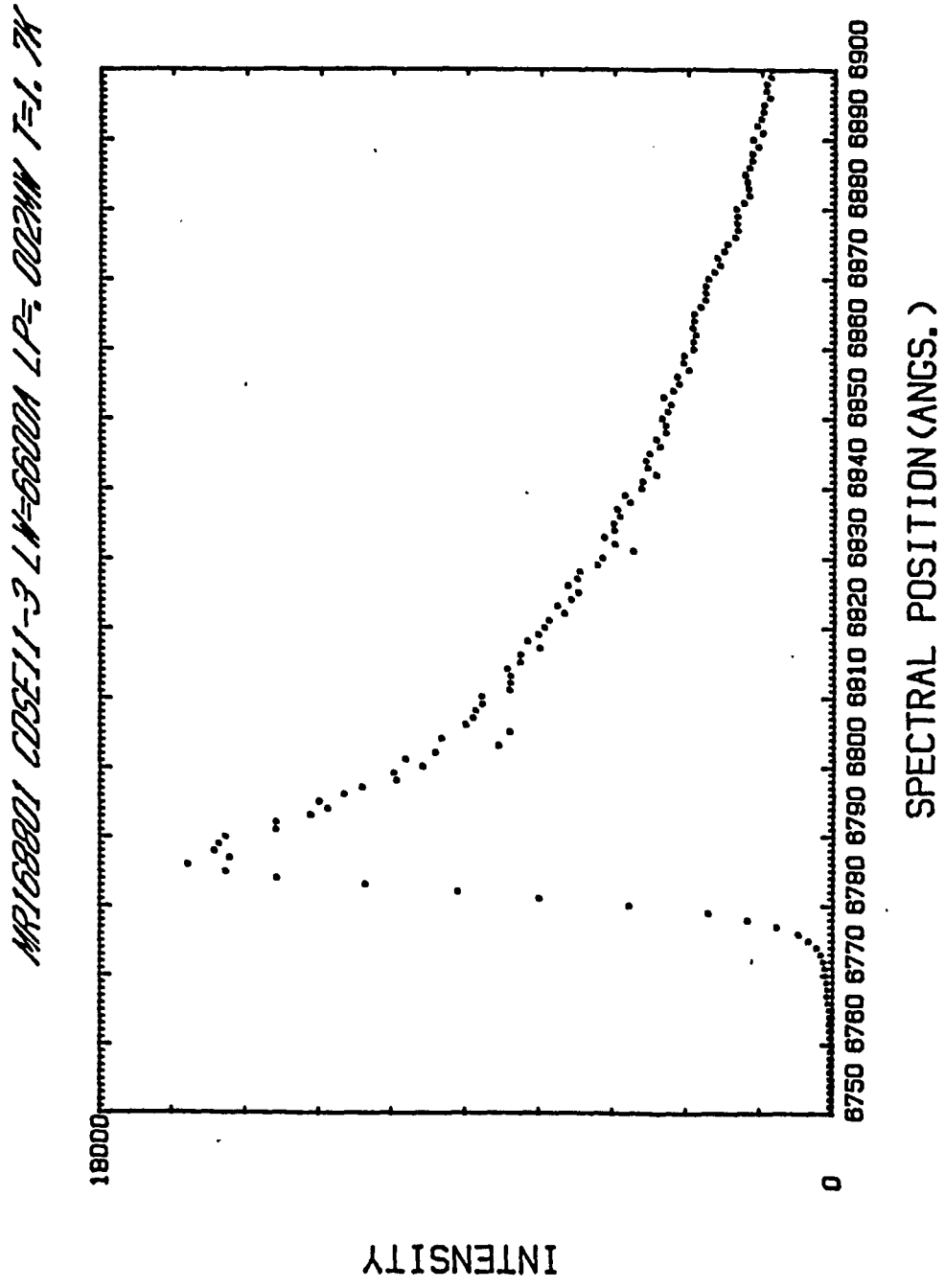

Fig. (III-6) Position of the spectra high-energy threshold versus carrier concentration obtained from the luminescence spectra. Note the non-monotonic character of the plot as a function of carrier concentration.

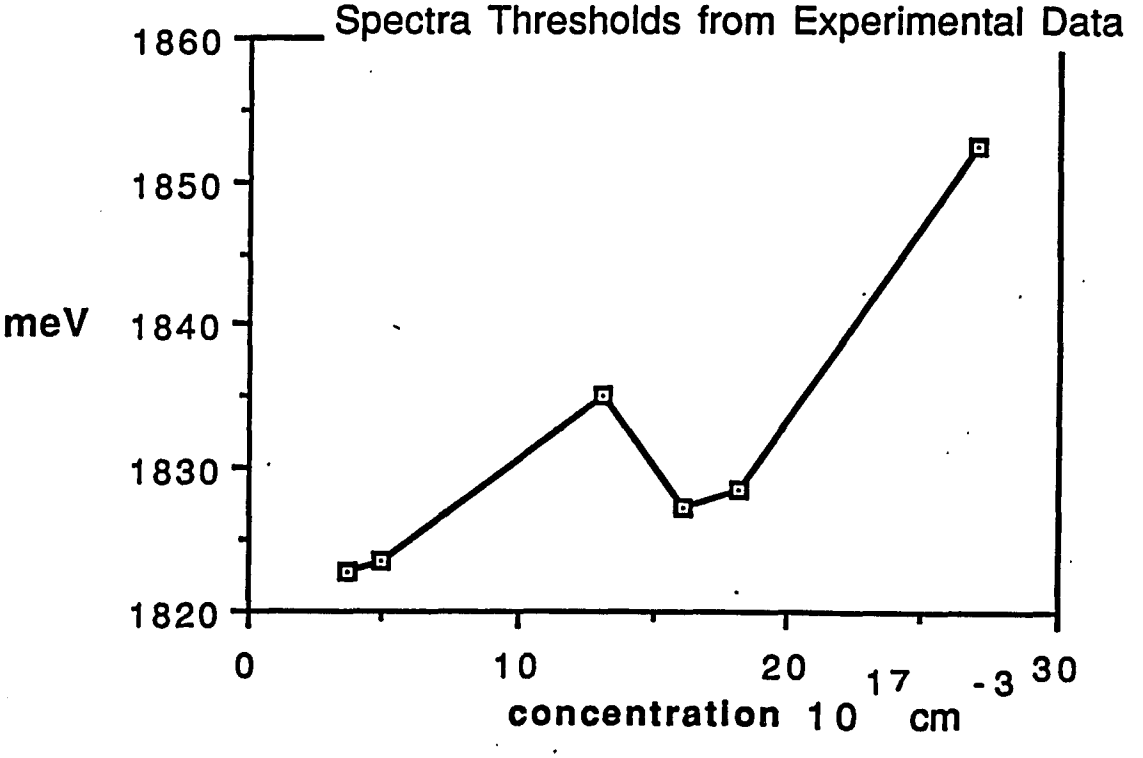

V. RESULTS II

High-Energy Threshold in Metallic Samples: Excitation Spectra

The excitation spectra are obtained by sweeping the exciting laser frequency and detecting the luminescence emitted by the sample at a fixed wavelength. Figures (III-7) (a to d) show the excitation spectra obtained for our CdSe samples. They all show a high-energy region with significant luminescent emission. There is also a sharp drop in the emission occuring **at the same** energy as the high-energy threshold of the luminescence spectra, within experimental uncertainty. At energies below this sharp drop there is usually some, but a considerably reduced level of, emission.

These spectra are certainly what we would expect for recombination between a Fermi electron and a hole at the top of the valence band. Figure (III-8) shows a schematic representation of the band diagram near k=0. For exciting energies higher than the difference between the Fermi level and the top of the valence band, there should be a great deal of absorption and therefore also of luminescence emission. For energies below this difference, absorption should be suppressed to a large extent. The sharp drop in the excitation spectra occur at this energy difference.

Moreover, we have looked for acceptor levels by exploring the luminescence spectra at wavelengths much longer than those corresponding to the high-energy threshold. Given that valence holes[8] are so much heavier than conduction band electrons, one expects the Rydberg for shallow acceptors to be considerably larger than for shallow donors. This is indeed the case; we have found levels higher than 50 meV above the valence band as we shall describe in the next section[9]. The point here is that these levels are quite distant from the high-energy threshold of the luminescence spectra. This is additional evidence against interpreting these thresholds as arising from decay of Fermi electrons into acceptor traps, so we shall assume that they correspond to the decay of Fermi electrons into a thermalized hole at the top of the valence band.

Fig. (III-7a) Excitation spectrum of sample M1. The sharp peak at 6880 A (6900 A for the other samples) is a reference signal. It corresponds to the detection of scattered radiation from the exciting laser light.

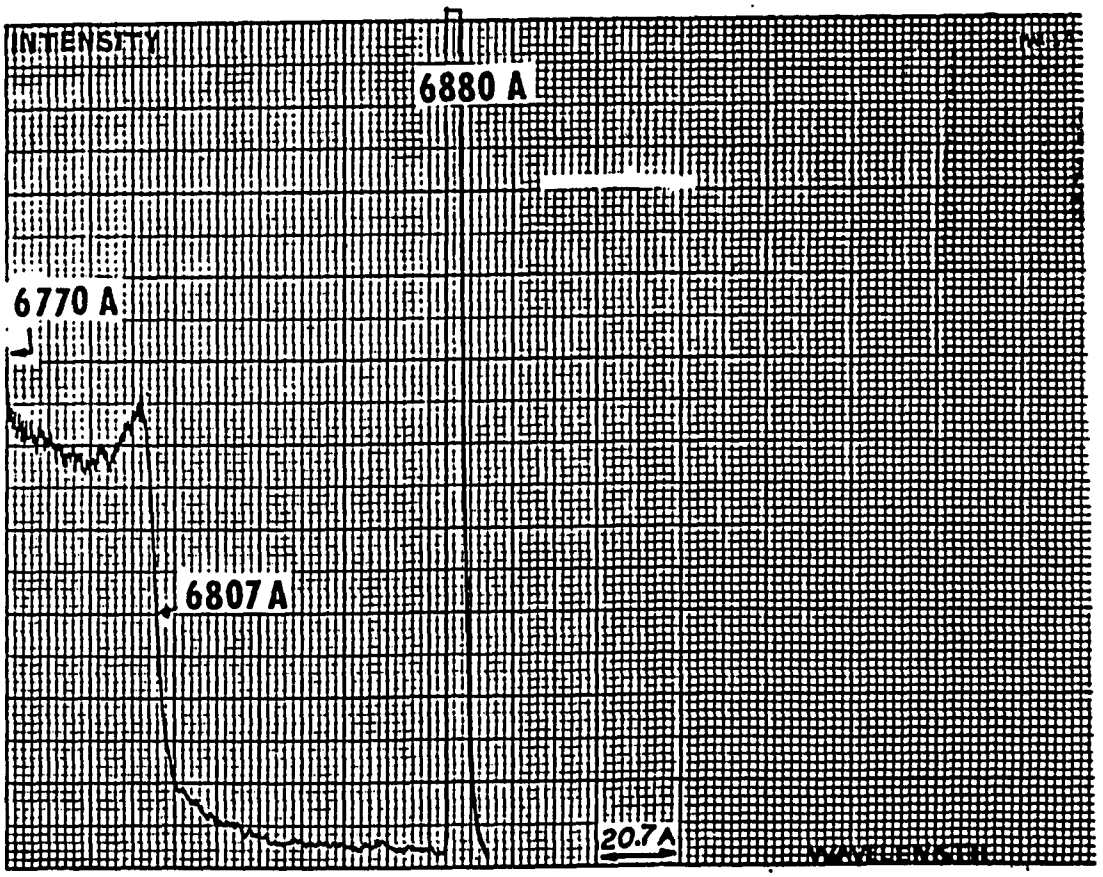

Fig. (III-7b) Excitation spectrum of sample M3.

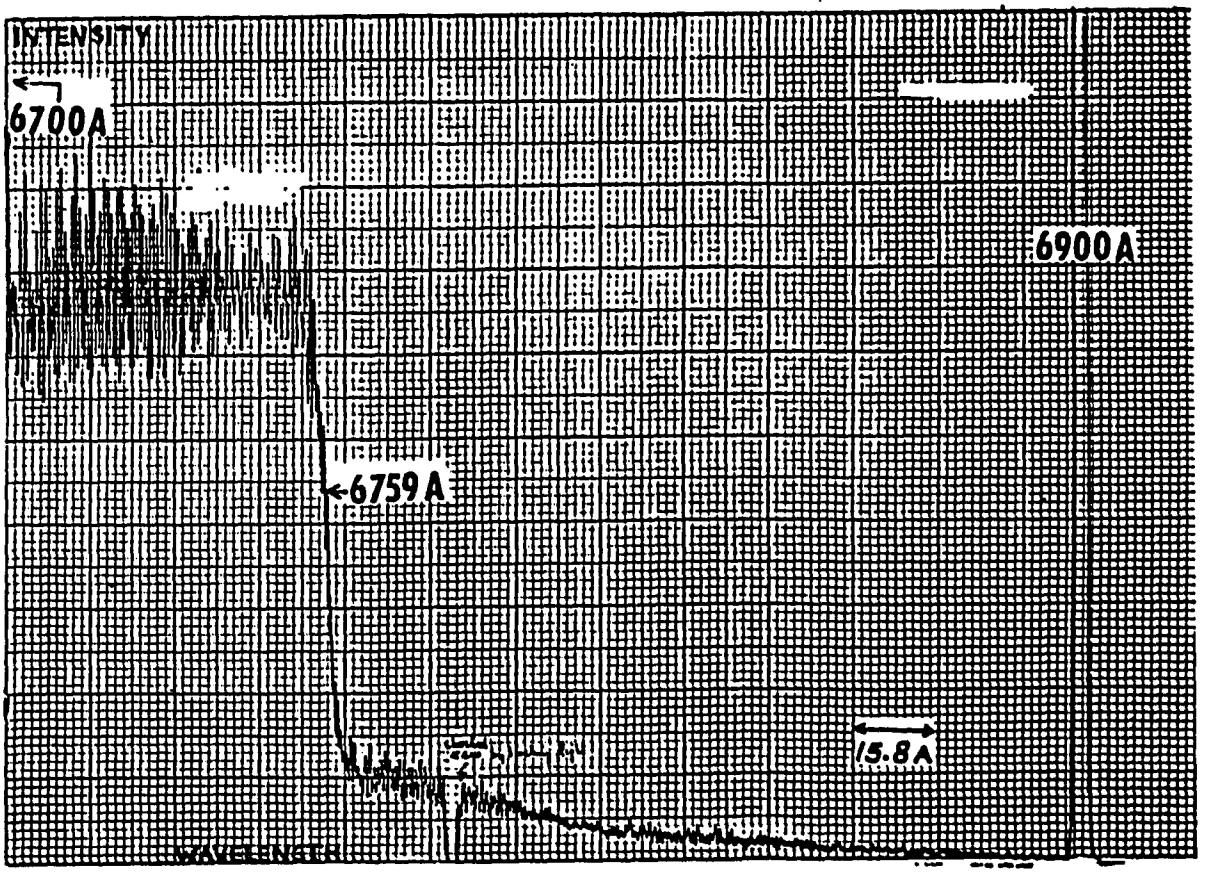

Fig. (III-7c) Excitation spectrum of sample M4.

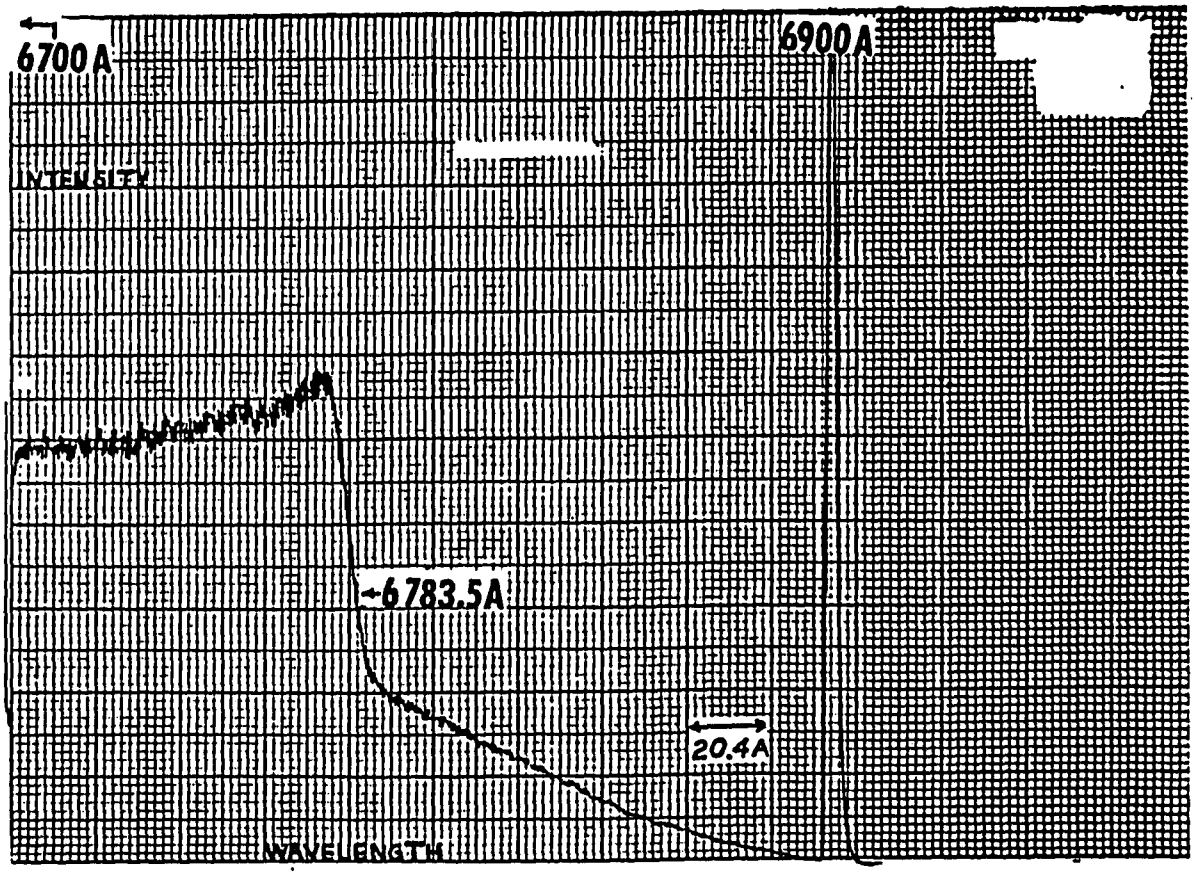

Fig. (III-7d) Excitation spectrum of sample M5.

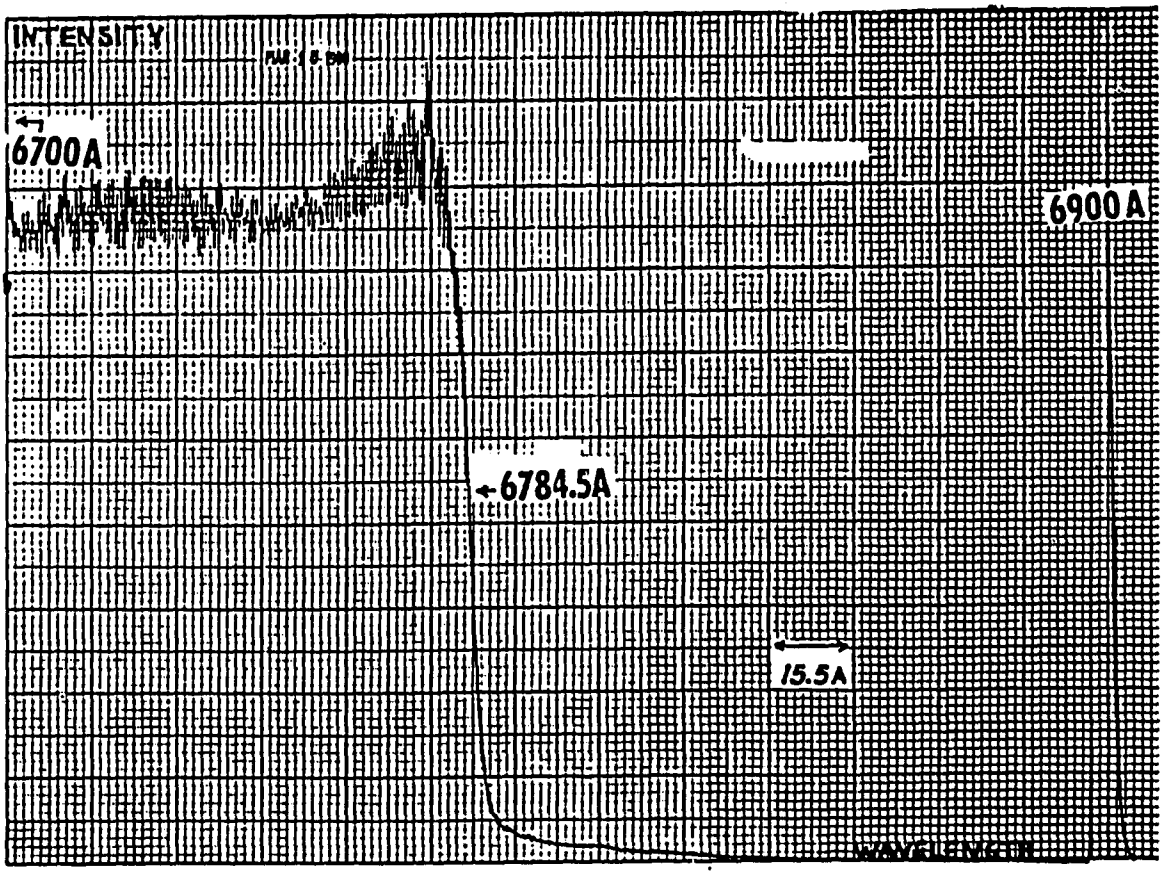

Fig. (III-8) Band diagram for CdSe near k = 0.

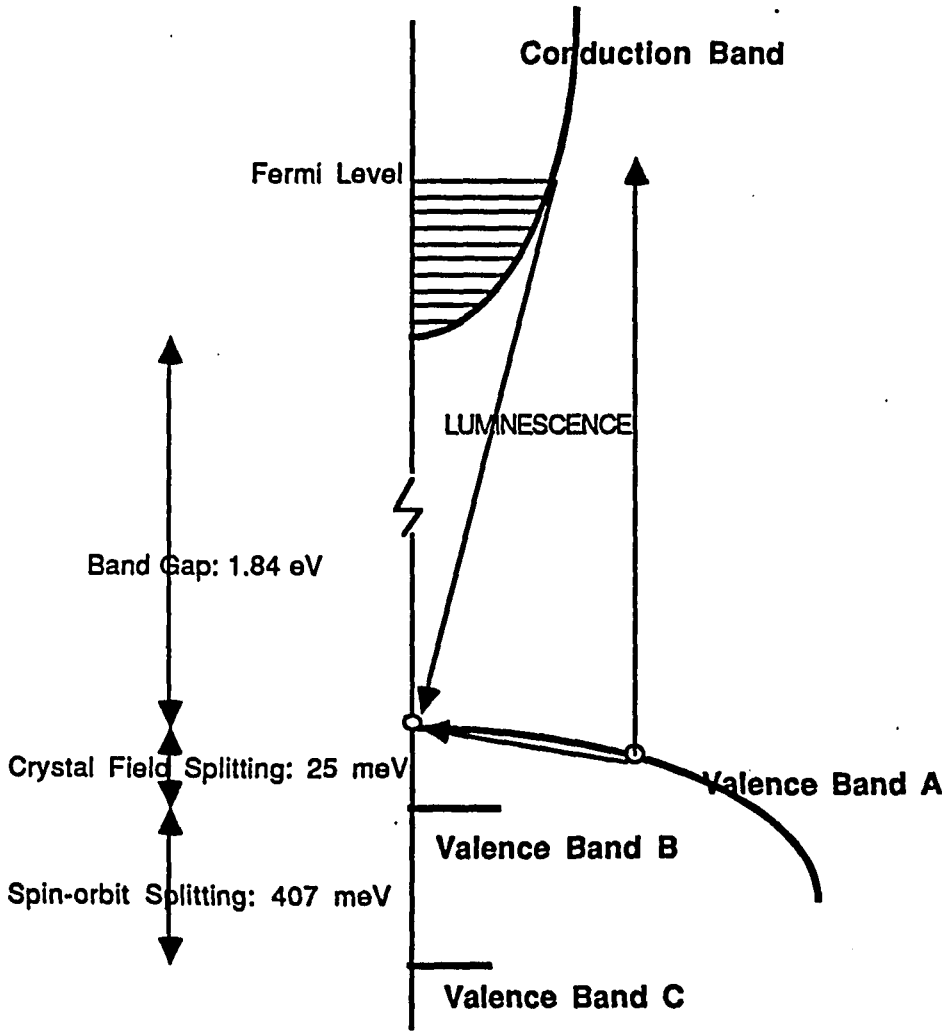

VI. RESULTS III

Long-Wavelength Luminescence: Evidence for Acceptor Levels

When both donors and acceptors are simultaneously present in an insulating crystal, it is possible to absorb a photon by promoting an electron from an acceptor state to a donor state. The recombination of the electron in a donor state back into the acceptor state gives rise to donor-acceptor pair bands in the luminescence spectrum. The energy required to make a donor-acceptor pair transition is[10]

$$E_{DA}(R) = E_G - E^o_A - E^o_B + e^2/\varepsilon R + J_{DA}(R), \qquad (1)$$

where E_G is the band-gap energy and E^o_A and E^o_B are the ionization energies of isolated acceptors and donors, respectively; $e^2/\varepsilon R$ is the Coulomb energy of the two ionized impurity centers separated by a distance R, while $J_{DA}(R)$ is a small correction term due to the interaction between the neutral donor and acceptor.

Luminescence spectra of insulating CdSe, obtained both by C. H. Henry *et al*[11] and by Yu and Hermann[12], are shown in Fig. (III-9). Donor-acceptor pair bands occur at frequencies much below the bound exciton peak. From these bands one can estimate the ionization energy of the acceptors, by using Eq.(1). Henry et. al.[11] thus obtain an approximate ionization energy of 109 meV for substitutional Li and Na, which behave as shallow acceptors in CdSe.

On the basis of our transport data we surmise that most of our metallic samples contain significant levels of compensation. In

fact, compensation plays a central role in explaining the non-monotonic carrier concentration dependence of the upper luminescence threshold in the model presented in section VIII, below. It was thus important for us to find further evidence of the presence of acceptors at these high concentration levels, in particular because of the well known unreliability of transport measurements in the determination of compensation levels.

For samples on the metallic side of the MI transition, donor-acceptor pair recombination develops into recombination of electrons from the Fermi sea into acceptor states. The ionization energy of the acceptors should still play a key role in determining the energy of the photons emitted in these transitions. Note that this ionization energy is bound to be affected by the presence of the Fermi sea of electrons through the Coulomb interaction. Moreover, given the large mass of valence electrons, and therefore the small size of Bohr radii for shallow acceptor states, central cell corrections to this energy may be non-negligible. It would not be surprising, therefore, if the ionization energy of the as yet undetermined acceptor impurities in our metallic CdSe samples turned out to be different from the 109 meV for substitutional Li and Na in insulating CdSe observed by Henry *et al*.[11]

Using the ionization energy value of 109 meV as a rough guide, we expected the luminescence emission coming from recombination of Fermi electrons into acceptor states to occur at wavelengths around 7100 A. We investigated the region between 6900 A and 7400 A.

Fig. (III-9) Luminescence spectra for insulating CdSe.*

The top figure shows data obtained by Henry *et al.* I_1 and I_2 denote excitons bound to acceptor and donor impurities, repectively. The donor-acceptor pair band peak occurs at 7180 A. The bottom figure shows data taken by Yu and Hermann. I_{2A} denotes the A exciton bound to a donor impurity. The donor-acceptor pair band is denoted by D_1. All samples are doped substitutionally with Li or Na, which act as acceptors in CdSe. Interstitial Li and Na are also present.

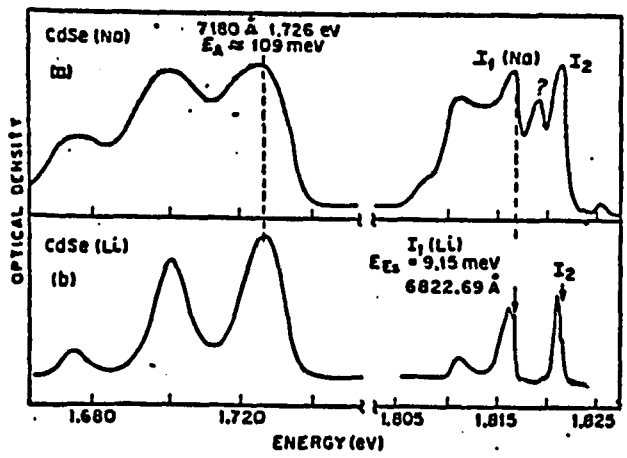

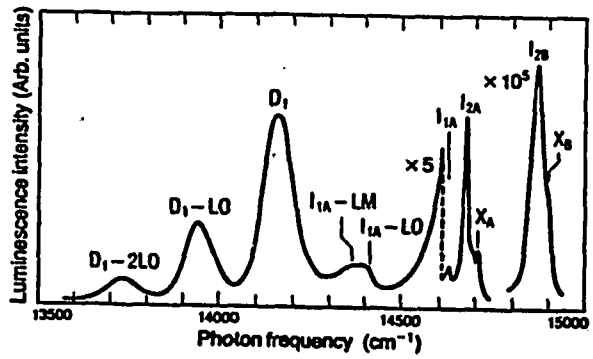

* Reprinted by permission of the American Institute of Physics, New York, New York.

Figures (III-10) (a) and (b) show the luminescence spectra of samples M3 and M5 obtained by exciting with light of 6600 A wavelength. These photons are energetic enough to excite valence electrons above the Fermi level, so that the signal from electrons ionizing the acceptor impurities is masked to a greater or lesser extent by the tail of the main luminescence line. For sample M5 we observe a peak near 7100 A, corresponding to 82 meV below the high-energy threshold for this sample. The jump occuring at 6900 A in both spectra is an artifact of removing a filter in order to increase the power of the exciting light and magnify the signal detected by the spectrometer.

Fig. (III-10a) Luminescence spectrum of sample M3 including long wavelength portion. The excitation light wavelength is 6600 A.

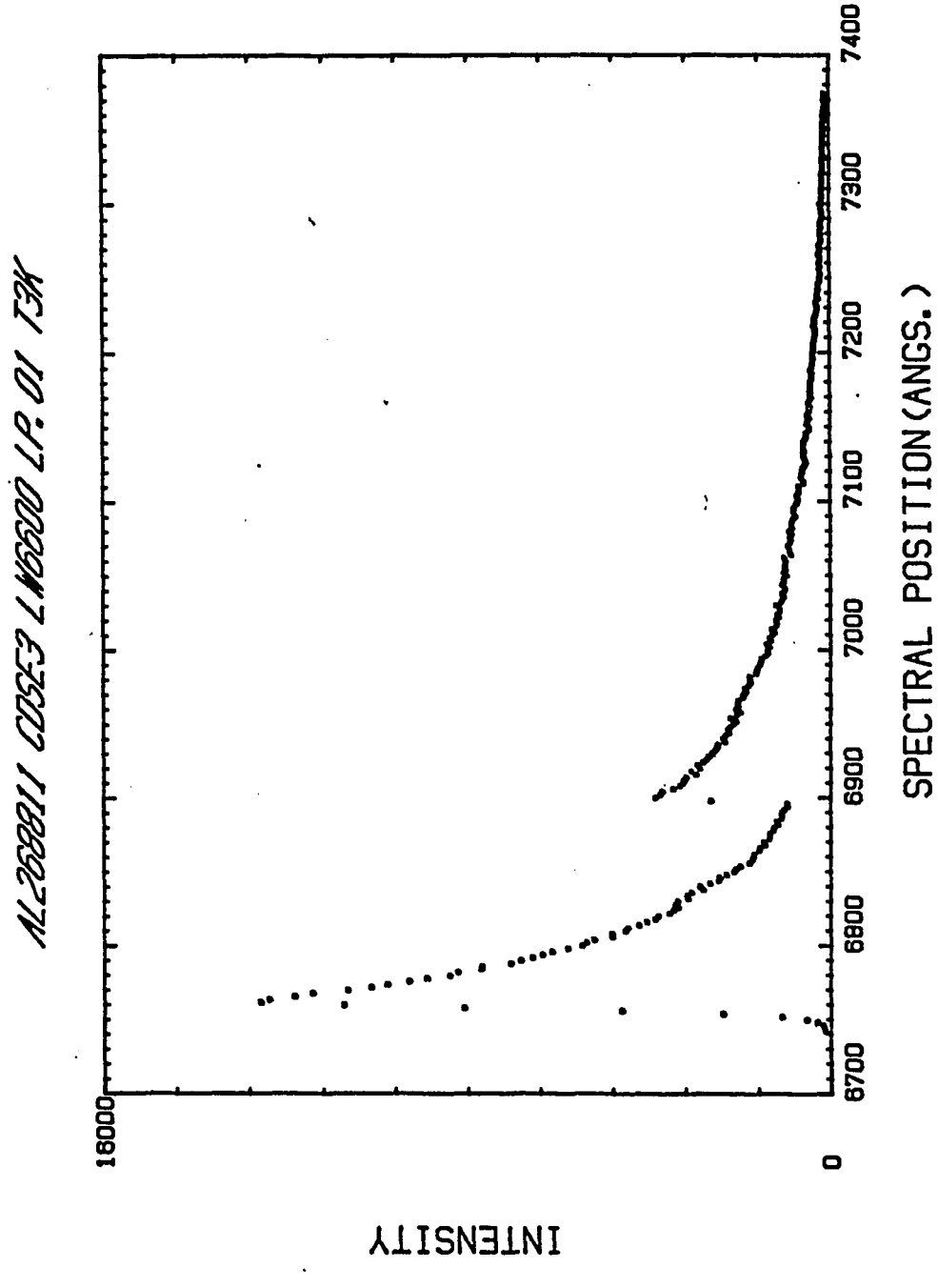

Fig. (III-10b) Luminescence spectrum of sample M5 including long wavelength portion. The excitation light wavelength is 6600 A. Long wavelength peak corresponds to recombination into acceptor states.

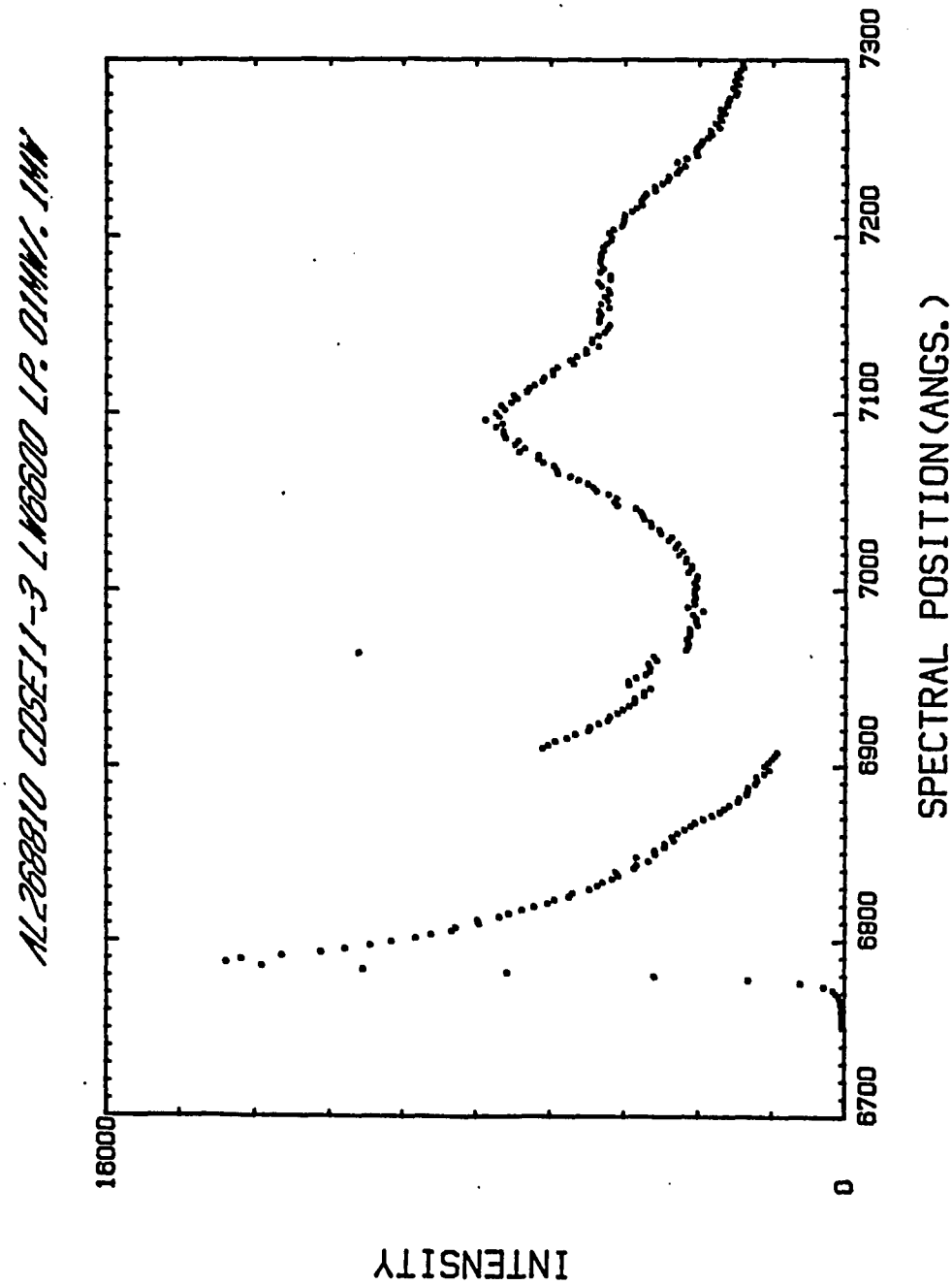

The main purpose of the above spectra is to indicate the relative strength of the long wavelength signals from samples M3 and M5. Below we show that this signal is also present in the case of sample M3. The fact that it is barely distinguishable from the tail in the spectrum (it shows as a little bump around 6970 A), suggests a considerably larger compensation in M5 than in M3.

Figures (III-11) (a), (b) and (c) show the long-wavelength luminescence spectra of samples M3 and M5 obtained by pumping with light of wavelengths 6850 A and 6970 A. These photons cannot excite valence electrons above the Fermi level, so that the tail of the main luminescence line is eliminated. We can then clearly observe a peak for sample M3 occuring close to 6970 A.

Note that the position of the peak is independent of exciting wavelength as shown for the case of sample M5 by Figs. (III-11) (b) and (c). The low energy shoulder in all figures is probably a phonon replica of the peak since it occurs approximately 25 meV away. The longitudinal optical phonon energy is 26.2 meV.

As far as we know this is the first time that recombination into acceptor states has been observed in n-doped semiconductors with carrier concentrations above the metal-insulator transition.

Fig. (III-11a) Long-wavelength luminescence spectrum for sample M3. Low energy exciting radiation was used to suppress the luminescence arising from the decay of electrons into the top of the valence band. This enables us to see the long wavelength peak coming from recombination with acceptor states above the valence band.

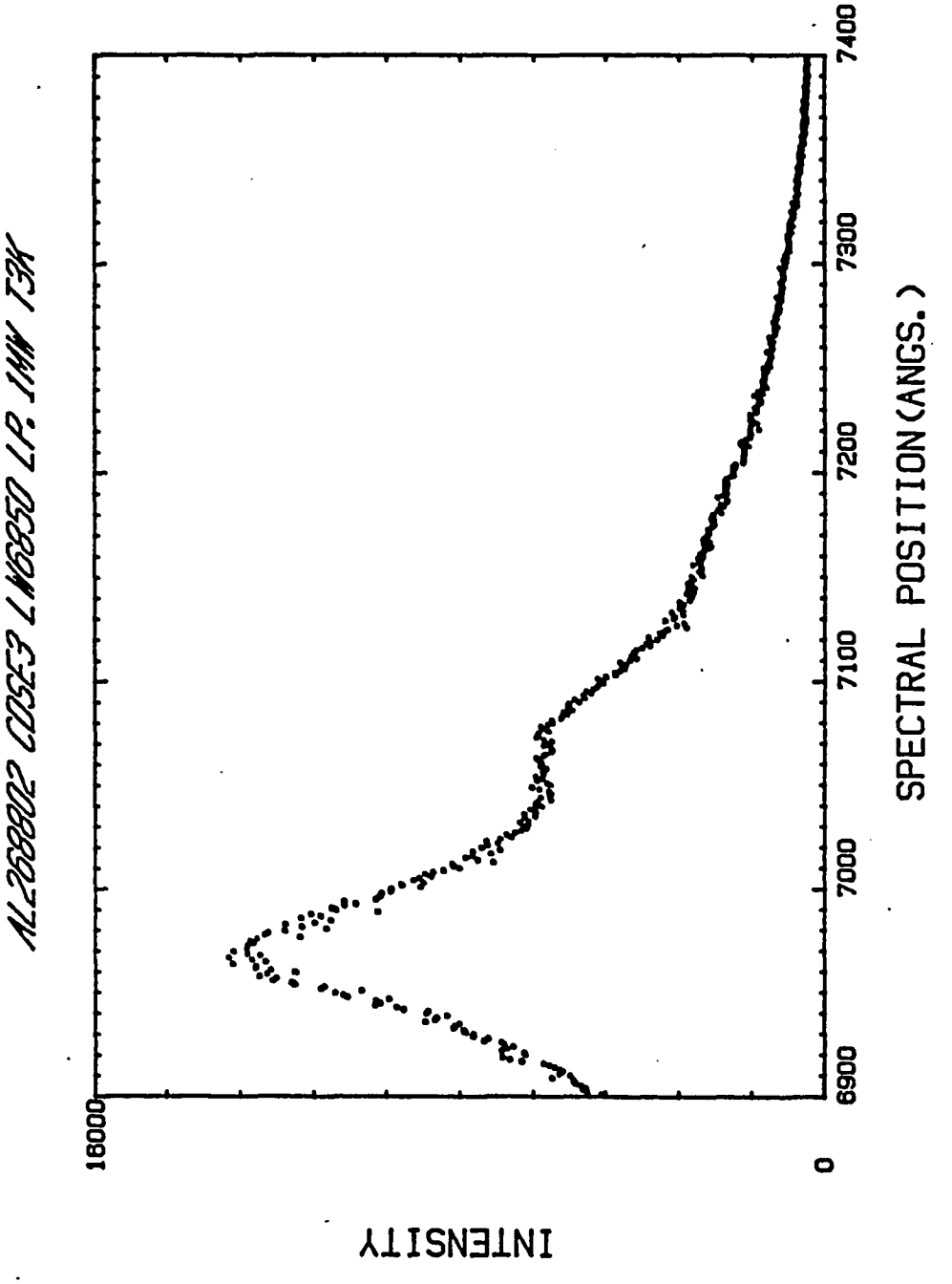

Fig. (III-11b) Long wavelength luminescence spectrum for sample M5. Exciting light wavelength is 6850 A.

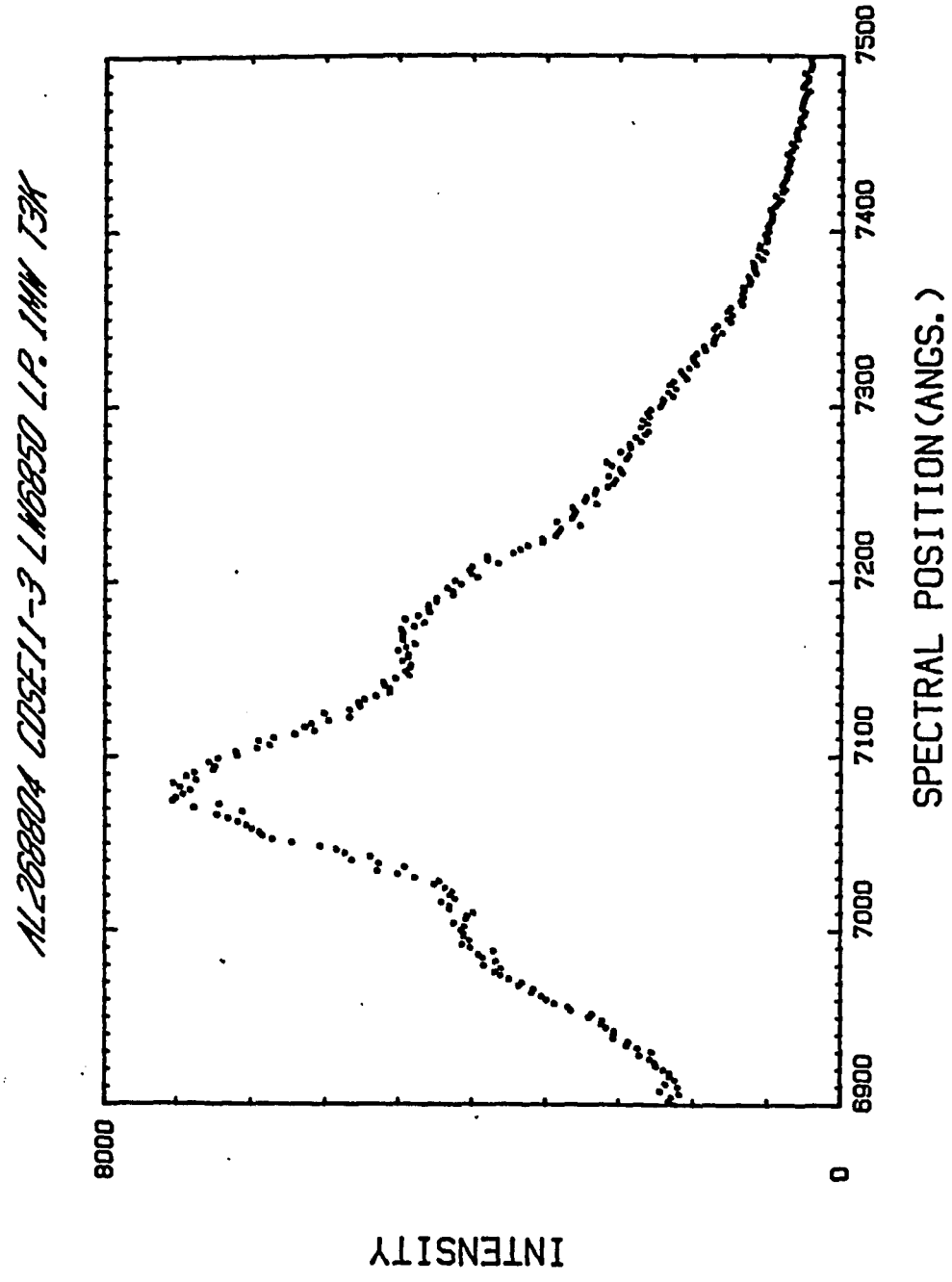

Fig. (III-11c) Long wavelength luminescence spectrum for sample M5. Exciting light wavelength is 6970 A. Note, by comparing with Fig. (III-10b) that the position of the peak is independent of exciting light wavelength.

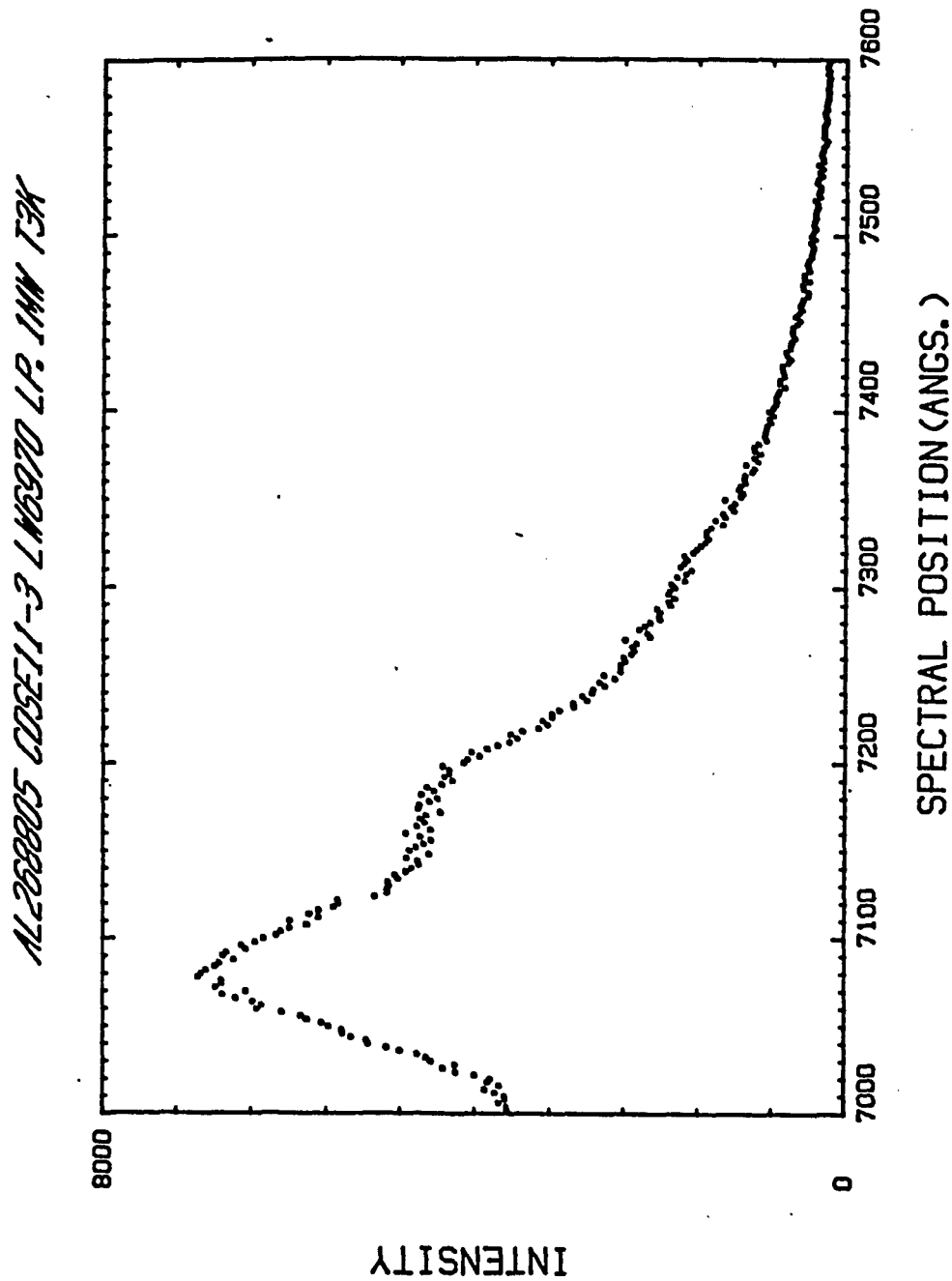

VII. APPLICATION OF GIRVIN'S MODEL TO CdSe

We calculate here the luminescence spectrum threshold by evaluating the energy emitted when an electron from the Fermi surface in the conduction band recombines with a hole at the top of the valence band. Following Girvin[1] we consider the following sources of electric potential which perturb the electron and hole energy levels: (i) phonons, (ii)electron-electron interaction, (iii) electron-hole interaction, (iv) random impurity potential.

The effect of the indium impurities is first evaluated by assuming that they are distributed on a periodic superlattice within the CdSe lattice, similarly to the treatment of Girvin for the case of CdS. The electric potential generated by this superlattice of positive point charges is calculated following the model of Wigner and Huntington[13] for the metallic hydrogen system. This treatment of the effect of the random impurity potential suffers from the obvious weakness that the impurity centers are considered as a regular array. Moreover, no consideration is given to the role of the acceptor impurities, which are present in significant numbers due to the heavy compensation in the samples. In the next section we attempt to remedy these omissions with a model for the effect of the random impurities based on work by L. Vina and M. Cardona.[4,5]

i) Phonons

a) Electron-phonon coupling.

The high level of doping present in the samples used in this study has a significant effect on the strength of the electron-phonon coupling and leads to important corrections to the electronic chemical potential. The formation of an interacting electron gas impinges on the strength of this coupling through the dielectric screening of the electric field associated with lattice distortions.[14]

The electronic coupling to longitudinal optical phonons has been treated by H. Frohlich[15] in his classic work on the effect of lattice fields on electrons in ionic crystals. According to Frohlich, the electron-phonon coupling is given by

$$V = \sum_{k,q} \left[\frac{4\pi e^2 \hbar\omega_{LO}}{\Omega q^2} \frac{1}{2} \left(\frac{1}{\varepsilon_\infty} - \frac{1}{\varepsilon_0} \right) \right]^{1/2} C^+_{k+q} C_k (B^+_{-q} + B_q), \qquad (2)$$

where ε_∞ and ε_0 are the high- and low-frequency dielectric constants, Ω is the volume of the sample, C^+_k is the electron creation operator, and B^+_q is the phonon creation operator.

This coupling leads to a correction to the conduction-band energy ΔE given by

$$\Delta E = -\alpha\hbar\omega_{LO} \qquad (3)$$

and a shift in the observed effective mass given by

$$m = m^*[1 - (1/6)\,\alpha], \qquad (4)$$

where α is the polaron coupling constant ($\alpha = 0.43$ in CdSe), m^* is the observed mass, and m is the bare conduction-band mass. [16]

The reason for the importance of the dielectric screening by the electron gas can be seen from the numbers in Table III-1. The electron plasma frequency ω_p for the highest density sample is approximately three times larger than the LO-phonon frequency. This means that the electron gas has time to respond to and partially cancel out the relatively slowly varying electric field associated with the lattice vibrations. This leads to a weakening of the electron-phonon coupling and a reduction in the LO phonon frequency.

Girvin argues that as a result of screening and exclusion effects which partially suppress the electron-phonon interaction, the screened polaron contribution to the electron chemical potential is quite small in his case (approximately 1 meV). Given that the unscreened electron-phonon coupling in CdSe is even weaker than in CdS, and that the screening is approximately as effective in both cases (ω_p/ω_{LO} are comparable), it seems safe to assume that the screened polaron contribution can also be neglected in our case. This is not quite true for samples M1 and M2, and our approximation will lead to overcorrections in the Fermi energy of these samples.

TABLE III-1. Plasma frequency based on the bare conduction-band mass and the high-frequency dielectric constant.
$\hbar\omega_{LO} = 26.2$ meV.

SAMPLE	$\hbar\omega_p$ (meV)
M1	26.2
M2	30.5
M3	49.6
M4	54.7
M5	58.2
M7	71.1

b) Screened valence polaron.

The screened valence hole-phonon coupling is larger than the screened electron-phonon coupling for conduction electrons and must be taken explicitly into account. The valence hole is more strongly coupled to the phonons due to its heavier mass. Moreover, it is not subject to exclusion effects since it is distinguishable from Fermi sea electrons, so there is no suppression of the hole-phonon interaction on this account.

According to Girvin,[1] the lowest order energy shift (in the hole-phonon couling constant) for the valence hole due to its

interaction with optical phonons in the presence of screening is given by

$$\Delta E = -\left(\frac{\omega_{LO}}{\omega_{TO}}\right)^{1/2} \frac{\alpha_\perp \hbar\omega_{LO}}{2} \left\{ \frac{-K}{(1-K^2)(1+K\sqrt{R})} - \frac{2(K^2-2)}{(1-R)^{1/2}(1-K^2)^{3/2}} \arctan\left[\sqrt{\frac{1-K}{1+K}}\frac{1-\sqrt{R}}{1+\sqrt{R}}\right] \right\}$$

for $K < 1$. The parameter K is defined by

$$K \equiv \sqrt{m / M_\perp}\, k_{TF} R_P^*,$$

where k_{TF} is the Thomas-Fermi wave vector and R_P^* is the screened polaron radius given by

$$R_P^* = a_0 \sqrt{|ry / \hbar\omega_{TO}|},$$

where ry is the effective Rydberg (based on the bare conduction band mass), and a_0 is the effective Bohr radius. The parameter R is defined by

$$R \equiv M_\perp / M_\parallel,$$

where the above masses refer, respectively, to the bare valence band masses perpendicular and parallel to the c-axis of the crystal. Finally,

$$\alpha_\perp \equiv (M_\perp / m)^{1/2} \alpha,$$

where α is the conduction band polaron coupling constant. According to Girvin,[1] the unscreened polaronic correction to the valence band energy is given by

$$\Delta E = \alpha_{\perp} \hbar\omega_{LO} \arcsin (1-R)^{1/2} / (1-R)^{1/2},$$

where all the parameters are as defined above.

ii) Electron-electron interaction

Because of the large Bohr radius in CdSe, the dimensionless inter-electron spacing parameter $r_s = [(4\pi/3)na_o^3]^{-1/3}$ ranges over values comparable to that of ordinary metallic elements, as shown in Table III-2; here n is the electron density and a_o is the effective Bohr radius. We must therefore take care to use an expression for the electron-electron interaction which is applicable in this regime. A number of treatments exist for the correlation energy of an interacting electron gas. That of Nozieres and Pines[17], based on an approximate interpolation between the contributions to the system energy arising from the long and short wavelength parts of the Coulomb interaction, applies in this density regime. The result obtained by these authors for the correlation energy is

$$E_c \cong (-0.115 + 0.031 \ln r_s) ry. \qquad (5)$$

Here ry stands for the effective Rydberg. Together with the Hartree-Fock terms, this expression gives the average energy shift per electron due to electron-electron interactions.

This expression must be modified to give the shift in the Fermi energy $\Delta\varepsilon_F$ due to correlations. We use Seitz's Theorem[18] for this, namely

$$\Delta\varepsilon_F = E_c + n\frac{\partial E_c}{\partial n}, \qquad (6)$$

where n stands for electron density.

The full expression for the Fermi level ε_F, in terms of the Fermi wave vector, k_F, and the Bohr radius, a_o, is thus

$$\varepsilon_F = \{(k_F a_o)^2 - (2/\pi)(k_F a_o) - 0.031\ \ln[\alpha(k_F a_o)] - 0.125\}ry \qquad (7)$$

where $\alpha = (4/9\pi)^{1/3}$. The first and second terms are, respectively, the kinetic energy of degeneracy and the exchange energy. The remaining terms represent the correlation energy. This treatment assumes that the electrons are imbedded in a uniform positive background.[19]

TABLE III-2. Inter-electron spacing parameter r_s, based on the bare conduction band mass and the high-frequency dielectric constant.

SAMPLE	r_s
M1	3.15
M2	2.84
M3	2.06
M4	1.93
M5	1.85
M7	1.62

iii) Electron-hole interaction

Here we study the correlation energy arising from the polarization of the electron gas by the valence hole. The quantity calculated is the self-energy of the valence hole treated to lowest order in perturbation theory including the dynamical screening of the interaction by the electron gas. The screening is treated in the random phase approximation. This correlation energy is given by

$$\Delta E = -\frac{\hbar}{\pi(2\pi)^3}\int d^3q \int_0^\infty d\omega \frac{4\pi e^2}{\varepsilon_\infty}\frac{1}{q^2}\,\mathrm{Im}\left[\frac{-1}{\varepsilon(q,\omega)}\right]\frac{1}{T(\vec{q})+\hbar\omega}, \qquad (8)$$

where $T(\mathbf{q})$ is the kinetic energy in the (anisotropic) valence band, and $\varepsilon(q,\omega)$ is Lindhard's dielectric function for the electron gas.[20]

Eq. (8) was evaluated numerically. Details of the procedure, as well as the text of the program used for the numerical evaluation are presented in Appendix II.

Approximations to the effect of the lattice dielectric screening lead to estimates of upper and lower bounds for the contribution of the electron-hole interaction to the Fermi energy. These approximations are also discussed in Appendix II.

iv) Interaction with impurity centers

Eq. (7) for the Fermi energy is obtained under the assumption that the electrons move in a uniform positive background. It is important that we correct for this assumption, because the interaction with the ionized impurity centers plays a very important role in explaining our observations.

As a first approximation we model the impurity centers as a regular array of ionized hydrogenic atoms embedded in the CdSe crystal. This follows the original model used by Girvin[1] to explain CdS luminescence data on the metallic side of the metal-insulator transition. This treatment, which assumes also that the crystal is uncompensated, fails to explain the smaller high-energy thresholds of samples M4 and M5 relative to that of the less concentrated sample M3. In the next section we shall introduce a model which takes into account both the randomness of the impurity potential as well as the presence of compensation. This latter treatment is capable of accounting for the main features of our luminescence data.

Girvin's treatment of the impurity potential makes use of the fact that the impurity centers appear hydrogenic against the crystal background. This is true both in CdS and in CdSe, and is due to the small size of the electronic core relative to the effective Bohr radius of the donors (a_0 = 38.3 A). This picture is confirmed by the fact that the donor binding energy[21] (19.5 meV) is very close to the Rydberg ($e^2/2a_0\epsilon_0$ = 20.0 meV).

We shall therefore assume initially that the indium donors are distributed on a periodic superlattice within the CdSe lattice. The sole effect of the CdSe lattice is assumed to be to provide a dielectric background, with dielectric constant equal to ϵ_0. With these assumptions, the indium superlattice system is equivalent, except for scale factors, to the metallic hydrogen system first studied by Wigner and Huntington.[13]

The energy of an electron due to its interaction with the hydrogenic ions is calculated by Wigner and Huntington using the Wigner-Seitz method. This energy is obtained by approximating the solution to the Schrodinger equation for a single electron in the presence of the ions and subtracting out the kinetic energy of the electron[22]. It is given by

$$\frac{E_H}{ry} = -\frac{3}{r_s} - \frac{1.85}{20.2 - 2.65r_s - \frac{6.72\mu^2}{20.2 - 0.6r_s}} - 0.0093 \quad , \qquad (9)$$

where $\mu = 3.84/r_s$, r_s is the dimensionless interelectron spacing, and ry is the effective rydberg. The conduction band bottom in metallic

hydrogen is obtained by taking $\mu = 0$. The corrections to this value for electrons with wave vectors k not equal to zero are very small.

We must now subtract out the interaction of the electron with the uniform positive background assumed in the previous section, and replace it with the above interaction. For a uniform positive background in the Wigner-Seitz cell, the electronic wave function at the band bottom is essentially flat. In that case, the energy of interaction between the electron and the positive background is given by $E_o = -2.4\ ry/r_s$. If we approximate the wave functions for higher wave vector by plane waves, the interaction energy is still given by the same formula. All parameters are based on the low frequency dielectric constant ε_o.

v) Wave vector non-conservation

The above calculation of the high-energy threshold location assumes that Fermi surface electrons can recombine with holes at the top of the valence band. Here we make some comments on the validity of this assumption.

Typical luminescence recombination times in CdSe are close to 200 picoseconds,[23] while valence hole thermalization times are much shorter, typically close to the inverse of a phonon frequency, or 25 femtoseconds for CdSe.[23] One would therefore expect most of the Fermi electron-valence hole recombinations in the kind of luminescence experiments we performed to occur with thermalized holes at the top of the valence band, unless forbidden by wave vector conservation.

S. M. Girvin[1] has argued that for heavily doped CdS samples --the same would be true for CdSe samples,--the radial momentum distribution for the lowest-energy valence hole becomes so broad that the $\Delta k = 0$ rule must completely break down. This is a consequence of impurity scattering, which strongly affects the valence hole momentum distribution because the density of scatterers is so large and because the hole is relatively heavy and not subject to exclusion principle constraints. In more picturesque language one could say that the random impurity distribution breaks the translational symmetry of the crystal and allows the $\Delta k = 0$ rule to be violated. This effect has been verified experimentally by J. I. Pankove and P. Aigrain[24] who carried out measurements of the absorption spectrum of doped germanium. They found that the strength of the indirect absorption threshold (which required a very large momentum transfer relative to the Fermi momentum of the present problem) rose rapidly with impurity density.

This shows that we are justified in assuming that Fermi electrons are allowed to recombine with thermalized holes at the top of the valence band.

vi) Results

In Table III-3 we list the various contributions to the theoretical calculation of the threshold location based on the Girvin model, presented above. Figure (III-12) shows a plot of the predicted thresholds, as a function of carrier concentration, as well as the thresholds as determined from experiment. The model predicts a monotonically increasing threshold with carrier

concentration. The size of the difference between theoretical and experimental results, close to 10 meV or less, is comparable with the results obtained by Girvin for CdS.

TABLE III-3. Energies (in meV) relevant to the calculation of the spectrum threshold. (A) Fermi energy of the interacting electron gas. (B) Energy of interaction of the Fermi electrons with hydrogenic ions in the Wigner-Huntington metallic hydrogen model. (C) Band bottom with uniform positive background. Relaxation energy of the electron gas around the valence hole: (D) upper bound; (E) lower bound. (F) Bare conduction band polaron energy. (G) Bare valence band polaron energy. (H) Screened valence polaron energy. Sum of all these terms plus the uncorrected fundamental band gap for undoped CdSe at 4.2 K, 1840 meV, giving a predicted spectrum threshold: (J) upper bound; (K) lower bound.

SAMPLE	A	B	C	D	E	F	G	H	J	K
M1	-4.4	-29.6	21.3	-19.0	-23.0	11.2	25.2	-8.1	1836.5	1832.6
M2	-2.8	-32.4	23.6	-20.0	-24.3	11.2	25.2	-7.6	1837.1	1832.9
M3	7.2	-43.4	32.5	-24.2	-29.6	11.2	25.2	-5.6	1842.8	1837.4
M4	10.7	-46.4	34.8	-25.1	-30.8	11.2	25.2	-5.0	1845.3	1839.6
M5	13.1	-48.0	36.1	-25.7	-31.6	11.2	25.2	-4.6	1847.2	1841.3
M7	22.6	-54.7	41.4	-27.7	-34.2	11.2	25.2	-3.2	1854.8	1848.2

Fig. (III-12). High energy threshold predictions for CdSe on the basis of the original Girvin model. Experimental results are also plotted for reference. Note the monotonic character of the theoretical predictions, in contrast to the experimental observations.

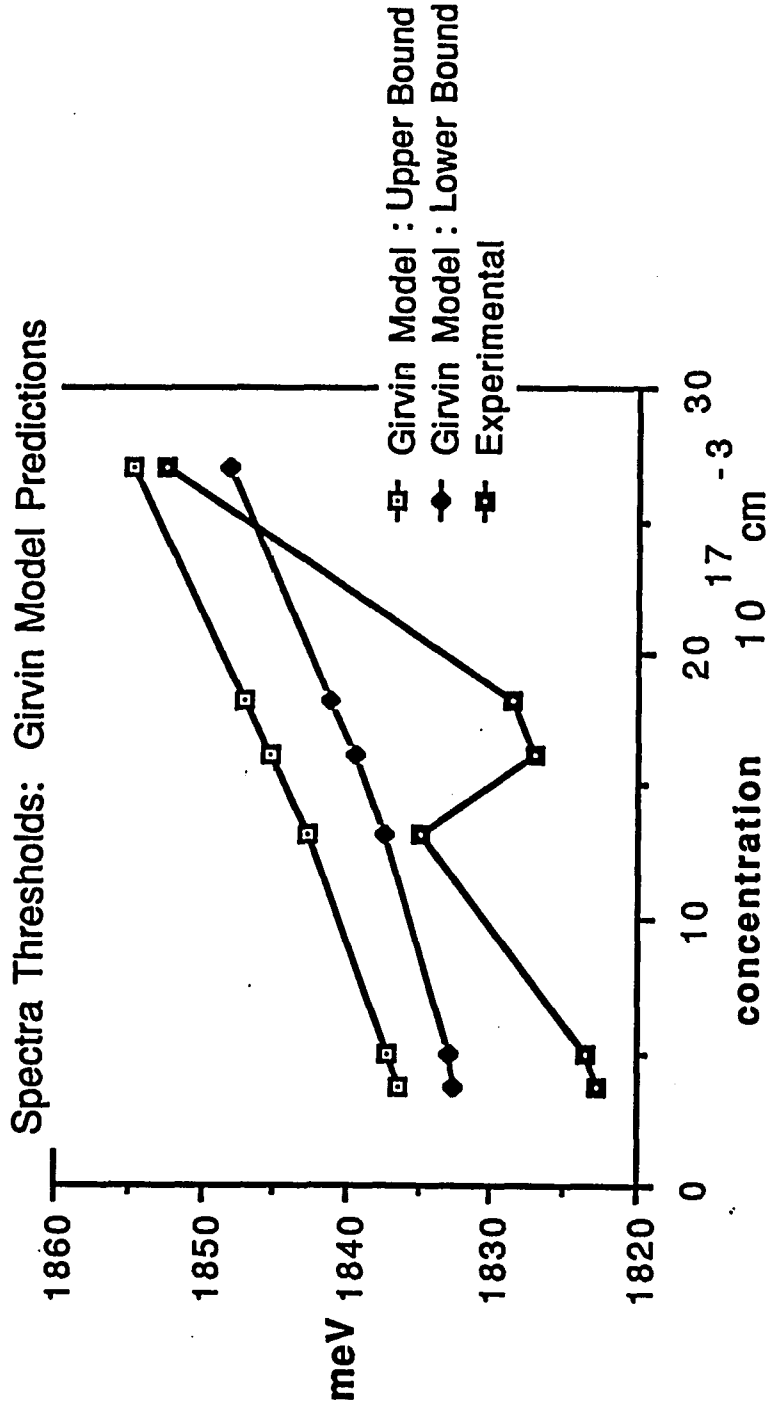

VIII. EFFECT OF COMPENSATION ON THE HIGH-ENERGY THRESHOLD: A MODEL

In Section VII we presented a model, due to Girvin, for the calculation of the high-energy threshold of the luminescence spectra for samples on the metallic side of the MI transition. This model predicts a monotonically increasing value of the threshold with increasing carrier concentration, as shown in Fig. (III-12). The experimentally determined thresholds, however, do exhibit a clear break in such a monotonic increase, between samples M3, on the one hand, and M4 and M5, on the other. This is also shown in Fig. (III-12).

One important element missing in the above model is the effect of compensation on the value of the threshold. In this section we present a modification of the Girvin treatment which allows us to model the effects of compensation. This model, based on work by L.Vina and M. Cardona,[4,5] is capable of reproducing the observed non-monotonic behavior of the high-energy threshold.

i) Vina-Cardona model for Band gap renormalization

Vina and Cardona treat the effect of impurities to second order in perturbation theory for the case of uncompensated semiconductors. Their perturbation Hamiltonian is given by the difference between the crystal potential with and without impurities present. They assume that the impurities are randomly distributed in the crystal, and that the perturbing potential can be

written as a sum of identical localized potentials centered at the impurity sites. The impurity centers are treated as screened "hydrogenic" Coulomb scatterers. The calculation assumes: a)dielectric screening by the lattice, and b)Lindhard dielectric screening by the electron gas.

The Vina-Cardona treatment represents a refinement over the Wigner model presented in the previous section in that, a)the electron screening is treated in a more sophisticated fashion, since the Wigner model assumes no screening inside a 'Wigner-Seitz' cell around the ion cores in the regular hydrogenic superlattice, and complete screening outside, and b)the impurity centers are assumed by Vina and Cardona to be randomly distributed in the crystal. Neither treatment, however, assumes multi-ion screening by the electron gas.

The band gap renormalization predicted by Vina and Cardona[4,5] is given by

$$\Delta E = a N_I^{\alpha}, \qquad (10)$$

where a and α are constants which depend on the band structure of the crystal, and the type of impurity scatterer[25], and N_I is the density of impurity scattering centers. The exponent α is predicted to lie between the values $\alpha=1/3$ and $\alpha=1$. Note that the Wigner model presented in Section VII, part v, predicts an α of 1/3.

This model was applied by Vina and Cardona to the case of heavily doped silicon and germanium for the study of band gap renormalization not only for the fundamental band gap but also for bands higher than the conduction band, for indirect and direct band

gap transitions. They studied the effects of both donor and acceptor dopants, on both sides of the metal-insulator transition, for a wide range of doping concentrations. Their calculated values of α yield close agreement with experiment. The experiments could not distinguish differences in α between donors and acceptors within the experimental scatter (of about 10% in α), but the calculated values differed by no more than 10%. Plots of the shifts in band gap energy for various band edges, from Refs. 4 and 5, for the case of silicon and germanium are shown in Fig. (III-13). All the shifts are toward lower energies.[26]

Fig. (III-13) Plots of the shifts in band gap energy for silicon and germanium for various band edges. These plots were obtained by Vina and Cardona, and are taken from Refs. 4 and 5.*

Th e horizontal axes correspond to doping concentration. The vertical axes correspond to band gap shift in meV.

The band gap shifts plotted below correspond to the following interband transitions:

A)For silicon: The energy E_1 is due to transitions between the highest valence band and the lowest conduction band along the Λ direction in the Brillouin zone (BZ) in a region from approximately $k = (\pi/4a)(1,1,1)$ to the edge of the BZ (L point). The region where the E_2 transition takes place is not very well defined, but corresponds to a higher interband transition.

B)For germ anium: The E'_0 gap corresponds to transitions between the $\Gamma_{25'}$ valence band and the Γ_{15} conduction band. The E_1 gap is related to transitions along the Λ direction of the BZ between the Λ_6 and the Λ_{4-5} valence bands to the Λ_1 conduction band. The E_2 transition is not very well defined.

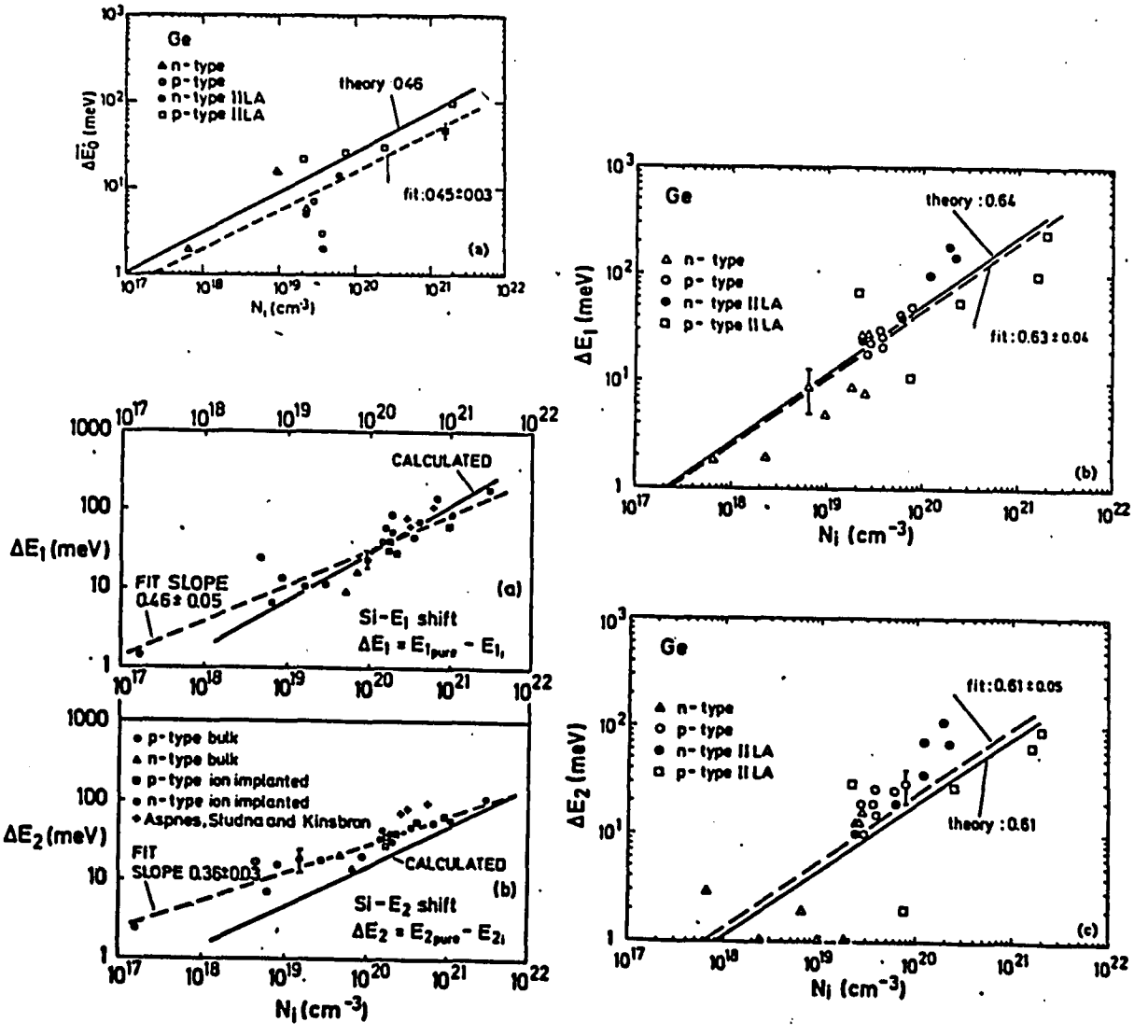

* Reprinted by permission of the American Institute of Physics, New York, New York.

ii) Band gap renormalization for compensated samples: a model

We model the band gap renormalization in the presence of donor and acceptor scatterers by adding a term to Eq. (10), so that

$$\Delta E = a_A N_A^{\alpha} + a_D N_D^{\alpha}, \qquad (11)$$

where N_A and N_D are the densities of acceptor and donor scattering centers, respectively. We assume that the exponent α is the same for both donors and acceptors, but allow the prefactors a_A and a_D to differ. There is some justification for setting both exponents equal, based on Vina and Cardona's calculations and data for silicon and germanium. For any given band gap, the value of α is not very sensitive to the nature of the scatterer, be it n-type or p-type, irrespective of the value of the band masses or whether the band edges are shifted relative to each other. A word of caution, however. In the work of Vina and Cardona for p-type silicon and germanium, screening is effected by valence band holes, whereas in our samples this screening comes about because of a deficit of electron charge near the scattering center (a different type of hole). We shall assume, somewhat arbitrarily, that α still remains nearly the same for donor and acceptor scattering in this case.

In writing Eq. (11) as the expression for band gap renormalization in the presence of compensation we are also, in effect, assuming that the contribution of the scatterers to the energy shift is additive, i.e., we disregard any correlations that

might be introduced into the band gap energy shift because of the presence of different types of impurities.

To obtain the value of the threshold energy, including the effects of compensation, we replace the electron-impurity interaction obtained from the metallic hydrogen model of Wigner and Huntington (Eq.(9)), with the expression in Eq. (11). We then add to this the remaining terms from the original Girvin model described in section VII. The values for a_A, a_D, and α are obtained by allowing these parameters to float freely in order to minimize the difference between the theoretical prediction for the high-energy threshold and the experimental values deduced from the luminescence spectra. More precisely, we minimize the expression

$$\sum_i \left[E_i^{th} - E_i^{exp} \right]^2 , \qquad (12)$$

where the sum runs over the various samples, and where E_i^{th} and E_i^{exp} stand for the theoretical and experimental threshold energies of the particular sample, respectively.

The results we obtain by this procedure are discussed in part (iv) of this section. The minimization process is carried out using all samples except M4. The parameters thus obtained are used to calculate the threshold energy for this sample.

iii) Estimates of compensation

The estimates of the compensation for the six metallic samples which we use in the calculation described above are derived from the results of transport measurements on these samples at temperatures below 100 K, as described in Chapter I of this thesis.

There is quite a large uncertainty associated with these values, as large as 50% or even larger, as we explain in that chapter. The relative values of compensation, however, should be closer to the actual relative compensations. In spite of the uncertainty in the determination of donor and acceptor impurity concentrations, the long wavelength luminescence results do indicate that there is a non-negligible amount of compensation in these samples.

The compensation values quoted in Table III-4, below, and used in the calculation of the luminescence high-energy thresholds are obtained, for samples M3 to M7, using the Vashishta-Singwi treatment for the electron screening. This is explained in Chapter I. Of the other models referred to in that chapter, the Toigo-Woodruff treatment gives very similar results, whereas the treatment of Brosens et al. gives unphysical results for sample M7 and was rejected on that basis. The compensations for samples M1 and M2, which are closer to the metal-insulator transition and therefore not fully degenerate, are obtained using R. Mansfield's formulation for the electron mobility,[27] since it is applicable to any level of degeneracy.

Table III-4. Compensation values for metallic samples.

SAMPLE	K
M1	0.65
M2	0.60
M3	0.31
M4	0.32
M5	0.32
M7	0.03

iv) Results and conclusions

In Table III-6 we list the high-energy thresholds obtained on the basis of the scheme presented above. They are also plotted in Fig. (III-14). The values of compensation used in the calculation were those derived from the mobility data.

The main feature of these results is that they reproduce the non-monotonic behavior observed experimentally. Thus, the inclusion of compensation offers a way of accounting for the non-monotonicity of the high-energy thresholds in the luminescence spectra. We note, in fact, that within the modified Girvin model presented in this thesis we have found no other way of reproducing a non-monotonic behavior, neither by adjusting the value of the lattice dielectric constant, nor by applying the Vina-Cardona model in its original form, Eq. (10); without compensation.

Table III-5 shows the predictions of this model, using the original Vina-Cardona expression for band-gap renormalization, for

the uncompensated case. They show a monotonic increase in the high-energy threshold with carrier concentration.

TABLE III-5. Spectrum thresholds as obtained using the Vina-Cardona expression for band-gap renormalization (Eq.(10)) for the uncompensated case. Note the monotonicity in the increase of the threshold with carrier concentration. The best exponent α equals 0.3.

SAMPLE	Spectrum Threshold (meV)
M1	1828.0
M2	1828.0
M3	1830.7
M4	1832.8
M5	1834.0
M7	1840.7

There are a few caveats regarding the results obtained using the model proposed in this section, however. First, the samples used in this work come from two different sources, as described in Appendix I. Given that crystal growing techniques allow for a wide margin of variation in impurity content, types and extent of defects, etc., the position of the high-energy threshold may be influenced by a number of uncontrolled variables not accounted for in the present model. In particular, if one considers the high-energy thresholds for the samples from the two sources separately, the results are monotonic with carrier concentration within each set of samples, in accordance with Girvin's model.

TABLE III-6. High-Energy threshold for the luminescence spectra obtained on the basis of the model presented in Section VIII. The results quoted are for the case which utilizes the upper bound estimate for the electron-hole interaction. The other case gives very similar values for the thresholds, an artifact of the minimization process. The values obtained for the parameters a_A, a_D, and α are: $a_A = -4.0 \times (10^{17})^{0.6}$ meV-$(cm^3)^{0.6}$, $a_D = -7.0 \times (10^{17})^{0.6}$ meV-$(cm^3)^{0.6}$, $\alpha = 0.6$.

SAMPLE	Spectrum Threshold (meV)
M1	1824.1
M2	1823.7
M3	1832.4
M4	1831.3
M5	1829.1
M7	1853.0

Secondly, as discussed in Chapter I of this thesis, there is a great deal of uncertainty in the determination of the compensation levels from transport measurements. This places real limitations on our conjecture that it is compensation which is responsible for the non-monotonic progression of the high-energy thresholds as a function of carrier concentration. Below we discuss to some extent the effect of varying the assumed level of compensation on our results.

It should be noted, moreover, that we are using three adjustable parameters, namely a_A, a_D, and α in Eq.(11), to fit six data points. This, of course, means that we cannot claim that our experiments have proven the correctness of this model, and cannot rule out possible alternative schemes.

The model shows some promising features, though. The values of the parameters a_A, a_D, and α obtained by the minimization procedure described on part (ii) of this section are not unreasonable. In particular, the exponent $\alpha = 0.6$ which we obtain is within the limits $1/3 < \alpha < 1$, claimed by Vina and Cardona, while the prefactors a_A and a_D separately give downward energy shifts on the order of a few tens of meV's. A downward shift is what is expected for both donors and acceptors on the basis of the Vina-Cardona model, and is also what these authors find experimentally for the cases of silicon and germanium. The fact that the shifts for donors and acceptors are of the same order of magnitude is also something that is observed for the cases of silicon and germanium by these same authors.

Moreover, if one manipulates the compensation parameters K (one at a time) away from the values obtained from the transport data and then looks for best values of the parameters a_A, a_D, and α, a reasonable fit is obtained within a fairly narrow range of the K's. This is shown in Figs. (III-15)(a) to (d), where we plot the residual error obtained from Eq.(12), normalized to the experimental uncertainty, versus compensation for each sample. These plots are based on fits to five of the samples (excluding M4). This does not, of course, exclude the possibility that there may exist a different set

of K values which would produce an even better fit. It does, however, show, (a)that there is a local minimum which is surprisingly sharp near the compensation values extracted from the transport data, and (b)that we cannot just fit any arbitrary set of compensation parameters to the experimental data on the basis of the scheme presented above.[28]

As mentioned before, the minimization process used to obtain the parameters a_A, a_D, and α was carried out excluding sample M4. The data for this sample was collected subsequently to the others and was used as an internal check on the model. As seen in Fig. (III-14), there is qualitative although not good quantitative agreement with the experimental results. The most important issue remains that the model is capable of yielding the observed non-monotonic behavior.

Finally, these results prompted a search for evidence of the presence of acceptors in these samples, since compensation plays such a central role in our explanation of the luminescence spectra. Initial studies of the long-wavelength luminescence, discussed in section IV, above, show that, indeed, there exists significant compensation in these samples, especially in sample M5. This work is still in progress and quantitative analysis based on these results will have to await a more detailed investigation.

Fig. (III-14) Plot of the spectra thresholds obtained using the model presented in this section versus carrier concentration. The experimental thresholds are also plotted for reference. Note that the model is able to predict the non-monotonic character of the increase of the threshold positions with carrier concentration.

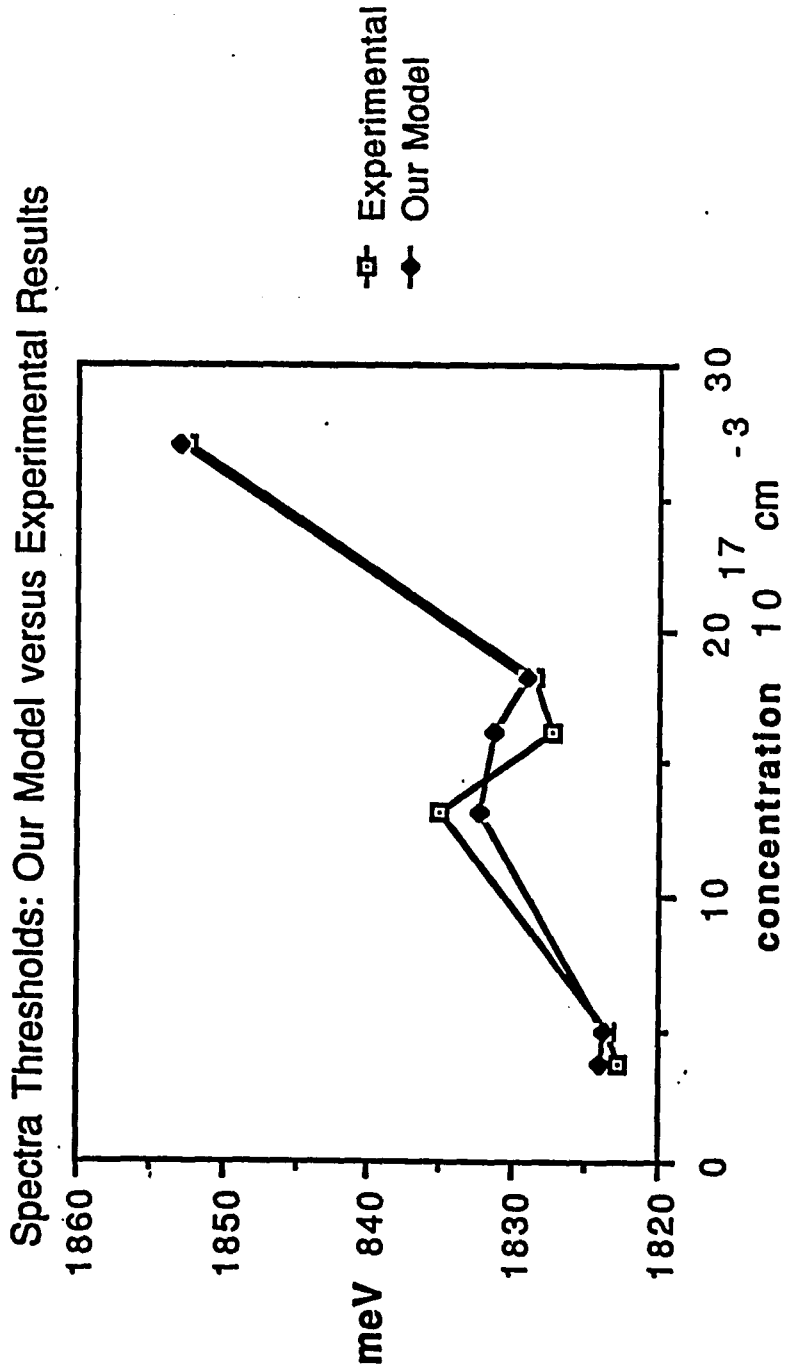

Fig. (III-15a) Residual error ΔE obtained from Eq. (12), normalized to the experimental uncertainty, obtained by varying the assumed value of the compensation for sample M1, as explained in the text. Here,

$$\Delta E = \frac{1}{\Delta\varepsilon}\sqrt{\sum_i (E_i^{th} - E_i^{exp})^2 / N}$$

where $\Delta\varepsilon$ is the experimental uncertainty, and N is the number of samples considered in the calculation.

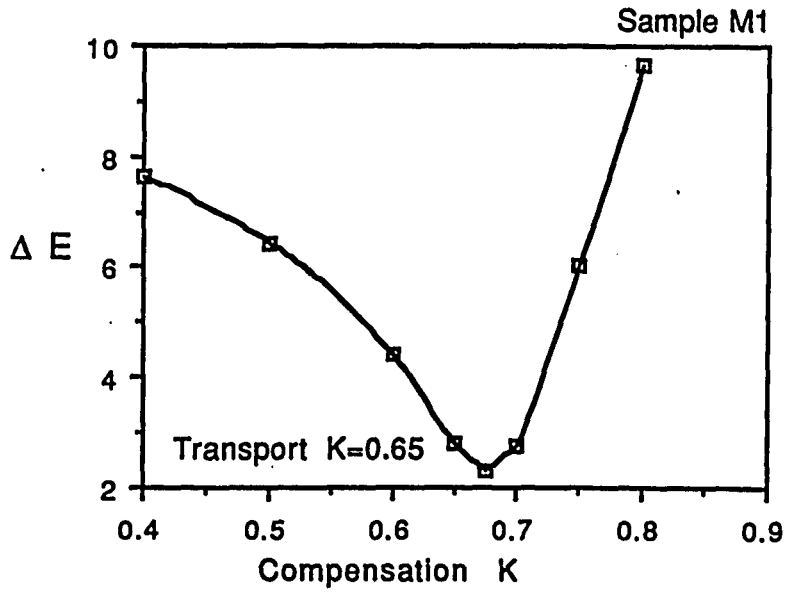

Fig. (III-15b) Residual error, normalized to the experimental uncertainty, obtained by varying the assumed value of the compensation for sample M3.

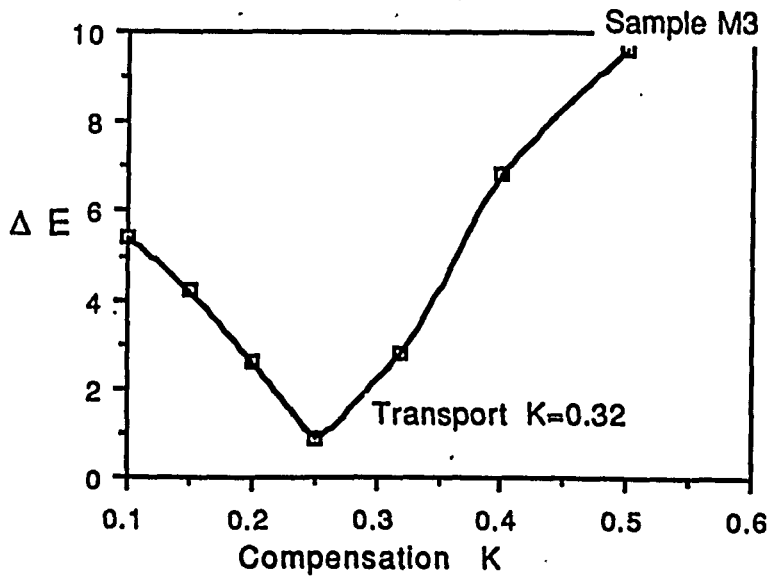

Fig. (III-15c) Residual error, normalized to the experimental uncertainty, obtained by varying the assumed value of the compensation for sample M5.

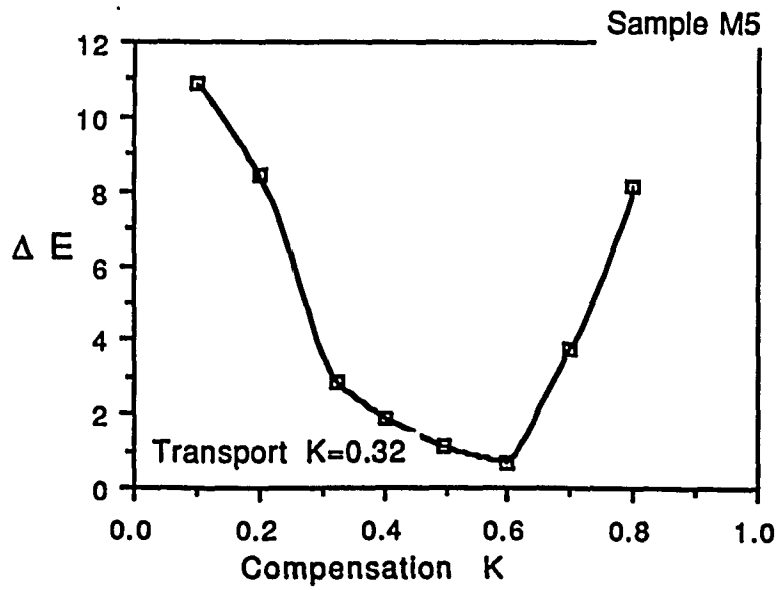

Fig. (III-15d) Residual error, normalized to the experimental uncertainty, obtained by varying the assumed value of the compensation for sample M7.

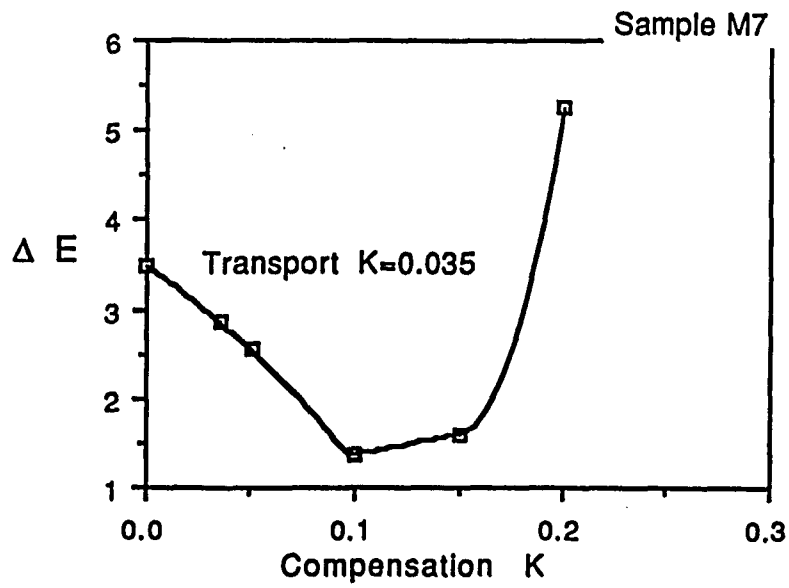

REFERENCES

[1] S. M. Girvin, Phys. Rev. B **17**, 1877 (1978).

[2] Hiroshi Kukimoto, Shigeo Shionoya, Seizo Toyotomi, and Kazuo Morigaki, J. Phys. Soc. Jpn. **28**, 110 (1970).

[3] E. Burstein, Phys. Rev. **93**, 632 (1954).

[4] L. Vina and M. Cardona, Phys. Rev. B **29**, 6739 (1984).

[5] L. Vina and M. Cardona, Phys. Rev. B **34**, 2586 (1986).

[6] Masato Hayashi, Hinoshi Saito, Shigeo Shionoya, Solid State Comm. **24**, 833 and 837 (1977). The experiments carried out by these authors show that in order to produce electron-hole plasmas or even high-density exciton systems in insulating CdSe, excitation energy densities many orders of magnitude larger than 1 W/cm^2 are needed.

[7] The spectra in Fig.1 were obtained at CCNY, whereas those in Fig.2 were obtained at Bell Laboratories, Murray Hill, N.J. Both sets of spectra give the same results.

[8] Here we refer to holes in the A band.

[9] Acceptor levels in insulating CdSe have been observed by Henry *et al.*, Ref. 8, and Yu and Hermann, Ref. 9. These levels, for substitutional Li and Na dopants, occured at about 109 meV above the valence band.

[10] F. E. Williams, J. Phys. Chem. Solids **12**, 265 (1960).

[11] C. H. Henry, K. Nassau, and J. W. Shiever, Phys. Rev. B **4**, 2453 (1971).

[12] Peter Y. Yu and Claudine Hermann, Phys. Rev. B **23**, 4097, (1981).

[13] E. P. Wigner and H. B. Huntington, J. Chem. Phys. **3**, 764 (1935).

[14] Because of the large average interelectron distance relative to the CdSe lattice constant, dielectric screening by the electron gas affects only the macroscopic longitudinal electric fields associated with these distortions.

[15] H. Frohlich, H. Pelzer, and S. Zienau, Phil. Mag. **41**, 221 (1950).

[16] The above results are obtained under the assumption that ω_{LO} is independent of wave vector. This is a reasonable assumption in our case since the Fermi sphere fills only a tiny fraction of the first Brillouin zone of the CdSe for all our samples. See Appendix I for dimensions of the Fermi sphere. The weak-coupling constant $\alpha = 0.43$ in CdSe.

[17] P. Nozieres and D. Pines, Phys. Rev. **111**, 442 (1958).

[18] G. D. Mahan, *Many-Particle Physics*, Plenum Press, New York, 379 (1981).

[19] The density parameter r_s, the Rydberg and therefore also the value of the Fermi energy, depend on the lattice dielectric constant ε. One must therefore make a judicious choice as to whether to use the static or the high frequency lattice dielectric constant. The Pines-Nozieres calculation for the correlation energy of the electron gas separates the contributions from low and high momentum transfers of the Coulomb interaction energy, where these momenta are defined relative to a quantity the same order of magnitude as the Thomas-Fermi wave vector ($h=2\pi$).The dominant low momentum elementary excitations of the electron gas, or plasmons, possess a minimum frequency given by the classical frequency of plasma oscillations, which in our case is typically two or three times larger than the optical phonon frequency. The short-range, or high momentum transfer contribution to the correlation energy acts over a characteristic length comparable to the Thomas-Fermi screening length λ_{TF}. This means that the relevant lattice response time for the short-range interaction is given by λ_{TF}/v_F, where v_F is the Fermi velocity. Typical times are an order of magnitude smaller than the inverse of the optical phonon frequency. It is thus reasonable to use the high frequency lattice dielectric constant in the expression for the correlation energy of the electron gas.

[20] J. Lindhard, Kgl. Danske Videnskab. Selskab, Mat.-Fys. Medd. **28**, No. 8 (1954).

[21] H. H. Woodbury and M. Aven, Phys. Rev. B **9**, 5195 (1974). The donor binding energy cited in this work is determined from optical measurements.

[22] Wigner and Huntington write the electron wave function in a Bloch-like form, $\exp(i\mathbf{k}.\mathbf{x})\Phi(\mathbf{x})$. E_H is obtained upon subtracting out the kinetic energy of the flat part of the wave functions.

[23] Private communication by Peter Delfyett and R.R. Alfano.

[24] J. I. Pankove and P. Aigrain, Phys. Rev. **126**, 956 (1962).

[25] The dependence on the type of impurity enters in this treatment through the impurity structure factor S(q) in the unit cell, where the Fourier transform of the impurity potential is given by $V(q)=4\pi\, S(q)/\varepsilon(q)\, q^2$, and $\varepsilon(q)$ is the Lindhard dielectric function.

[26] In the Vina-Cardona treatment, the carrier-impurity part of the Hamiltonian is given by Eq. (5) of Ref. 11,

$$H_{ei} = \sum_{\bar{k},\, n;\, \bar{k}',\, n'} \left\langle \bar{k}',\, n' \middle| V_I \middle| \bar{k},\, n \right\rangle c^{+}_{\bar{k}',\, n'} c_{\bar{k},\, n}$$

where V_I represents the difference between the crystal potential with and without impurities present, and $|k,n\rangle$ represents the state of an electron with momentum k in band n. V_I is then written as a sum of identical localized potentials V^{imp} centered at the

impurity sites. The randomness of the impurity locations is taken into account by performing an ensemble average over these localizations.

The first-order contribution to the energy shift in the band gap is given by Eq. (11) of Ref. 11,

$$\Sigma^{(1)}(\bar{k}) = N_I \langle \bar{k}, n | V^{imp} | \bar{k}, n \rangle ,$$

where N_I is the density of impurity scattering centers. This represents the shift due to the fact that the average periodic potential has been slightly altered due to the presence of the impurities. This contribution is generally fairly small compared to the second order correction.

The second order shift is given by Eq. (16) of Ref. 11,

$$\Delta^{(2)}_{\bar{k}, n} = N_I \sum_{\bar{q}, m} \frac{\left| \langle \bar{k}, n | V^{imp} | \bar{k} + \bar{q}, m \rangle \right|^2}{e_{\bar{k}, n} - e_{\bar{k} + \bar{q}, m}} ,$$

where $e_{k,n}$ is the unperturbed energy of this electron. Both donor and acceptor scattering centers give the same sign for the shift because the interaction part enters as a square in this expression.

A simple Thomas-Fermi model for the electron dielectric screening gives a shift in band gap energy proportional to

$$\Delta^{(2)}_{\bar{k}, n} \sim \frac{N_I}{(q^2 + q^2_{TF})^2} \sim \frac{N_I}{(q^2 + C N_I^{1/3})^2} ,$$

where C is a constant. This means that small q transfers yield contributions proportional to $N_I^{1/3}$, whereas large q transfers yield contributions proportional to N_I. The total result depends on which process is dominant, but will lie between these two limits.

[27] R. Mansfield, Proc. Roy. Soc. London B 69, 76 (1956).

[28] These plots show that the data would be better fit by a more compensated sample M5 relative to M3.

APPENDIX I

Samples

Samples of n-CdSe doped with indium were obtained from two different sources, as specified in Tables A-1 and A-2, below. Six of the samples, of which four are on the insulating side of the transition, were purchased from Cleveland Crystals (CC); the remaining samples were provided by the Institute of Physics, Polish Academy of Sciences in Warsaw (PAS). For ease of identification the prefixes I and M denote insulating and metallic, respectively. The concentrations listed in both tables were determined from the room temperature value of the Hall coefficient, making the usual assumption that the ratio of the Hall mobility to the drift mobility is unity, that is, $r_H = \mu_H/\mu_D = 1$. Based on measurements of the temperature dependence of the Hall coefficient, we estimate that for insulating samples all but at most 10% of the carriers have been activated into extended states at room temperature. Resistivities and carrier concentrations have been determined, using the van der Pauw method, to within 3%.

Both for luminescence and transport measurements the samples were cut with their faces perpendicular to the c-axis to a size of approximately 3mm X 4mm X 0.8mm. Electrical leads were placed close to the edges or along the sides of the samples. The c-axis was determined, using x-ray diffraction (Laue method), to within 5 degrees for the transport measurements. These samples were reoriented at the AT&T Bell Laboratories with an x-ray

goniometer, to better than 20 minutes of arc for the luminescence and excitation spectra studies at this facility

TABLE A-1: INSULATING SAMPLES

Label	n_o(RT) 10^{17} cm^{-3}	ρ(RT) Ω-cm	Fermi T Kelvin	n_o/n_c	source	CCNY label
I1	1.0	0.090	71	0.33	CC	CdSe1-1
I2	1.2	0.078	80	0.40	CC	CdSe8-1
I3	1.6	0.059	100	0.53	CC	CdSe7
I4	2.18	0.043	119	0.73	PAS	CdSe14-3-3
I5	2.2	0.044	119	0.73	PAS	CdSe14-3-1
I6	2.4	0.040	126	0.80	CC	CdSe6

TABLE A-2: METALLIC SAMPLES

Label	n_0(RT) 10^{17} cm^{-3}	ρ(RT) Ω-cm	Fermi T Kelvin	k_F A^{o-1}	source	CCNY label
M1	3.7	0.032	166	0.022	PAS	CdSe10-5
M2	5.0	0.022	206	0.024	PAS	CdSe12
M3	13.2	0.009	394	0.034	CC	CdSe3
M4	16.1	0.008	450	0.036	PAS	CdSe11-2-1-2
M5	18.2	0.008	488	0.038	PAS	CdSe11-3-1
M6	18.5	0.007	494	0.038	PAS	CdSe11-3-2
M7	27.2	0.003	638	0.043	CC	CdSe4-3

TABLE A-3: SOME CdSe PARAMETERS

Critical Concentration n_c used in this thesis: 3×10^{17} cm^{-3}.

Conduction band mass near k = 0: 0.13 m_e, where m_e=free electron mass

Valence band masses near k= 0[1]

	Band A	Band B	Band C
Longitudinal	2.50 m_e	0.18 m_e	0.71 m_e
Transverse	0.45 m_e	0.90 m_e	0.40 m_e

Optical frequencies[2] at 80 K

Longitudinal: 26.1 meV

Transverse: 21.3 meV

Average dielectric constants[2]

$\varepsilon_0 = 9.4$

$\varepsilon_\infty = 6.2$

Size of the Brillouin Zone along the Γ-M line: 0.84 A^{-1}

REFERENCES

[1] Donald Long, *Energy Bands in Semiconductors*, John Wiley & Sons, Inc.,N.Y. (1968).

[2] D. L. Rode, *Semiconductors and Semimetals* **10**, 84 (1975).

APPENDIX II

Evaluation of the electron-hole Interaction Energy

Equation (7) in Chapter III was evaluated in the following manner.

There are two contributions to the imaginary part of the inverse dielectric function[1], one from the plasmon pole and one from the branch cut due to single particle excitations. The contribution of the plasmon pole to the imaginary part of the inverse dielectric function is given by

$$\mathrm{Im}\left[\frac{1}{\varepsilon_{RPA}(\vec{k},\omega)}\right]_{\text{plasmon-pole}} = -\frac{\pi}{2}\omega_k\delta(\omega-\omega_k), \qquad (1)$$

where ω_k is the plasmon energy for wave vector k.

We obtain ω_k by evaluating the following sum rule numerically[2]

$$\int_0^\infty d\omega\ \mathrm{Im}\left[\frac{1}{\varepsilon(\vec{k},\omega)}\right]\times\omega = -\frac{\pi}{2}\omega_p^2, \qquad (2)$$

where ω_p is the plasma frequency.

Upon substituting the plasmon pole contribution in Eq. (2), we obtain

$$\omega_k^2 = \omega_p^2 + \frac{2}{\pi}\int_0^\infty \mathrm{Im}\left[\frac{1}{\varepsilon(\vec{k},\omega)}\right]_{\text{pair-excitations}}\times\omega d\omega . \qquad (3)$$

We then use this value of ω_k in the expression for the electron-hole interaction. The plasmon-pole contribution to this energy is, thus,

$$\Delta E = -\frac{\hbar}{\pi(2\pi)^3}\int_{-\infty}^{\infty} dk_{\parallel}\int_{0}^{\infty} dk_{\perp}\frac{4\pi e^2}{\varepsilon_\infty}\frac{\pi}{2}\left[\frac{k_\perp}{k_\perp^2+k_{\parallel}^2}\right]\left\{\frac{\omega_k}{\frac{1}{2}\hbar^2\left[\frac{k_\perp^2}{M_\perp}+\frac{k_{\parallel}^2}{M_{\parallel}}\right]+\hbar\omega_k}\right\}, \quad (4)$$

where the parallel and perpendicular directions are taken with respect to the crystal c-axis. The masses are the valence band masses.

For the contribution due to single-particle excitations we use Lindhard's dielectric function[2], and integrate over the range of k and ω where the imaginary part of this dielectric function is different from zero.

Both the plasmon pole contribution and the contribution due to single-particle excitations are evaluated by numerical integration. Below we reproduce the text of the programs used for these integrations.

A full treatment of this problem should include the use of a frequency dependent lattice dielectric function. Nevertheless, for the plasmon pole contribution, the high frequency dielectric function provides a good approximation, since $\omega_k > \omega_p >> \omega_{LO}$. For the contribution due to single-particle excitations, we can get approximate upper and lower bounds to this contribution by using ε_o and ε_∞, respectively. The essential features of our results remain the same within the range of values determined by these bounds.

The text of the programs for the numerical integrations used to evaluate the electron-hole interaction are reprinted below.

```
C THIS ROUTINE EVALUATES THE CONTRIBUTION OF THE
C ELECTRON-HOLE PAIR EXCITATIONS TO THE ELECTRON-
C HOLE INTERACTION ENERGY

      REAL kFT,k0,v0,xm,hbar
      REAL Mpar,Mper
      EXTERNAL ff
      COMMON k0,v0,kFT,Mpar,Mper,hbar,xm
C BARE  MASSES
      xm=1.0931e-28
      Mpar=1.9858e-27
      Mper=3.5525e-28
      k0=3.626
      kFT=4.10
      hbar=1.05459e-27
      v0=hbar*k0/xm
C     hbar is Plancks constant over 2 pi in CGS
C     w is the frequency omega
      CALL INT1
      STOP
      END

      REAL FUNCTION ff(kpar,kper,w)
      REAL k0,v0,kFT,kpar,kper,Mpar,Mper,hbar,xm,w
      REAL k,T,x,y,A1,A2,A3
      COMMON k0,v0,kFT,Mpar,Mper,hbar,xm
      k=SQRT(kpar**2+kper**2)
      T=(hbar/2.)*(kper**2/Mper+kpar**2/Mpar)
      IF(k .EQ. 0.)THEN
      PRINT *,'k=0.'
      k=1.e-15
      END IF
      IF(T .EQ. 0. .AND. w .EQ. 0.)THEN
      PRINT *,'T and w =0.'
      T=1.e-30
      END IF
      x=e1(kFT,k,k0,v0,xm,w,hbar)
      y=e2(kFT,k,k0,v0,xm,w,hbar)
      IF(x .EQ. 0. .AND. y .EQ. 0.)THEN
      write(6,*) 'x=0. and y=0.'
      GO TO 10
      END IF
      A1=kper/k**2
      A2=y/(x**2+y**2)
      A3=1./(T+w)
      ff=A1*A2*A3
10    CONTINUE
      RETURN
      END

     REAL FUNCTION e1(kFT,k,k0,v0,xm,w,hbar)
      REAL kFT,k,k0,v0,xm,w,hbar
      REAL x1,x2,x3,x4,x5,x6,x7,x8,x9,x10
C  This function computes the real part
```

```
C  of the dielectric susceptibility
      x1=hbar*(k**2)/(2.*xm)
        x2=k*v0
        x3=1.-((w-x1)**2/x2**2)
        x4=(w-x2-x1)/(w+x2-x1)
        x4=ABS(x4)
      x5=LOG(x4)
        x6=1.-((w+x1)**2/x2**2)
        x7=(w+x2+x1)/(w-x2+x1)
        x7=ABS(x7)
        x8=LOG(x7)
        x9=(kFT/k)**2
        x10=k0/(4.*k)
        e1=1+x9*(0.5+x10*(x3*x5+x6*x8))
        RETURN
        END

        REAL FUNCTION e2(kFT,k,k0,v0,xm,w,hbar)
        REAL kFT,k,k0,v0,xm,w,hbar
        REAL y1,y2,y3,y4,y5,y6,y7,y8
C  This function computes the imaginary part
C  of the dielectric function.
        e2=0.
        y1=hbar*(k**2)/(2.*xm)
        y2=k*v0
        y3=(kFT/k)**2
        y4=y2-y1
        y5=y2+y1
        y6=k0/k
        y7=((w-y1)**2)/y2**2
        y8=2.*k0
        IF(k .GT. y8)THEN
        GO TO 500
        END IF
        IF(w .LE. y4)THEN
        e2=(3.141593/2.)*(w/y2)*y3
        END IF
        IF(w .GT. y4 .AND. w .LE. y5)THEN
        e2=(3.141593/4.)*y6*(1.-y7)*y3
        END IF
        GO TO 600
500     CONTINUE
        y4=-1.*y4
        IF(w .GT. y4 .AND. w .LE. y5)THEN
        e2=(3.141593/4.)*y6*(1.-y7)*y3
        END IF
600     CONTINUE
        RETURN
        END

        SUBROUTINE INT1
```

```
      REAL a1,a2,a3,b1,b2,b3,N1,N2,N3,INT
      REAL del1,del2,del3,k
      REAL x1,x2,x3,i1,i2,i3,NN3
      REAL k0,v0,kFT,Mpar,Mper,hbar,xm,func
      EXTERNAL ff
      COMMON k0,v0,kFT,Mpar,Mper,hbar,xm
C initialize integral to 0.
      INT=0.
C upper and lower limits of integration
      a1=-20.
      b1=20.
      a2=0.
      b2=20.
      a3=0.
      N1=134.
      N2=66.
      N3=66.
C compute deltas
      del1=(b1-a1)/N1
      del2=(b2-a2)/N2
      N1=N1-1.
      N2=N2-1.
      NN3=N3-1.
      DO 100 i1=0.,N1,1.
      x1=a1+del1/2.+i1*del1
      DO 101 i2=0.,N2,1.
      x2=a2+del2/2.+i2*del2
      k=SQRT(x1**2+x2**2)
      b3=k*v0+hbar*k**2/(2.*xm)
      del3=b3/N3
      DO 102 i3=0.,NN3,1.
      x3=del3/2.+i3*del3
      func=ff(x1,x2,x3)
      INT=INT+func*del1*del2*del3
102   CONTINUE
101   CONTINUE
100   CONTINUE
      PRINT *,'INTEGRAL=',INT
      PRINT *,' CdSe n0=27.e17, epsilon0 .e-h'
      PRINT *, 'k0,v0,kFT, all divided by 1.e6.'
      PRINT *, ' ai=20., N1=134,N2=66'
      RETURN
      END
```

```
C THIS ROUTINE EVALUATES THE CONTRIBUTION OF THE
C PLASMON POLE TO THE ELECTRON-HOLE INTERACTION
C ENERGY

      REAL kFT,k0,v0,xm,hbar
      REAL Mpar,Mper
      COMMON k0,v0,kFT,Mpar,Mper,hbar,xm
      xm=1.0931e-28
      Mpar=1.9858e-27
      Mper=3.5525e-28
      k0=3.626
      kFT=4.1
C ALL k's are divided by 1e6
      hbar=1.05459e-27
C     hbar is Plancks constant over 2 pi in CGS
C     w is the frequency omega
      v0=hbar*k0/xm
      CALL INT1
      STOP
      END

     REAL FUNCTION e1(kFT,k,k0,v0,xm,w,hbar)
      REAL kFT,k,k0,v0,xm,w,hbar
      REAL x1,x2,x3,x4,x5,x6,x7,x8,x9,x10
C  This function computes the real part
C  of the dielectric susceptibility
     x1=hbar*(k**2)/(2.*xm)
      x2=k*v0
      x3=1.-((w-x1)**2/x2**2)
      x4=(w-x2-x1)/(w+x2-x1)
      x4=ABS(x4)
     x5=LOG(x4)
      x6=1.-((w+x1)**2/x2**2)
      x7=(w+x2+x1)/(w-x2+x1)
      x7=ABS(x7)
      x8=LOG(x7)
      x9=(kFT/k)**2
      x10=k0/(4.*k)
      e1=1+x9*(0.5+x10*(x3*x5+x6*x8))
      RETURN
      END

      REAL FUNCTION e2(kFT,k,k0,v0,xm,w,hbar)
      REAL kFT,k,k0,v0,xm,w,hbar
      REAL y1,y2,y3,y4,y5,y6,y7,y8
C  This function computes the imaginary part
C  of the dielectric function.
      e2=0.
      y1=hbar*(k**2)/(2.*xm)
      y2=k*v0
      y3=(kFT/k)**2
      y4=y2-y1
      y5=y2+y1
      y6=k0/k
```

```
      y7=((w-y1)**2)/y2**2
      y8=2.*k0
      IF(k .GT. y8)THEN
      GO TO 500
      END IF
      IF(w .LE. y4)THEN
      e2=(3.141593/2.)*(w/y2)*y3
      END IF
      IF(w .GT. y4 .AND. w .LE. y5)THEN
      e2=(3.141593/4.)*y6*(1.-y7)*y3
      END IF
      GO TO 600
500   CONTINUE
      y4=-1.*y4
      IF(w .GT. y4 .AND. w .LE. y5)THEN
      e2=(3.141593/4.)*y6*(1.-y7)*y3
      END IF
600   CONTINUE
      RETURN
      END


      SUBROUTINE INT1
      REAL a1,a2,b1,b2,b3,N1,N2,N3,NN3,INT
      REAL del1,del2,del3,k,x,y,B,B1,B2,T,NN2
      REAL x1,x2,x3,i1,i2,i3,INT2,wp,wk,kc
      REAL k0,v0,kFT,Mpar,Mper,hbar,xm,func
      COMMON k0,v0,kFT,Mpar,Mper,hbar,xm
C initialize integral to 0.
      INT=0.
C calculate plasma frequency. Given that we have
C divided k's by 1e6, wp has been divided by 1e12.
C This still means calculated energy shift must be
C multiplied by 1e6.
      wp=kFT*v0*0.57735
      kc=wp/v0
      a1=-1.*kc
      b1=kc
      a2=0.
      N1=50.
      N2=50.
      N3=50.
C compute deltas
      del1=(b1-a1)/N1
      N1=N1-1.
      NN2=N2-1.
      NN3=N3-1.
      DO 100 i1=0.,N1,1.
      x1=a1+del1/2.+i1*del1
      b2=kc**2-x1**2
      b2=SQRT(b2)
```

```
      del2=b2/N2
      DO 101 i2=0.,NN2,1.
      x2=a2+del2/2.+i2*del2
      k=SQRT(x1**2+x2**2)
      b3=k*v0+hbar*k**2/(2.*xm)
      del3=b3/N3
      INT2=0.
      DO 102 i3=0.,NN3,1.
      x3=del3/2.+i3*del3
      x=e1(kFT,k,k0,v0,xm,x3,hbar)
      y=e2(kFT,k,k0,v0,xm,x3,hbar)
      B=y/(x**2+y**2)
      INT2=INT2+B*x3*del3
102   CONTINUE
      wk=2.*INT2/3.1415926
      wk=wp**2+wk
      wk=SQRT(wk)
      T=(hbar/2.)*(x1**2/Mpar+x2**2/Mper)
      B1=x2/k**2
      B1=3.1415926*B1/2.
      func=B1*wk/(T+wk)
      INT=INT+func*del1*del2
101   CONTINUE
100   CONTINUE
      PRINT *,'INTEGRAL=',INT
      PRINT *,'This is the plasmon pole contribution'
      PRINT *,' for CdSe n0=27.e17, epsilon0'
      PRINT *, 'k0,v0,kFT, all divided by 1.e6. '
      RETURN
      END
```

REFERENCES

[1] David Pines, *Elementary Excitations in Solids*, W.A. Benjamin, Inc., New York (1964).

[2] Arnold J. Glick and Richard A. Ferrell, Annals of Phys. **11**, 359 (1960).

APPENDIX III

The Hall Coefficient and the van der Pauw Method

A correction to L. J. van der Pauw's original formulation[1]

The van der Pauw method is a widely used experimental technique for the determination of the resistivity of electrically conducting materials. This method is based upon a theorem derived by van der Pauw,[1] and its usefulness lies in the fact that it is applicable to any flat sample of arbitrary shape if the electrical contacts are sufficiently small and located at the circumference or edge of the sample. van der Pauw's original paper also contains a prescription for obtaining the Hall coefficient, again applicable to any flat sample of arbitrary shape. We have found, however, that the formulation for extracting the Hall coefficient needs a correction in order to account for magnetoresistive effects. In this appendix we present this correction and experimental data to support it.

Fig. (A3-1) shows a flat sample of arbitrary shape with four small contacts at arbitrary places along the circumference. The contacts, denoted by A, B, C and D, are placed in successive order along the edge of the sample. van der Pauw defines a resistance $R_{AB,CD}$ as the potential difference V_{DC} between the contacts D and C per unit current through the contacts A and B.

Fig. (A3-1) van der Pauw geometry for resistivity and Hall coefficient measurements.

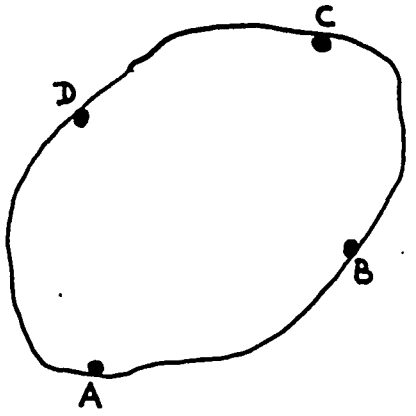

The Hall coefficient is derived to be

$$R_H = (d\,\Delta R_{BD,AC})/H, \tag{1}$$

where $\Delta R_{BD,AC}$ is the change of the resistance $R_{BD,AC}$ due to a magnetic field H applied perpendicular to the sample,[2] and d is the thickness of the sample. As it stands, this formula is only correct in the limit as the applied magnetic field tends to zero. In practice, however, it can lead to significant errors since the Hall coefficient is always measured at finite fields.

Below we derive the correction to Eq. (1). We assume that the voltages are measured at constant current. The current passes through contacts B and D, and the voltage is measured between contacts A and C.

In the presence of a magnetic field H, the voltage $V_{CA}(H)$ is given by

$$V_{CA}(H) = -\int \mathbf{E}_D(H).d\mathbf{l} \; -\int \mathbf{E}_H(H).d\mathbf{l}, \tag{2}$$

where $\mathbf{E}_D(H)$ is the "drift" electric field in the direction of the current lines, and $\mathbf{E}_H(H)$ is the Hall electric field, perpendicular to the current lines. We suppress any explicit notation of the position dependence of fields or current densities. The "drift" field can be written

$$\mathbf{E}_D(H) = \rho(H)\,\mathbf{J}, \tag{3}$$

where $\rho(H)$ is the value of the resistivity at field H, and $\mathbf{J}$ is the current density vector. Therefore,

$$V_{CA}(H) - V_{CA}(0) = -\{[\rho(H)/\rho(0)] - 1\}\int \mathbf{E}_D(0).d\mathbf{l} - \int \mathbf{E}_H(H).d\mathbf{l}, \quad (4)$$

where we have made use of the fact, demonstrated by van der Pauw, that for constant current the current density at any given point does not change when a magnetic field is applied.

The Hall coefficient at field H is thus given by

$$R_H(H) = -[d/H\, I]\int \mathbf{E}_H(H).d\mathbf{l} = (d/H)\{ R_{BD,AC}(H) - [\rho(H)/\rho(0)]\, R_{BD,AC}(0) \}, \quad (5)$$

where I is the total current passing through the sample between contacts B and D. It can be shown that the integral $-\int \mathbf{E}_H(H).d\mathbf{l}$ is independent of the contact positions A, B, C and D as long as these are consecutively placed along the circumference of the sample. One can then make a conformal mapping onto a bar shaped sample and adjust the positions of A, B, C and D without altering their order so that they map onto a classical configuration for the measurement of Hall effect. If the input currents into both samples are the same, and if they have the same thickness then, as shown by van der Pauw, the voltage difference between conformally mapped points will be the same. It is not too difficult to see then that $-\int \mathbf{E}_H(H).d\mathbf{l}$ is indeed the Hall voltage.

We now rewrite Eq. (5) in the following form

$$R_H(H) = (d/H)\{ \Delta R_{BD,AC} - [\Delta\rho/\rho(0)] R_{BD,AC}(0) \}, \quad (6)$$

where

$$\Delta R_{BD,AC} = R_{BD,AC}(H) - R_{BD,AC}(0), \text{ and}$$

$$\Delta\rho = \rho(H) - \rho(0).$$

Comparing Eqs. (1) and (6) we see that an extra correction term is needed beyond the original van der Pauw formula in order to compute the Hall coefficient when the magnetoresistance is non-negligible.

We can recast the expression for the Hall coefficient into still another useful form if we make the reasonable assumption that the magnetoresistance does not change upon reversal of magnetic field direction,[3]

$$R_H(H) = (d/2H) \{ R_{BD,AC}(H) - R_{BD,AC}(-H) \}. \qquad (7)$$

It is this latter formula which we have used most often in extracting the Hall coefficient from our data.

An Example: Data for samples I2 and I5

Below we present some data to support the above results. These data were taken for sample I2 at temperatures 10 K and 8.5 K, and for sample I5 at 1.2 K. The quite voluminous amount of data taken for other CdSe samples at different temperatures tell the same story. Notice that given the non-negligible magnitude of the magnetoresistance the results from Eq. (1) are quite inconsistent for reversed directions of magnetic field, and that as the magnetoresistance becomes more sizeable this inconsistency becomes more pronounced. Notice also that the correction term in

Eq. (6) removes this inconsistency, and that Eq. (7) gives results which are very close to Eq. (6).

Sample I2

Temperature: 10 K

H	$\Delta\rho/\rho_o$	$\Delta R_{BD,AC}$	$\Delta R_{BD,AC} - [\Delta\rho/\rho(0)]R_{BD,AC}(0)$	$[R_{BD,AC}(H) - R_{BD,AC}(-H)]/2$
kG		Ω	Ω	Ω
up				
0	0	0	0	0
2	-0.000	0.062	0.064	0.064
3	-0.001	0.090	0.095	0.093
4	-0.002	0.118	0.129	0.126
5	-0.003	0.143	0.160	0.158
6	-0.004	0.166	0.187	0.192
down				
2		-0.065	-0.063	
3		-0.096	-0.091	
4		-0.134	-0.123	
5		-0.172	-0.155	
6		-0.217	-0.196	

Fig. (A3-2a) van der Pauw formulation: $\Delta R_{BD,AC}$ versus H, for sample I2 at 10 K. Note the different slopes between up and down magnetic field directions.

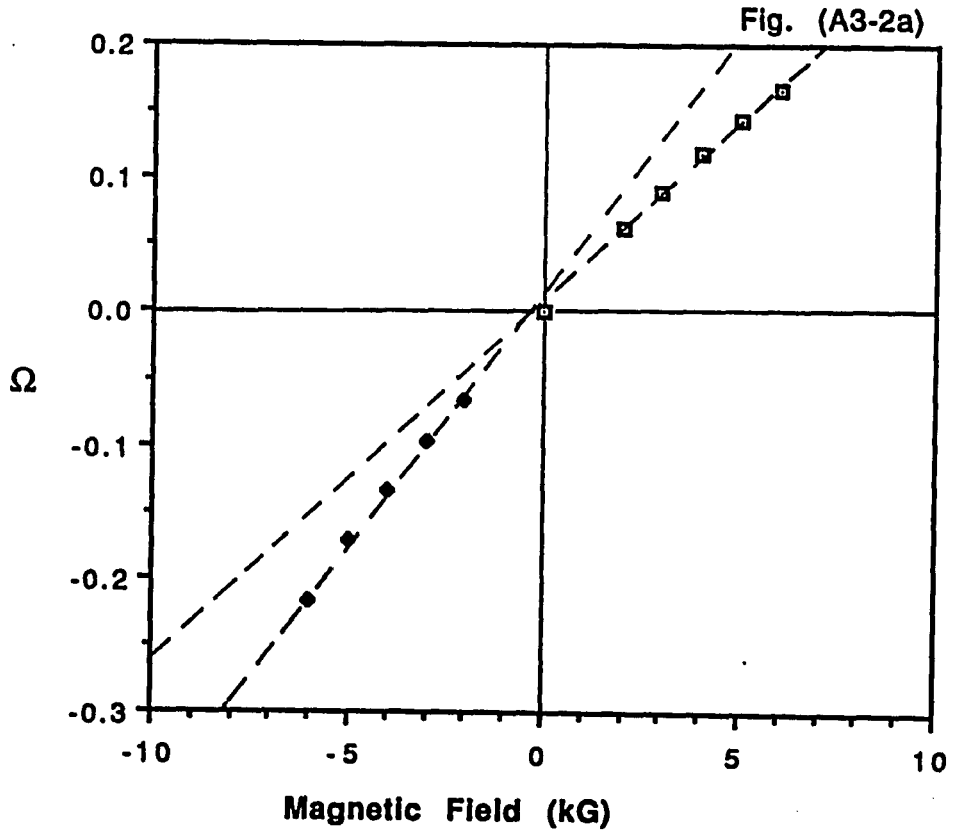

Fig. (A3-2b) Corrected formulation: $\Delta R_{BD,AC} - [\Delta\rho/\rho(0)]R_{BD,AC}(0)$ versus H, for sample I2 at 10 K. The slopes for the up and down magnetic field directions are the same within the experimental uncertainty.

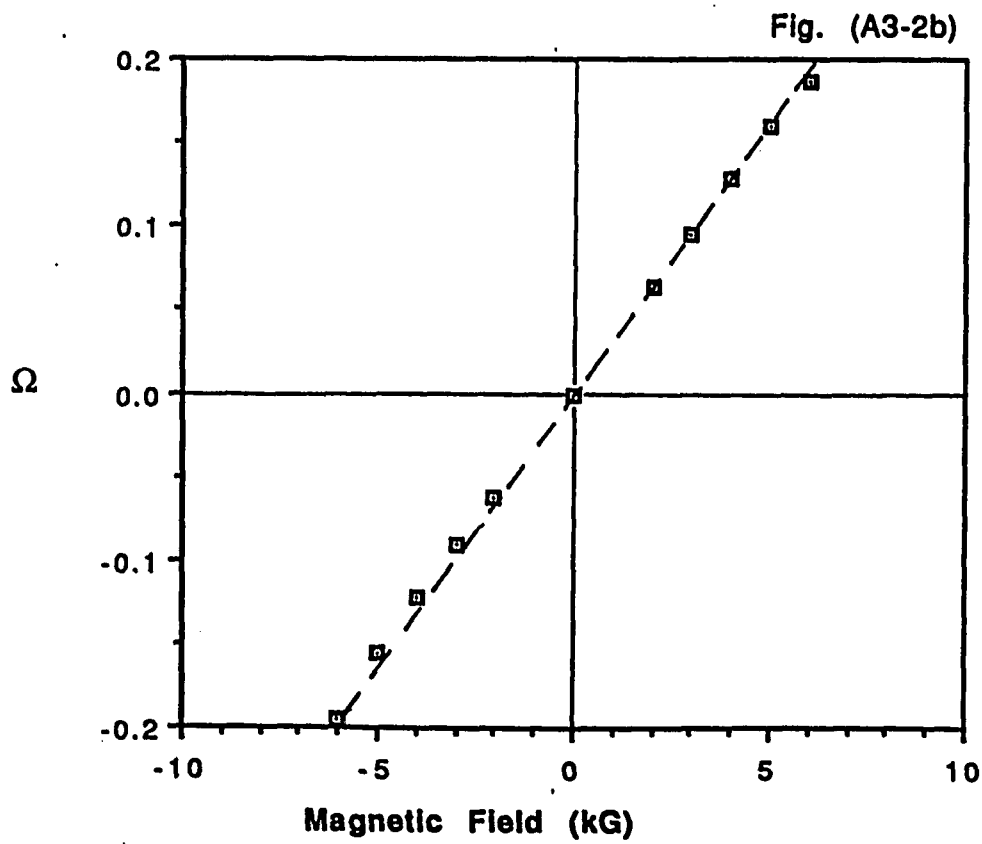

Sample I2

Temperature: 8.5 K

H	$\Delta\rho/\rho_o$	$\Delta R_{BD,AC}$	$\Delta R_{BD,AC} - [\Delta\rho/\rho(0)]R_{BD,AC}(0)$	$[R_{BD,AC}(H) - R_{BD,AC}(-H)]/2$
kG		Ω	Ω	Ω
up				
0	0	0	0	0
2	-0.001	0.054	0.055	0.058
3	-0.001	0.099	0.109	0.103
4	-0.002	0.119	0.141	0.140
5	-0.004	0.149	0.184	0.182
6	-0.005	0.174	0.219	0.225
down				
2		-0.061	-0.060	
3		-0.106	-0.096	
4		-0.161	-0.139	
5		-0.216	-0.181	
6		-0.276	-0.231	

Fig. (A3-3a) van der Pauw formulation: $\Delta R_{BD,AC}$ versus H, for sample I2 at 8.5 K. Note the different slopes between up and down magnetic field directions.

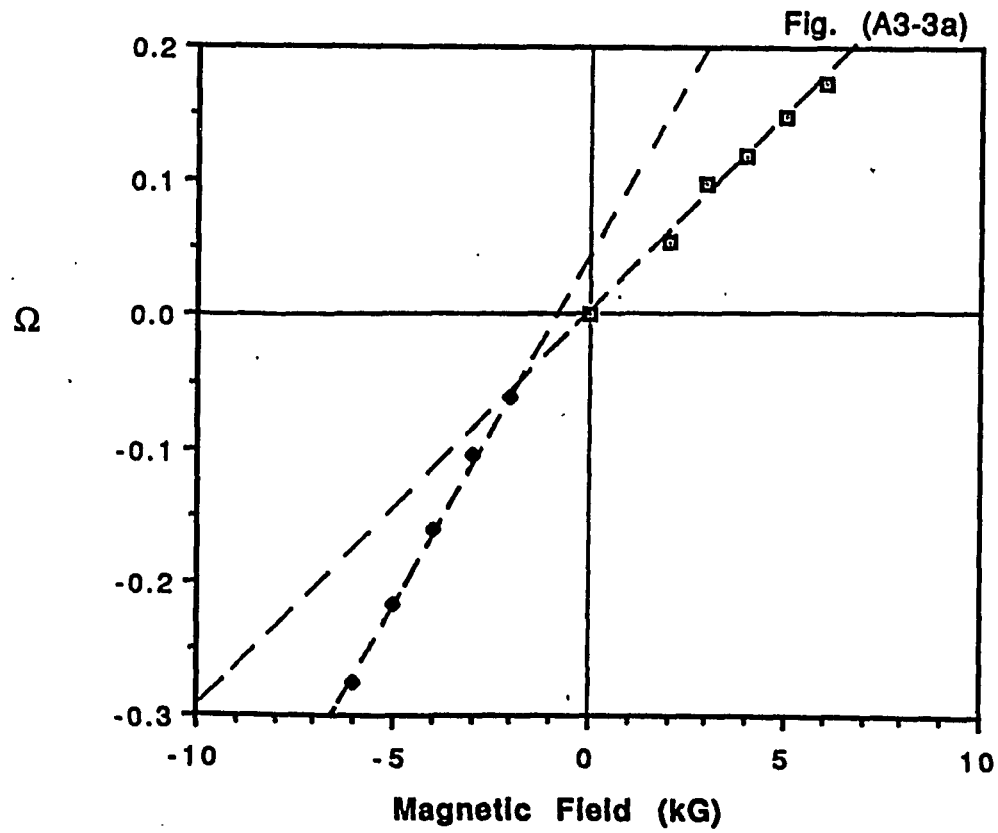

Fig. (A3-3b) Corrected formulation: $\Delta R_{BD,AC} - [\Delta\rho/\rho(0)]R_{BD,AC}(0)$ versus H, for sample I2 at 8.5 K. The slopes for the up and down magnetic field directions are the same within the experimental uncertainty.

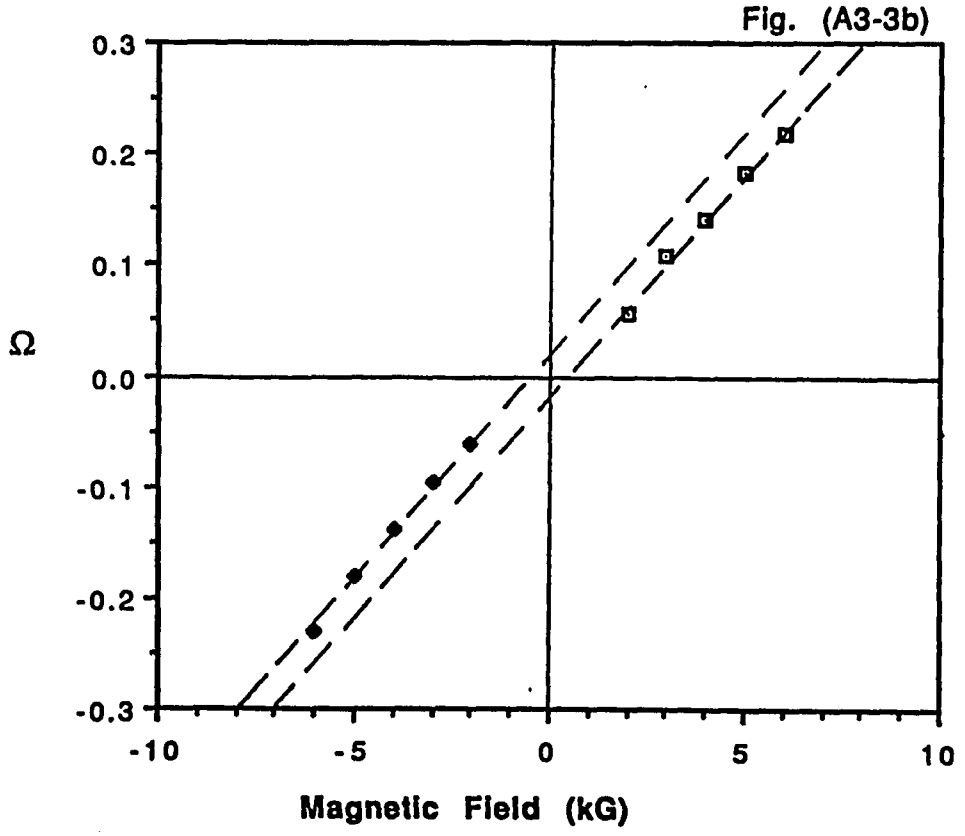

Sample I5

Temperature: 1.2 K

H	$\Delta\rho/\rho_o$	$\Delta R_{BD,AC}$	$\Delta R_{BD,AC} - [\Delta\rho/\rho(0)]R_{BD,AC}(0)$	$[R_{BD,AC}(H) - R_{BD,AC}(-H)]/2$
kG		Ω	Ω	Ω
up				
0		0	0	0
1	-0.002	0.003	0.004	0.004
2	-0.006	0.005	0.010	0.010
3	-0.012	0.006	0.015	0.015
5	-0.027	0.008	0.028	0.027
7	-0.043	0.011	0.041	0.040
10	-0.063	0.016	0.061	0.059
down				
1		-0.006	-0.005	
2		-0.014	-0.010	
3		-0.024	-0.015	
5		-0.046	-0.026	
7		-0.069	-0.039	
10		-0.102	-0.056	

Fig. (A3-4a) van der Pauw formulation: $\Delta R_{BD,AC}$ versus H, for sample I5 at 1.2 K. Note the different slopes between up and down magnetic field directions.

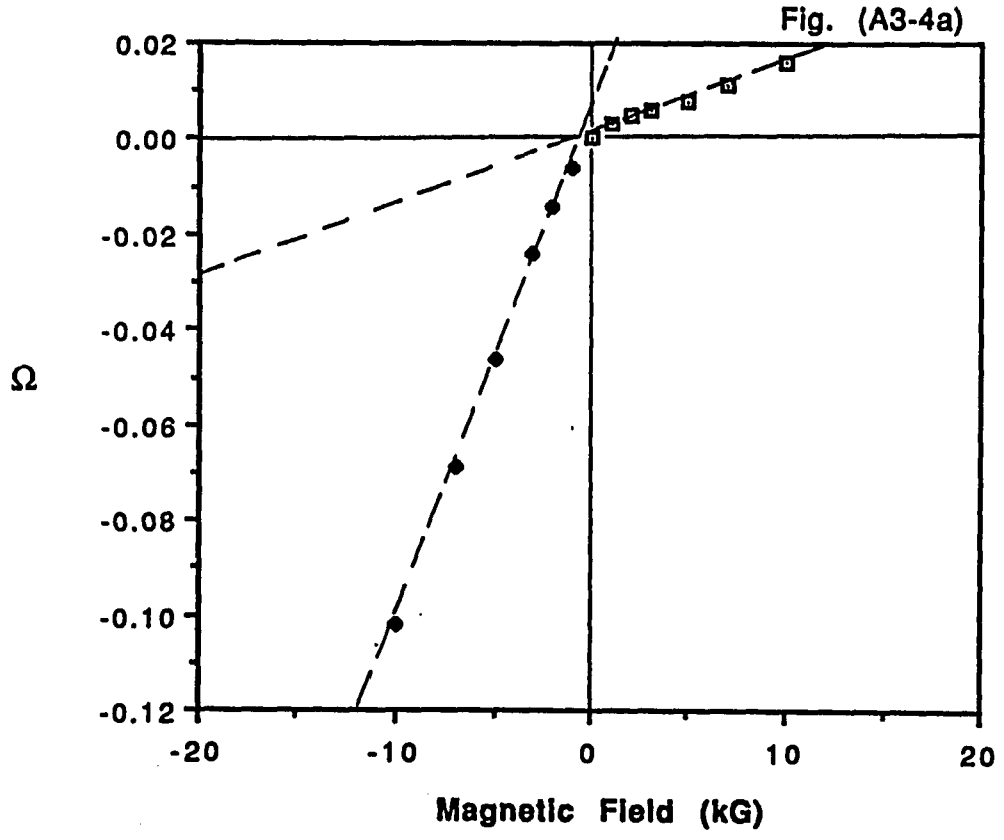

Fig. (A3-4b) Corrected formulation: $\Delta R_{BD,AC} - [\Delta\rho/\rho(0)]R_{BD,AC}(0)$ versus H, for sample I5 at 1.2 K. The slopes for the up and down magnetic field directions are the same within the experimental uncertainty.

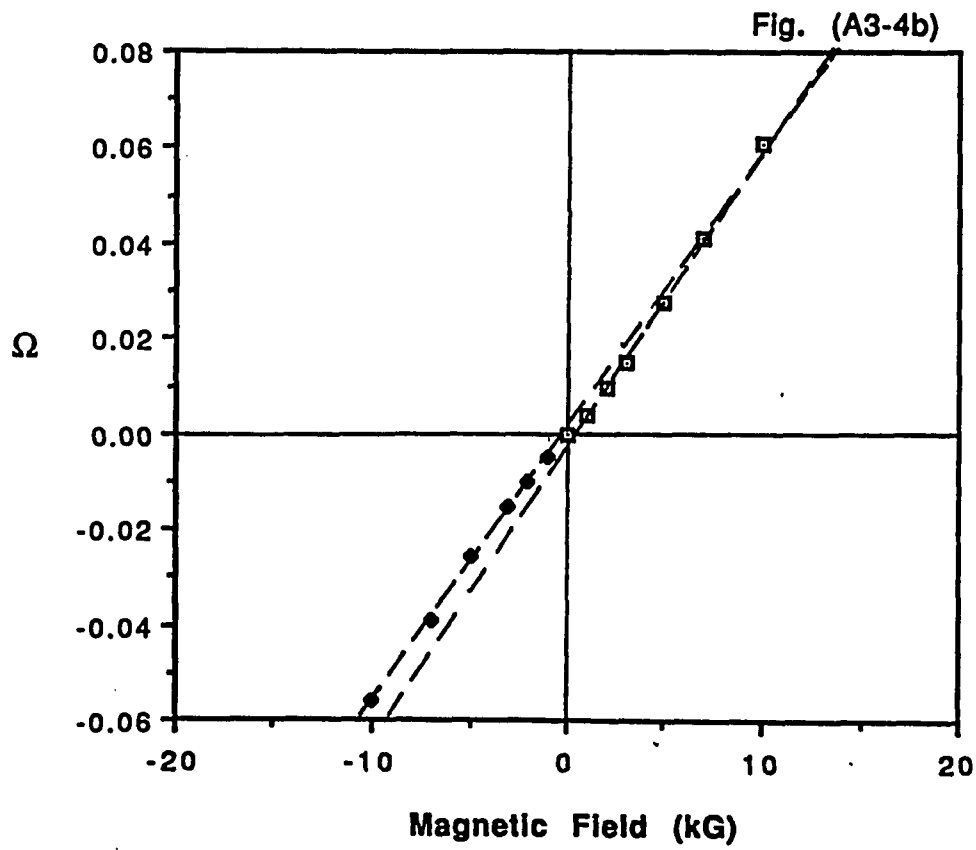

REFERENCES

[1] L. J. van der Pauw, Philips Res. Reps. **13**, 1 (1958).

[2] We assume negligible sample magnetization compared to the applied magnetic field.

[3] Note that all our measurements are done with the magnetic field in the direction of the crystal c-axis. The electrical contacts are placed on the sides of the sample, away from the top and bottom flat surfaces which are perpendicular to the c-axis. In principle a reversal of the magnetic field direction should not, therefore, introduce any variations due to anisotropy into the measured magnetoresistance.

BIBLIOGRAPHY

Allen, F. R., and Adkins, C. J., Phil. Mag. **26**, 1027 (1972).

Amitay, M. and Pollak, M., J. Phys. Soc. Jpn. Suppl. 21, 549 (1966).

Brosens, F., DeVreese, J. T., and Lemmens, L. F., Phys. Rev. B **21**, 1363 (1980).

Brosens, F., Lemmens, L. F., and DeVreese, J. T., Phys. Status Solidi **74**, 45 (1976).

Burmeister, R. A., and Stevenson, D. A., Phys. Status Solidi **24**, 683 (1967).

Burstein, E., Phys. Rev. **93**, 632 (1954).

Cuevas, M., Phys. Rev. **164**, 1021 (1967).

Davis, E. A., and Compton, W. D., Phys. Rev. A **140**, 2183 (1965).

Devreese, J. T., Brosens, F., and Lemmens, L. F., Phys. Rev. B **21**, 1349 (1980).

Emin, D., The Hall Effect and its Applications, edited by C. L. Chien and C. R. Westgate, Plenum Press, 281 (1979).

Erginsoy, C., Phys. Rev. **79**, 1013 (1950).

Falicov, L., and Cuevas, M., Phys. Rev.**164**, 1025 (1967).

Finlayson, D. M., Irvine, J., and Peterkin, L. S., Phil. Mag. B **39**, 253 (1979).

Fistul', V. I., Heavily Doped Semiconductors (Plenum, New York, 1969).

Friedman, L., and Holstein, T., Ann. Phys. **21**, 494 (1963).

Friedman, L., and Pollak, M., Phil. Mag. B**38**, 173 (1978).

Fritzsche, H., J. Phys. Chem. Solids **6**, 69 (1958).

Fritzsche, H., Phil. Mag. B **42**, 835 (1980).

Fritzsche, H., Phys. Rev. **99**, 406 (1955).

Frohlich, H., Pelzer, H., and Zienau, S., Phil. Mag. **41**, 221 (1950).

Geldart, D. J. W., and Taylor, R., Can. J. Phys. **48**, 155 (1970).

Girvin, S. M., Phys. Rev. B **17**, 1877 (1978).

Glick, A. J., and Ferrell, R. A., Annals of Phys. **11**, 359 (1960).

Gruenewald, M., Mueller, H., Thomas, P., Wuertz, D., Solid State Commun. **38**, 1011 (1981).

Hayashi, M., Saito, H., Shionoya, S., Solid State Commun. **24**, 833 and 837 (1977).

Henry, C. H., K. Nassau, and Shiever, J. W., Phys. Rev. B **4**, 2453 (1971).

Hirsch, M. J., Holcomb, D. F., Disordered Semiconductors, edited by M. A. Kastner, G. A. Thomas and S. R. Ovshinsky (Plenum Press, New York, 1987) 45; Proceedings of the Eighteenth International Conference of the Physics of Semiconductors, Stockholm, August 11-15, 1986.

Holas, A., Aravind, P. K., and Singwi, K. S., Phys. Rev. B **20**, 4912 (1979).

Holstein, T., Phys. Rev. **124**, 1329 (1961).

Hutson, A. R., J. Appl. Phys. **32**, 2287 (1961).

Jaroszynski, J., and Dietl, T., Acta Physica Polonica, A **69**, 1017 (1986).

Johnson, V. A., and Lark-Horovitz, K., Phys. Rev. **82**, 977 (1951).

Klein, R. S., Phys. Rev. B 31, 2014 (1985).

Koon, D. W., and Castner, T. G., Solid State Commun. **64**, 11 (1987).

Kukimoto, H., Shionoya, S., Toyotomi, S., and Morigaki, K., J. Phys. Soc. Jpn. **28**, 110 (1970).

Lax, M., and Narayanamurti, V., Phys. Rev. B **24**, 4692 (1981).

Le Hir, M. J. F., J. Phys. (Paris) **28**, 563 (1967).

Lindhard, J., Kgl. Danske Videnskab. Selskab, Mat.-Fys. Medd. **28**, No. 8 (1954).

Long, D., Energy Bands in Semiconductors, John Wiley & Sons, Inc., N.Y. (1968).

Mahan, G. D., Many-Particle Physics, Plenum Press, New York, 379 (1981).

Mansfield, R., Proc. Roy. Soc. London B **69**, 76 (1956).

Meyer, J. R., and Bartoli, F. J., Phys. Rev. B **24**, 2089 (1981).

Meyer, J. R., and Bartoli, F. J., Phys. Rev. B **36**, 5989 (1987).

Mott, N. F., and Davis, E. A., Electronic Processes in Non-Crystalline Materials, 2nd Edition (Clarendon Press, Oxford, 1979) 239.

Mousty, F., Ostoja, P., and Passari, L., J. Appl. Phys. **45**, 4576 (1974).

Nemeth, R., and Muhlschlegel, B., Solid State Commun. **66**, 999 (1988).

Nozieres, P., and Pines, D., Phys. Rev. **111**, 442 (1958).

Pankove, J. I., and Aigrain, P., Phys. Rev. **126**, 956 (1962).

Pines, D., Elementary Excitations in Solids, W.A. Benjamin, Inc., New York (1964).

Rode, D. L., Semiconductors and Semimetals **10**, 84 (1975).

Sasaki, W., Phil. Mag. B **52**, 427 (1985).

Schiff, L. I., Quantum Mechanics, Third Edition, McGraw-Hill Book Company, 326.

Singwi, K. S., Sjolander, A., Tosi, M. P., and Land, R. H., Phys. Rev. B **1**, 1044 (1970).

Singwi, K. S., Tosi, M. P., Land, R. H., and Sjolander, A., Phys. Rev. **176**, 589 (1968).

Toigo, F., and Woodruff, T. O., Phys. Rev. B **2**, 3958 (1970); **4**, 371, 4312 (1971).

van der Pauw, L. J., Philips. Res. Repts. **13**, 1 (1958).

Vashishta, P., and Singwi, K. S., Phys. Rev. B **6**, 875 (1972).

Vina, L., and Cardona, M., Phys. Rev. B **29**, 6739 (1984).

Vina, L., and Cardona, M., Phys. Rev. B **34**, 2586 (1986).

Wigner, E. P., and Huntington, H. B., J. Chem. Phys. **3**, 764 (1935).

Williams, F. E., J. Phys. Chem. Solids **12**, 265 (1960).

Yu, P. Y., and Hermann, C., Phys. Rev. B **23**, 4097, (1981).

Zubarev, D. N., Usp. Fiz. Nauk **71**, 71 (1960) [Soviet Phys. Usp. **3**, 320 (1960)].